TEST FACILITY DEVELOPMENT FOR SMALL CENTRIFUGAL COMPRESSORS (DESIGN STAGE)

BY

FAHAD A. AL-SULAIMAN

A Thesis Presented to the

DEANSHIP OF GRADUATE STUDIES

KING FAHD UNIVERSITY OF PETROLEUM & MINERALS

DHAHRAN, SAUDI ARABIA

In Partial Fulfillment of the
Requirements for the Degree of

MASTER OF SCIENCE

In

MECHANICAL ENGINEERING

Rabia II 1424 H
June 2003

بسـ ـ ـم الله الرحـ ـ ـمن الرحـ ـ ـ ـ ـيم

{سبحانك لا علم لنا إلا ما علمتنا إنك
أنت العليم الحكيم}

Dedicated

To

My Parents

and

My Family

ACKNOWLEDGMENTS

All Praise and Glory to Allah The Almighty Who Alone made this small objective to be accomplished. I feel honored and privileged to Glorify His name and gave due reverence to only Allah The Almighty for bestowing me with spirit, strength, patience and health to complete this work. Peace and Blessings of Allah be upon his Prophet Muhammad.

The research described in this was carried out in mechanical engineering department at King Fahd University of Petroleum & Minerals. I acknowledge the support given by this university to conduct this research.

I acknowledge, with deep gratitude, appreciation and inspiration for the careful guidance and encouragement given to me by my thesis advisor, Dr. Amro Al-Qutub. He has not only taken keen interest in the work by giving constructive comments with patience, in spite of his very busy schedule, but also performed himself the work with me at every step of the thesis. I am especially thankful and grateful to my thesis committee members, Dr. Rached Ben-Mansour and Dr. Sami El-Ferik for their useful comments on the research work conducted and review of the thesis.

I would also like to recognize and appreciate the patience, forbearance and courage of members of my household, especially my parents. I am also thankful to all faculty and staff members of ME Department who helped me in one-way or another.

TABLE OF CONTENTS

LIST OF TABLES

LIST OF FIGURES

THESIS ABSTRACT

Name Name: **Fahad Abdul-Aziz Al-Sulaiman**
Title of Study: **Test Facility Development For Small Centrifugal Compressors: Design Stage**
Major Filed: **Mechanical Engineering**
Date of Degree: **Rabi II 1424 H (June 2003)**

The trend of the centrifugal compressors applications now, is to use a small and light unit with high pressure ratio and efficiency. To achieve this, the rotational speed of the compressor must be very high, over 30,000 rpm, to increase tip speed. These characteristics of such compressors reduce the manufacturing and operating costs and improve, in general, the performance of the system.

The objective of the present work is to design a test rig for small centrifugal compressors for studying the performance, including efficiency and operating range (surge and choke). The design of the test rig takes into account safety, flexibility of use, reliability and uncertainty analysis. The design also takes into consideration the American Society of Mechanical Engineering, Performance Test Codes 10 (ASME PTC 10). The study contains the following major results:

- Aero-thermodynamics analysis of the impeller to estimate the power requirement for different compressors geometries, as well as torque and total pressure and temperature ratios estimation. This analysis was used to develop three codes. The results of these codes help to select the proper driver and instrumentation for the test facility. The results of the codes indicate the need for a driver with 500 kW to run the compressor for a given impeller tip radius ranged from .0286 to 0.1143 m to satisfy the objective. Also, the maximum expected total pressure ratio is over 8 and the maximum expected mass flow rate is 3.35 kg/s.
- The design of the test rig including general layout and selection of the driver unit.
- Measuring techniques, with consideration to ASME PTC 10 including single sample uncertainty analysis of the instrumentation. The uncertainty analysis helps to recommend some correlation terms.

Master of Science Degree
Mechanical Engineering Department
King Fahd University of Petroleum & Minerals
Dhahran, Saudi Arabia
Rabi II, 1424 (June 2003)

ملخص الرسالة

الاسم: فهد بن عبد العزيز آل سليمان

العنوان: تطوير جهاز إختبار لضواغط الطرد المركزية (مرحلة التصميم)
التخصص الرئيسي: الهندسة الميكانيكية
تاريخ الدرجة: يونيو 2003 م، ربيع الثاني 1424 هـ

إن توجة العام لتطبيقات ضواغط الطرد المركزي هوإيجاد وحدة صغيرة وخفيفة ذات ضغط نسبي وكفاءة عاليتين. ولتحقيق ذلك لابد أن تكون سرعة دوران الضاغط عالية جدا (أكثرمن 30000 دورة في الدقيقة) وذلك لزيادة سرعة طرف المروحة الطاردة. هذه الخواص تقلل من تكلفة التصنيع و التشغيل وتحسن بشكل عام أداء النظام.

الهدف من هذا البحث هو تصميم جهاز اختبار ضواغط الطرد المركزي الصغيرة لدراسة أدائها، وهذا يشمل الكفاءة ونطاق التشغيل.وقد أخذ في الحسبان عند تصميم جهاز الإختبار الأمان، مرونة العمل، الإعتمادية ودقة التحليل. التصميم أخذ في الإعتبار معاير الأداء رقم 10 للجمعية الأمريكية للمهندسين الميكانيكين. الدراسة تشمل النتائج الرئسية الاتية:

- التحليل الهوائي والحراري الديناميكي للمروحة الطاردة لتقدير متطلبات الطاقة لأشكال وأحجام مختلفة من الضواغط بالإضافة إلى عزم التدوير و نسبتي الضغط و الحرارة. هذا التحليل استخدم لتطوير ثلاثة برامج تساعد في اختيار المدور المناسب باللإضافة إلى أجهزة القياس المناسبة. وقد دلت النتائج إلى الحاجة لإستخدام محرك ذو قدرة تصل إلى 500 كيلو وات لتدوير مروحة ضاغط نصف قطرها الخارجي يتراوح طوله من 0.0286 إلى 0.1143 متر. ومن المتوقع أن تصل أعلى نسبة ضغط إلى أكثر من 8 وأعلى تدفق هواء يصل إلى 3.35 كيلو غرام في الثانية باستخدام هذا المحرك.
- تصميم جهاز الإختبار ويشمل التخطيط العام واختيار المدور المناسب.
- تركيب منظومة أجهزة القياس مع الأخذ في الإعتبار معاير الأداء رقم 10 للجمعية الأمريكية للمهندسين الميكانيكين بالإضافة إلىتحليل دقة أجهاز القياس وذلك لعينة واحدة، وهذا يساعد على التقليل من نسبة الخطأ في نتائج القياس.

درجة الماجستير في العلوم
قسم الهندسة الميكانيكية
جامعة الملك فهد للبترول والمعادن
الظهران- المملكة العربية السعودية
ربيع الثاني عام 1424 هـ

CHAPTER 1

INTRODUCTION

1.1 BACKGROUND

A centrifugal compressor consists primary of a stationary casing containing a rotating impeller, which increases the velocity of the gas, and a fixed diffuser where the gas is decelerated to increase the static pressure. The centrifugal compressor is widely used in petrochemicals and chemicals plants, natural gas pipelines, air separation plants, A/C, automobile turbochargers, power generation units, aircrafts, etc. The trend of centrifugal compressor applications these days is to use a small and light unit with high pressure ratio and efficiency, as well as low power requirement and wide operation range. Mitsubishi Heavy Industries, Ltd worked on the development of high-perfomance and compact centrifugal compressor stage, Masutani et al. (1999). Many others companies are also working on compact high-pressure centrifugal compressors, such as Elliot and Atlas Copco. This type of compressor is used by Saudi Aramco. To achieve high-pressure ratio, the tip speed of the impeller have to operate at transonic and or supersonic speeds thus

leading to high rotational speeds, over 30,000 rpm. These characteristics of such compressor will reduce the manufacturing and operating costs and improving, in general, the performance of the system. Research on this type will enhance the understanding and development of small centrifugal compressors under different operating conditions, which may lead to improvements in compressor performance. Extensive numerical and experimental research is running to improve the performance of the centrifugal compressor.

The numerical research represents only a guidance that can predict the compressor performance since it depends on many assumptions. The core of any reliable performance analysis that can the compressor user based on is the experimental investigation. However, the quality of the experimental outputs is based on the design of the test facility used. That is the instrumentations used for the measurement and the layout of the test rig.

The instrumentations need to be accurate enough to reflect the actual measured values. Also, they must be located into the proper locations, so the calculated values from the measurements represent the actual desired values. Still with the careful selection of the instrumentations, the level of their accuracies is limited. This brings the needs to implement the uncertainty analysis on the instrumentations.

One major parameter in the design of compressor test facility layout is the driver unit selection. Driver unit selection is based on many factors, such as its ability to control the compressor near the surge line, as well as its flexibility to test several compressor configurations.

The test facility design is important in the experimental investigations to predict the actual performance of a given compressor. In other words, the quality of the experimental results depends on the design of the test facility.

1.2 OBJECTIVE

The objective of the present work is to design a test facility for small centrifugal compressors for studying the perfomance, including efficiency and operating range (surge and choke). The design of the test rig takes into account safety, flexibility of use, reliability and results quality (uncertainty analysis). The design also takes into consideration the American Society of Machanical Engineering, Performance Test Codes 10 (ASME PTC 10).

1.3 LITERATURE REVIEW

The research in the field of performance test of centrifugal compressors may be divided into two main categories based on rotational speed: the low speed (<30,000 rpm) and the high speed (>30,000 rpm). From test rig design point of view, rotating speeds of

the impeller is of great concern. High rotational speeds pose technical challenges when designing bearings, seals, as well as balancing of the drive unit. The experimental results of these studies are important references in designing centrifugal compressors. Stall and surge, for example, are two important parameters for the perfomance study of the compressor, which are difficult to predict through numerical study.

Large number of experimental research was completed on the performance of low speed compressors due to design simplicity. Rodgers (1997) described the development of subscale single- stage centrifugal compressor with dimensionless specific speed of 1.8, impeller tip diameter 8.75 in and 14,000 rpm. He compared the results with recent CFD results. Representative application of this type of research is on gas booster compressor. Wernet et al. (2001) investigated the surge in a centrifugal compressor using digital PIV and discussed its advantaged. The outer diameter was 431 mm and the rotational speed was 21,789 rpm. Engeda (1997) tested three types of diffusers, a vaneless, conventional vaned and low solidity vaned. He compared the rotating stall and surge characteristics of a centrifugal compressor with these types and stated the influence of each one on the performance. Also, he noticed that the type of the diffuser had no considerable effect in the inducer and impeller stall, as will as the conventional type is slightly more stable than the others. This investigation was at three different speeds: 18,800, 24,000 and 28,000 rpm. Liberti et al. (1996) used the same test rig as Engeda (1997) to investigate the effect of the vaneless diffuser width on the performance with an outer impeller diameter equal to 0.244 m . They used two vaneless diffusers with parallel walls and different width, to

study the performance. Roduner; Köppel; Kupferschmied and Gyarmathy (1999) used both pneumatic and fast-response (time-resolving) probes to compare the measurements data of unsteady high-speed flow in a centrifugal compressor. Again the same group published two other papers (2000) on the development and application of the fast-response aerodynamic probe system in turbomachines: one on flow, surge and stall in a centrifugal compressor and the other about the comparison of averaging methods applied to centrifugal compressor measurements. The impeller diameter was 0.28 m and the maximum speed was 17,720 rpm.

Also, more research was done on the numerical side. Arima et al. (1998) applied three-dimensional Navier-Stokes computations, using an algebraic Reynolds turbulence stress model, to study the complex flow fields of a transonic centrifugal compressor impeller. In addition to that, they investigated the secondary flow that generated by the complex curvature and tip-clearance flow. The aim of the above study was to analyze the perfomance and compared the results with experimental data. Schlechtriem and Lötzerich (1997) detected the tip leakage vortex breakdown in a modern, wide-cord, transonic rotor caused by interaction of the vortex with the passage shock. Clayton et al (1998) conducted a wide numerical study of the three-dimensional turbulent flow in an unshrouded impeller of a high-speed centrifugal compressor, using STAR-CD code.

In brief, more research have been done for low speed centrifugal compressor where subsonic flow is dominant at this case comparing to transonic and supersonic flow for high-speed type. In other words, low speed centrifugal compressor is easier to analyze

numerically and investigate experimentally.

On the other hand, limited information in the open literature is available on the high-speed centrifugal compressors. In the experimental side, fewer cases were studied. This is mainly due to the difficulty of the measurements at the rotor inlet and exit, in addition to the construction of the test rig itself. Different experimental techniques were used to satisfy dynamic similarity. For example, Krain et al. (1995) studied the aerodynamics of a full scale impeller with transonic inlet conditions, using a backswept rotor design for 586 m/s tip speed and a mean relative tip Mach number of 1.3. The test rig used in this investigation was driven by two inline DC-motors with a total power of 1500 kW to drive a small impeller with an outer tip diameter of 0.224 m. A planetary gear was used to transmit the motor shaft speed to the rotor shaft speed with a maximum final speed 50,000 rpm. In addition to advanced control system for the speed, mass flow rate, bearing cooling, gearbox cooling and vibration monitoring were implemented to assure safe and reliable operation, which indicate the complexity and technical challenges involved in the construction of high speed centrifugal compressor test facility. Krain and Hoffmann (1998) used the latter test rig to investigate the flow physics in high-pressure ratio centrifugal compressor. In addition to that, as stated in the second paper Pak, Krain and Hoffmann (1992) and Eisenlohr et al (1998) used the same test rig in their investigation. Pak et al. (1992) studied the flow field analysis of a high-pressure ratio centrifugal compressor. Eisenlohr et al (1998) used Krain et al. (1995) results to validate four different viscous 3D-solvers. Actually, the main geometrical parameters including

the blade angles of the impeller are identical. So, large amount of performance and flow characteristics can be obtained from a well-designed and constructed test rig of a compressor.

Fink, (1988) studied the detailed time resolved surge measurements of a small high-speed centrifugal compressor driven by a radial turbine. This study focused on the surge since the numerical approach cannot be accepted alone, especially in such condition. Due to the fact that the complete turbocharger was used in this test rig with the turbine driven by compressed cold air, there are limitations on the type and size of the tested impellers. The test rig requires large blow down facility to operate. This compressor was designed to operate at speeds up to 70,000 rpm with pressure ratios over than 3. The outer tip diameter was 0.128 m

Investigation of a low Reynolds number and high Mach number through a super-scale test facility of very small centrifugal compressors was performed by Shirley (1998). The test facility was 75 times larger than the full-scaled device and operated under 1/75 atmospheric pressure conditions to correctly match the Reynolds number, which was about 20,000. The investigated compressor has impeller outer diameter equal to 0.6 m and rotational speed equal to 26,000 rpm while the full-scaled compressor has impeller tip diameter equal to 0.004 m and rotational speed equal to 1,909,860 rpm. One of the main difficulties raised in this test rig was the use of vacuum test loop, which requires vacuum pump, heat exchanger for cooling and special seals. Numerical solution on the same test rig conditions was accepted due to the acceptable similarity with the experimental results.

Justen et al. (1999) estimated the influence of the unsteadiness on the operating performance of the centrifugal compressor stage which was done by the measurements at choke and surge limits for different diffusers geometries. The impeller outer diameter was 0.27 m and the rotational speed was 35,200 rpm. Hunziker et al (2001) completed the study of the numerical and experimental investigation of a centrifugal compressor with an inducer casing bleed system and showed its effectiveness and compared the results with non-bleeding system. The impeller exit diameter was 0.1676 m. Kim et al (2001) reported experimentally the efficiency of a centrifugal compressor with two different inlet flow directions and noticed clear difference between them and based on that they developed an improved inlet using numerical simulations. The impeller has an outer diameter equal to 0.1433 m and design rotational speed equal to 38,976 rpm. Colantuoni and Colella, (1993) described the procedure of adopting the design for a transonic impeller having 1.31 relative Mach number at the inducer tip, 45 degree back-swept exit blade angle and a tip speed of 636 m/s. They emphasized on the aero-design and performance analysis for a 9:1 pressure ratio compressor. The tip diameter at the impeller exit was 0.279 m and the rotational speed was 43,500 rpm. This type of compressor is used for small aeroengines.

In the numerical analysis of high-speed compressors, Eisenlohr et al. (1998) compared between four different viscous 3D-solvers in the calculations of the design speed to investigate the suitability of these programs in the various design procedures with special attention on the area from the rotor inlet up to the splitter blades. They validated the numerical analysis through the comparison with the information gained by

the same test rig mentioned above, which was used by Krain, et al. A performance prediction method at design and off-design values of mass rate and rotational speed for a low-pressure ratio (2.2:1) centrifugal compressor capable of rotating at a speed up to 90,000 rpm was reported by Al-Zubaidy and Dahgan (1992). The possibility of a novel centrifugal compressor, driven by a variable speed electric motor, in addition to the component design of a centrifugal compressor, which is used in air conditioners, was studied by Yun et al. (1996). Most of the studies emphasized on the perfomance and flow analysis of the compressor both numerically and experimentally with some concentration on the transonic flow, which is dominant at high speed.

1.4 CONCLUSION

In conclusion, people have worked more in the numerical analysis of the centrifugal compressor because it is easier, cheaper and takes less time compared to the experimental investigation. However, experimental studies for centrifugal compressor performance are the key and the reference for any good design. The relatively low confidence in results of numerical studies of centrifugal compressor performance is due to:

- Complexity of the flow (very complex structure and boundary condition).
- Surface finish of different parts (affecting flow rate, friction losses and separation).
- Very complex shock system in case of supersonic and transonic condition.

These are difficult to simulate in the numerical solution. Open literature on experimental studies of high-speed centrifugal compressors is scarce. This means that there is a need for a source for this type of study, especially the experimental side. In addition, there are plenty of applications of such type of compressors in the local area; however, the proper test rig is not available in KSA. To transfer this technology in the right way, the real state of the performance analysis for a small and high-speed centrifugal compressor need to be conducted, i.e. assuring dynamic and geometrical similarity.

1.5 WORK DONE

The present study contains the following:

1. Aero-thermodynamics analysis of the impeller to estimate the power requirement for a given compressor geometry
2. Study and design the test rig: general layout and selection.
3. Design the measuring techniques, with consideration to ASME PTC 10 including instrumentation single sample uncertainty analysis.

1.6 IMPORTANT RESULTS

The main results from this study are:

1. Codes that can calculate and plot the mass flow rate, pressure ratio, temperature ratio, input power and torque for different rotational speeds and compressor geometries.
2. Design of test facility for compressor, including power and general layout.
3. Instrumentation setup and deciding types as well as specification of sensors.
4. Procedure for reporting single sample uncertainty of the instrumentations.

CHAPTER 2

PERFORMANCE ANALYSIS

2.1 INTRODUCTION

One of the main requirements of designing the centrifugal compressor test facility is calculating the required input power and rotational speed to select the proper drive unit. This can be achieved through using the proper analysis. In addition to that, input torque, mass flow rate, stagnation pressure and temperature ratios can help in estimating the range of operating conditions and selection of instrumentation. Based on the analysis a computer program was constructed to perform the calculations for different impeller sizes and configurations.

2.2 ANALYSIS

The operating conditions for a given centrifugal compressor can be obtained theoretically through using some assumptions, as well as some modifications from the literature. Equations needed to find input power, input torque, mass flow rate, stagnation pressure and temperature ratios, as well as some other related equations were derived. Hill and Peterson (1992), represents one of the best sources for these derived equations.

2.2.1 Problem Analysis:

Geometry

The geometry of the analyzed impeller is shown in figures 2.1 and 2.2. Where r_1 is the impeller inlet radius, r_h is the impeller hub radius, r_2 is the impeller tip radius, β_1 is the inlet impeller blade angle and β_2 is exit impeller blade angle.

Major Assumptions:

- Ideal gas,
- Bulk flow,
- No preswirl at the inlet.

The bulk flow assumption will be corrected for boundary layer effect using the average mass flow rate during the computer program calculations. Usually, during the experimental investigation for this type of compressor the fluid is air, so the assumption of ideal gas is applicable here.

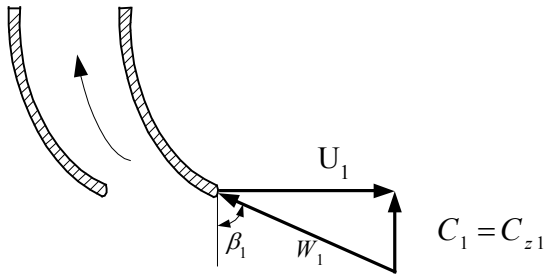

Figure 2.1 Impeller inlet geometry and velocity vector

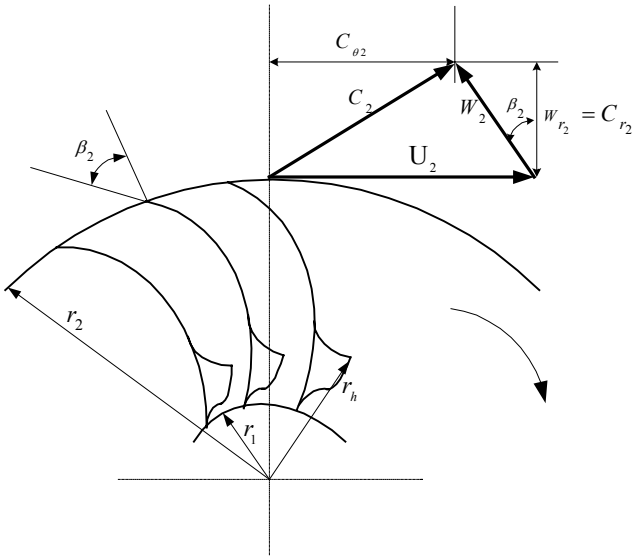

Figure 2.2 Impeller exit geometry and velocity vector

2.2.2 Governing Equations:

Actual mass flow rate

The flow factor is used to account for the off-design condition. When the relative flow is parallel to inducer tip, the flow is considered to be in ideal case (design condition); otherwise it is in off design condition. The ideal mass flow rate is defined as:

$$\dot{m}_{ideal} = A_1 C_{z1ideal} \rho_1 \ . \tag{2.1}$$

Using the definition of the flow factor, the actual mass flow rate can be written as:

$$\dot{m}_{act} = \phi_f \ \dot{m}_{ideal} \tag{2.2.a}$$

So, the actual mass flow rate can be written as:

$$\dot{m}_{act} = \phi_f \ A_1 C_{z1ideal} \rho_1 \ . \tag{2.2.b}$$

where the subscript 1 denotes the impeller inlet, A_1 is the inlet area, $C_{z1ideal}$ is the ideal axial velocity and ρ_1 is the static density.

With the known value of the tip impeller inlet radius, r_1, and the hub radius, r_h, the area at the inlet can be calculated as:

$$A_1 = \pi (r_1^2 - r_h^2), \tag{2.3}$$

and the axial velocity, in ideal case, see figure 2.1.

$$C_{z1ideal} = \frac{U1}{\tan \beta_1} = \frac{\Omega r_1}{\tan \beta_1},$$

in which U_1 is the blade velocity at tip of the impeller inlet, β_1 is the impeller blade angle at the inlet and Ω is the angular velocity. To account for the actual case the effect of the flow factor must be included:

$$C_{z1} = \frac{\phi_f \Omega r_1}{\tan \beta_1}, \tag{2.4}$$

The static density at the inlet is defined as a function of Mach number. Using the isentropic relation, the static density is equal to:

$$\rho_1 = \rho_{01}\left(1+\frac{\gamma-1}{2}M_1^2\right)^{\left(-\frac{1}{\gamma-1}\right)}$$

where ρ_{01} is the impeller inlet stagnation density, M_1 is the Mach number at the impeller inlet and γ is the specific heat ratio.

The Mach number can be defined as

$$M_1 = \frac{C_{z1}}{\sqrt{\gamma R T_1}},$$

where R is the gas constant and T_1 is the inlet static temperature that can be defined as:

$$T_1 = T_{01} - \frac{C_{z1}^2}{2C_p},$$

in which C_p is the specific heat. Thus the Mach number can be written as:

$$M_1^2 = \frac{C_{z1}^2}{\gamma R(T_{01} - \frac{C_{z1}^2}{2C_p})}$$

and the static density is equal to

$$\rho_1 = \rho_{01}\left[1 + \frac{\gamma - 1}{2}\frac{C_{z1}^2}{\gamma R(T_{01} - \frac{C_{z1}^2}{2C_p})}\right]^{\frac{-1}{\gamma - 1}} \tag{2.5}$$

Substitute equations 2.4 and 2.5 into 2.1 to get the actual mass flow rate as function of impeller geometry, operating speed and inlet conditions:

$$\dot{m}_{act} = \rho_{01}\left[1 + \frac{\gamma - 1}{2}\frac{(\frac{\phi_f \Omega r_1}{\tan\beta_1})^2}{\gamma R(T_{01} - \frac{(\frac{\phi_f \Omega r_1}{\tan\beta_1})^2}{2C_p})}\right]^{\frac{-1}{(\gamma - 1)}} \pi(r_1^2 - r_h^2)(\frac{\phi_f \Omega r_1}{\tan\beta_1}) \tag{2.6}$$

Slip Factor

From the geometry and operation of the compressor the flow at the impeller exit slips. Between each two blades in the impeller pressure gradient is developed due to

Coriolis acceleration and since there is no solid boundary to support pressure gradient at the exit, flow slips, Hill and Peterson (1992). There are some formulas that can be used to calculate the slip factor. The one, which was discussed by Wiesner (1967) and modified by Hill and Peterson (1992), is a representative formula that takes into account several factors. It takes into consideration number of the impeller blades, N_b, exit impeller blade angle, β_2, blade velocity at the impeller tip, U_2, and exit radial relative velocity of the impeller, W_{r2}, as shown in the equation below, see figure 2.2.

$$\sigma_S = (1 - \frac{2}{N_b}\sqrt{\cos\beta_2})(1 - \frac{W_{r_2}}{U_2}\tan\beta_2) \tag{2.7}$$

The exit radial relative velocity can be derived from the mass flow rate:

$$W_{r_2} = \frac{\dot{m}_{act}}{\rho_2 A_2} = \frac{\dot{m}_{act}}{\rho_2(\pi 2 r_2 b)} \tag{2.8}$$

The subscript 2 indicates the impeller exit and *b* is the impeller width. Substitute the value of W_{r_2} into equation 2.7 to get:

$$\sigma_S = (1 - \frac{2}{N_b}\sqrt{\cos\beta_2})(1 - \frac{\frac{\dot{m}_{act}}{\rho_2 (\pi 2 r_2 b)}}{\Omega r_2}\tan\beta_2),$$

Simplify to obtain:

$$\sigma_S = (1 - \frac{2}{N_b}\sqrt{\cos\beta_2})(1 - \frac{\dot{m}_{act}}{2\rho_2 \pi^2 r_2^2 b(\frac{rpm}{30})}\tan\beta_2) \tag{2.9.a}$$

The slip factor can also be defined as:

$$\sigma_S = \frac{C_{\theta 2}}{U_2} \tag{2.9.b}$$

Impeller exit static density

To calculate the slip factor, the impeller exit static density needs to be found first. The general procedure to derive the required equation to find the density was done by Hill and Peterson (1992). Some improvements were done on this procedure as shown below.

This procedure includes the following assumptions:

- Neglect the thickness of the vanes.
- Neglect the boundary layer displacement thickness.
- Assume the isentropic efficiency of the rotor : $\eta_{cr} \approx \frac{1+\eta_c}{2}$, η_c is the stage isentropic efficiency.

Using the isentropic relation, the static density ratio can be written as:

$$\frac{\rho_2}{\rho_1} = \frac{\rho_{02}}{\rho_{01}} \left[\frac{1 + \frac{\gamma - 1}{2} M_2^2}{1 + \frac{\gamma - 1}{2} M_1^2} \right]^{\frac{1}{\gamma - 1}} ;$$

Using the isentropic relation to replace the stagnation density ratio with the stagnation pressure ratio to get:

$$\frac{\rho_2}{\rho_1} = \left(\frac{P_{02}}{P_{01}}\right)^{\frac{1}{\gamma}} \left[\frac{1+\frac{\gamma-1}{2}M_2^2}{1+\frac{\gamma-1}{2}M_1^2}\right]^{\frac{1}{\gamma-1}} ; \tag{2.10}$$

The stagnation pressure ratio can be written in terms of the blade velocity at the impeller tip and the absolute tangential velocity at the impeller exit. This can be achieved by using the isentropic relation, isentropic efficiency and the definition of the power,

$$\frac{P_{02}}{P_{01}} = \left[1+\eta_{cr}\left[\frac{U_2 C_{\theta 2} - U_1 C_{\theta 1}}{C_p T_{01}}\right]\right]^{\frac{\gamma}{\gamma-1}} ;$$

The assumption for the case of no pre-swirl is valid for the analyzed compressor and thus $C_{\theta 1}$ is equal to zero. Also, the isentropic rotor efficiency, η_{cr}, can be replaced by the stage isentropic efficiency, η_c. That is,

$$\eta_{cr} \approx \frac{1+\eta_c}{2} ;$$

The rotor efficiency is modeled from the experimental results done by Krain et al. (1995). These results were selected since they are close to the operation conditions of the desired test facility of the compressor. Also, because Krain et al. (1995) study was chosen as a reference to validate four different advanced codes, which indicates the confident in their results, see Eisenlohr et al. (1998). The chosen efficiency model for validation was:

Stage efficiency = 0.8545*exp (-1E-06*rpm)

The main purpose of pressure ratio validation is to check whether the code can predict the compressor performance accurately, as shown in section 2.4.

Substitute η_{cr} into the above pressure ratio equation and with some simplifications the pressure ratio can be written as:

$$\frac{P_{02}}{P_{01}} = \left[1 + \left(\frac{1+\eta_c}{2}\right)\left(\frac{\gamma-1}{\gamma}\right)\left(\frac{U_2}{\sqrt{RT_{01}}}\right)^2\left(\frac{c_{\theta 2}}{U_2}\right)\right]^{\frac{\gamma}{\gamma-1}}; \tag{2.11}$$

The Mach number at the impeller inlet can be written as:

$$M_1 = \frac{C_{Z1}}{\sqrt{\gamma R T_1}} = \frac{C_{Z1}}{\sqrt{\gamma R (T_{01} - \frac{C_{Z1}^2}{2C_p})}};$$

Substitute for C_{Z1} in term of the angular velocity and the inlet angle and then square the Mach number to get:

$$M_1^2 = \frac{\left(\frac{\phi_f \Omega r_1}{\tan\beta_1}\right)^2}{\gamma R\left(T_{01} - \frac{\left(\frac{\phi_f \Omega r_1}{\tan\beta_1}\right)^2}{2C_p}\right)}; \tag{2.12.a}$$

Similarly, as the inlet Mach number, the exit Mach number can be written:

$$M_2^2 = \frac{C_2^2}{\gamma R(T_{02} - \frac{C_2^2}{2C_p})}; \tag{2.12.b}$$

where C_2 is the absolute velocity at the impeller exit and from figure 2.2 it can be written as:

$$C_2 = \sqrt{(U_2 - W_{r2}\tan\beta_2)^2 + W_{r2}^2}; \tag{2.13}$$

The derived above equations, 2.9.b and 2.11 can be substituted into equation 2.10 to get the density at the impeller exit. The exit stagnation density can be written in the proper form as:

$$\rho_2 = \rho_1 \left[\left[1 + \left(\frac{1+\eta_c}{2} \right) \left(\frac{\gamma - 1}{\gamma} \right) \left(\frac{U_2}{\sqrt{RT_{01}}} \right)^2 \sigma_s \right]^{(\frac{1}{\gamma-1})} \left[\frac{1 + \frac{\gamma-1}{2} M_2^2}{1 + \frac{\gamma-1}{2} M_1^2} \right]^{\frac{-1}{\gamma-1}} \right]; \tag{2.14}$$

where M_1^2 and M_2^2 as defined in equations 2.12 .a and 2.1.b, respectively.

Input Power

The power that the impeller consumes is defined as:

$$\mathrm{P} = \dot{m}_{act}\left((U C_\theta)_2 - (U C_\theta)_1 \right) \tag{2.15}$$

Where $C_{\theta 2}$ is the absolute tangential velocity at the impeller exit and defined as:

$$C_{\theta 2} = \sigma_s U_2 \tag{2.16}$$

With the assumption that there is no pre-swirl at the inlet, C_{θ_1} is equal to zero and from equation 2.15 and 2.16 the power can be written as:

$$\mathrm{P} = \dot{m}_{act}\, \sigma_S U_2^2 \tag{2.17}$$

Substitute into equation 2.17 for the slip factor and write blade velocity at the impeller tip as a function of the angular velocity, the power can be obtained as:

$$\mathrm{P} = \dot{m}_{act}\left[(1 - \frac{2}{Nb}\sqrt{\cos\beta_2})(1 - \frac{\dot{m}_{act}}{2\rho_2 \;\; \pi^2 \;\; r_2^2 \;\; b(\frac{rpm}{30})} \tan\beta_2)(\Omega r_2)^2 \right] \tag{2.18}$$

<u>Further parameters</u>

- The input torque:

$$\mathrm{T} = \mathrm{P}/\Omega; \tag{2.19}$$

- The stagnation impeller exit temperature:

$$T_{02} = \frac{\mathrm{P}}{\dot{m}_{act} C_p} + T_{01}; \tag{2.20}$$

- The impeller stagnation temperature ratio:

$$T_{0201r} = T_{02} / T_{01}; \tag{2.21}$$

- The compressor exit isentropic stagnation temperature:

$$T_{04s} = \eta_{cr}(T_{02} - T_{01}) + T_{01} \ , \tag{2.22}$$

where η_{cr} is the compressor efficiency.

- The stagnation pressure ratio:

$$\frac{P_{04}}{P_{01}} = (\frac{T_{04s}}{T_{01}})^{(\gamma/(\gamma-1))}; \tag{2.23}$$

2.3 IMPLEMENTATIONS OF THE ANALYZED EQUATIONS INTO THREE COMPUTER CODES

Some commercial codes have been written to estimate the operating conditions of the centrifugal compressors. However, most of them are written for industries to evaluate the operating conditions during the operation not for the designing purposes. For example, in Centrifugal Compressor Tracking Program developed by Ronald, P. Lapina, to calculate polytropic head and efficiency curves the discharge pressure and power curves are needed. On the other hand, there are limited codes that can calculate the operating conditions of the compressor for the designing purposes. An example of that is the code developed by PCA Engineering Inc. The results of the developed code in this project is compared with some experimental results, as explained below for the purpose of validations

The analyzed equations above are used to write three computer codes. All the three programs have the same general layout and exact procedure to implement the input. In additions to that, the definitions of the used variables and some comments were written. The input information is as follows:

- Impeller size (inlet, exit and hub radiuses).
- Impeller configuration (inlet and exit tip angles, blades number and impeller width).

- Gas properties, ideal gas only, (specific heat ratio, gas constant and constant pressure specific heat).
- Inlet conditions (stagnations inlet temperature, pressure and density).

To account for the bulk flow assumption in the analysis an estimated coefficient for the average mass flow rate was implemented in the codes. It was chosen based on a thorough experimental investigation in smooth pipes, see Schlichting, (1979) and for more details see Nikuradse, (1932). Also, to account for the flow separation (off design condition) an estimated flow angle, 10^{o} for separation was implemented based on experimental results. The characteristics of the three codes are:

- The first code calculates and plots the input power, input torque, stagnation temperature and pressure ratios vs. mass flow rate for different rpm and impeller size(s). An example of the results of this code is shown in figures 2.3-2.6 and the code is available in appendix A.1.
- The second code calculates and plots the input power, input torque, stagnation temperature and pressure ratios, as well as mass flow rate vs. rpm for different impeller sizes and impeller exit tangential velocities. A typical example of the results is shown in figures 2.7-2.11 and the code is shown in appendix A.2
- The third code calculates and plots the stagnation pressure ratio vs. compressor size for different input power and rpm. An example of the results is shown in figure 2.12 and the code exists in appendix A.3.

The impeller configuration used to get the above figures (2.3-2.12) is:

- Impeller inlet tip radius: 0.025 m.
- Impeller hub radius: 0.008 m.

- Impeller exit tip radius: 0.0381 m.
- Impeller inlet blade angle (from the radial axis): 45^0 for case one and 67^o for case two.
- Impeller exit blade angle (from the radial axis): 25^0.
- Impeller width: .005m.

These radiuses and the width of the impeller are for the reference size, which is called Z. Using multiple sizes option; the codes can provide the plots of different impeller sizes and width. In multiple sizes option only the impeller radius and width are change with a factor according to the desired option.

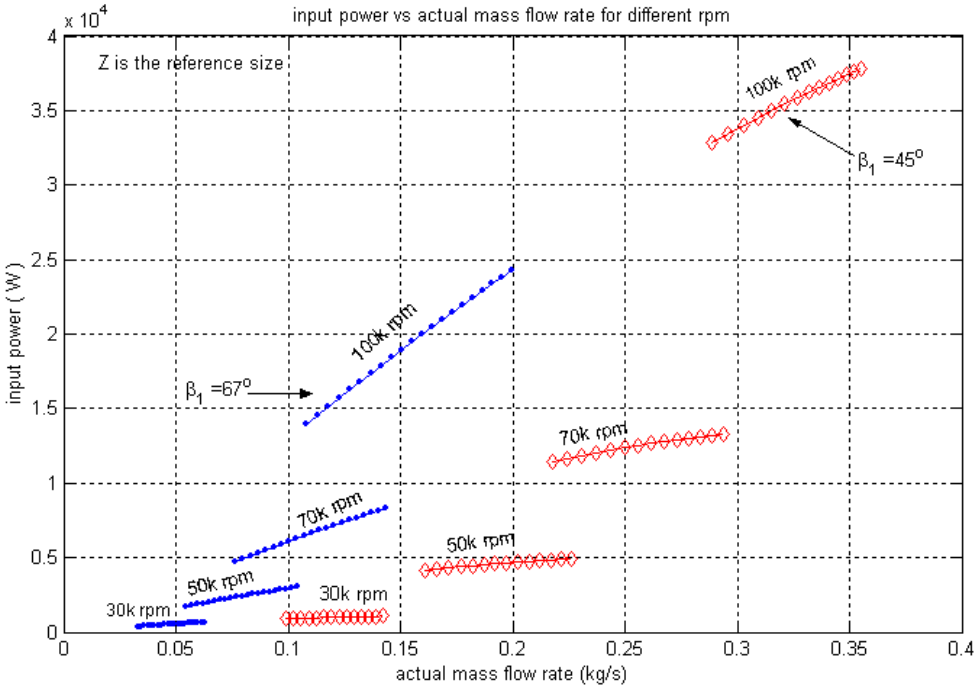

Figure 2.3 Input power vs. actual mass flow rate for different rpm and a given size, Z=1.

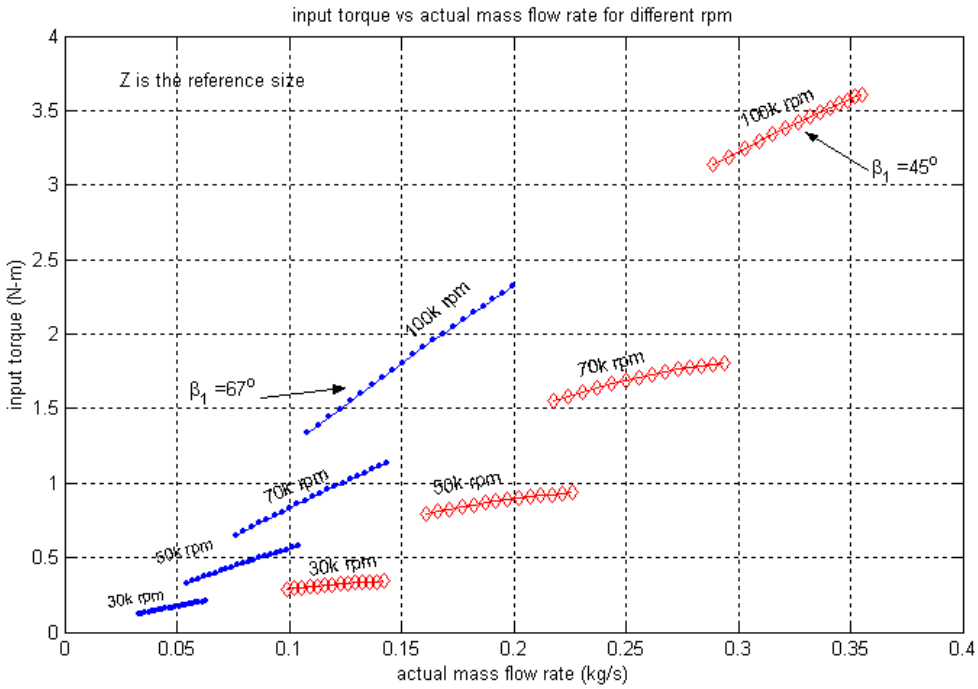

Figure 2.4 Input torque vs. actual mass flow rate for different rpm and a given size, Z=1.

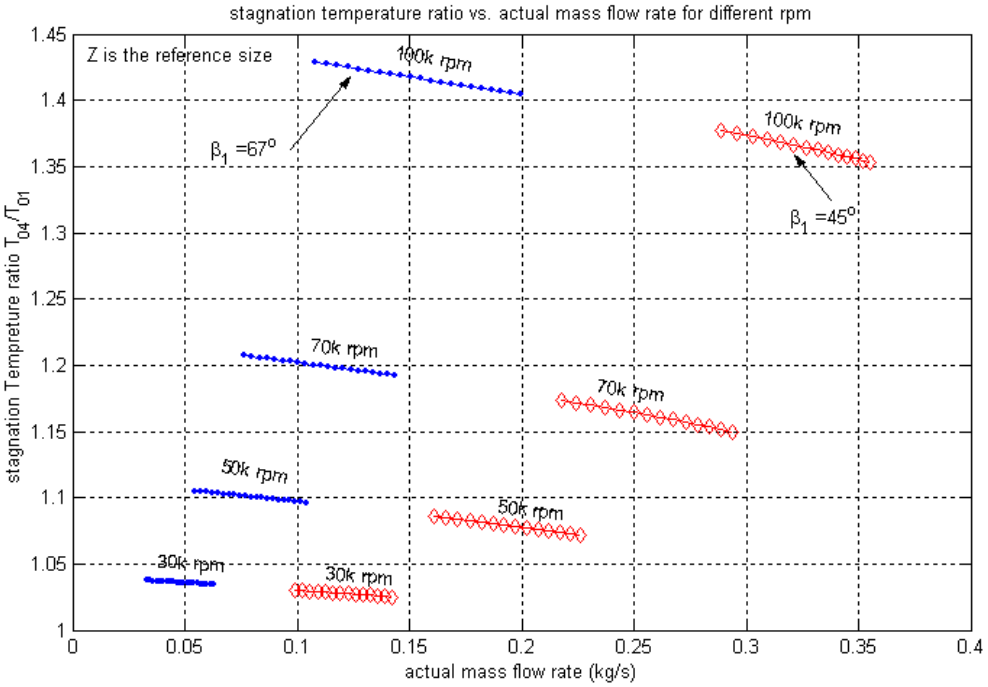

Figure 2.5 Stagnation temperature ratio vs. actual mass flow rate for different rpm and a given size, Z=1.

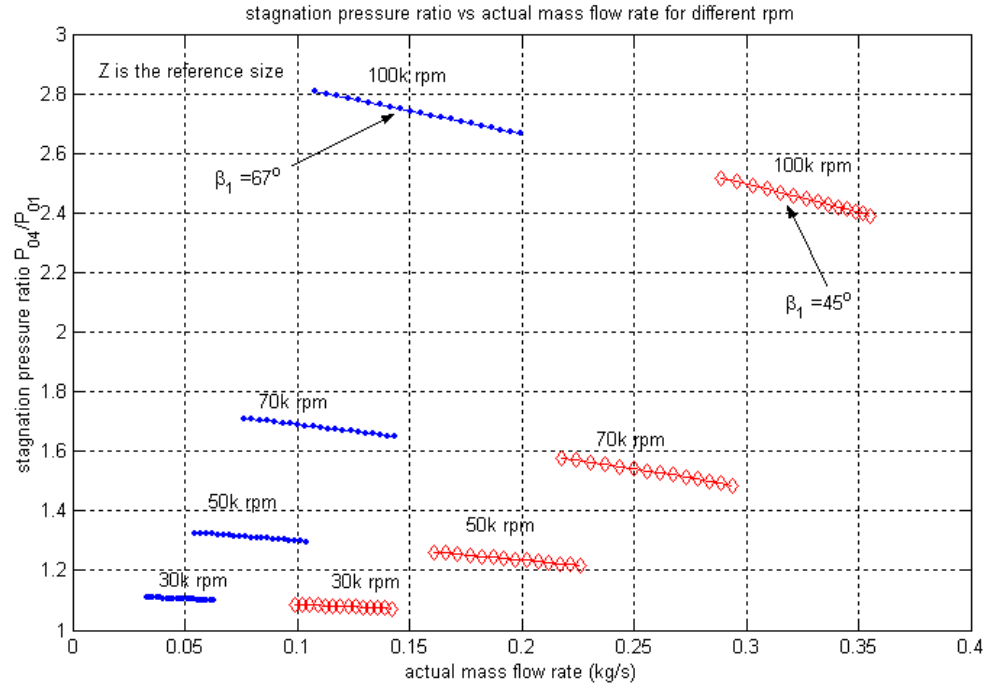

Figure 2.6 Stagnation pressure ratio vs. actual mass flow rate for different rpm and a given size, Z=1.

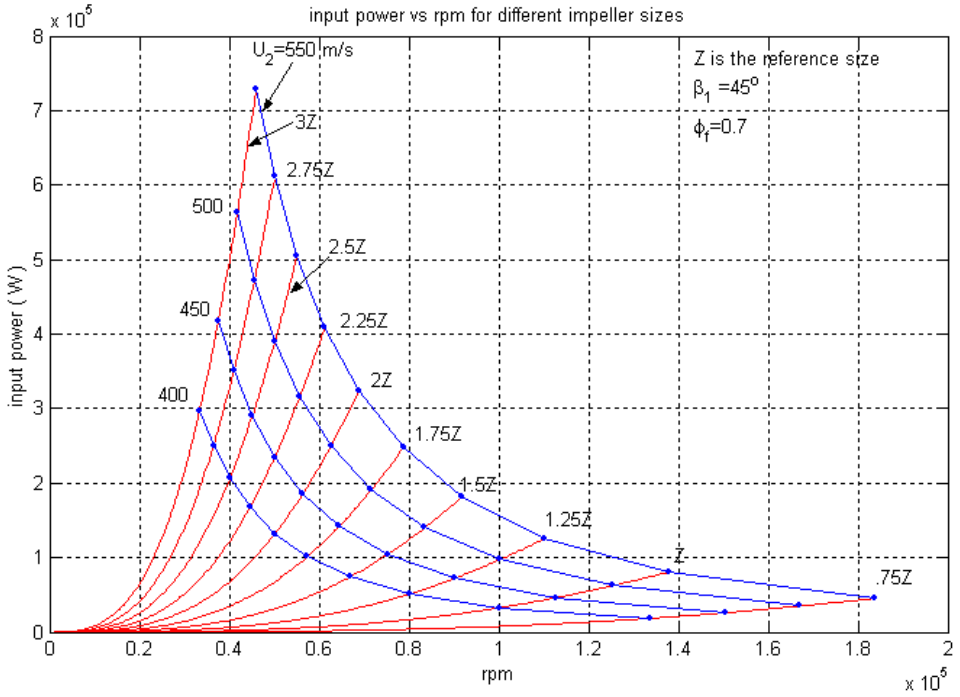

Figure 2.7.a Input power vs. rpm for different impeller sizes and exit tangential velocities where $\beta_1 = 45^0$ and $\phi_f = 0.7$.

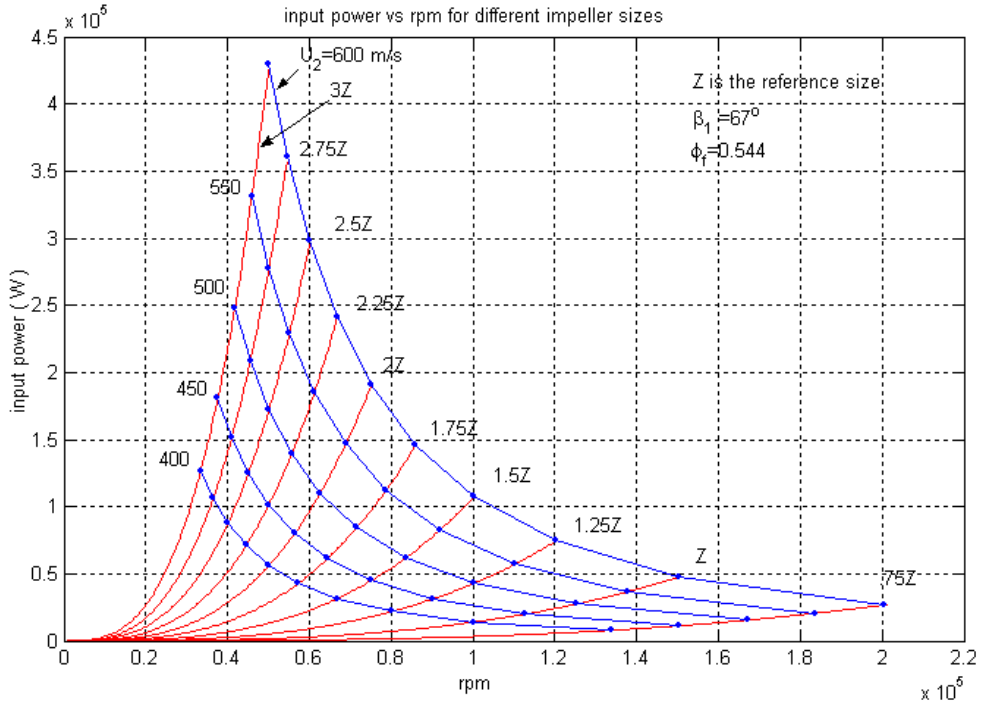

Figure 2.7.b Input power vs. rpm for different impeller sizes and exit tangential velocities where $\beta_1 = 67^0$ and $\phi_f = 0.544$.

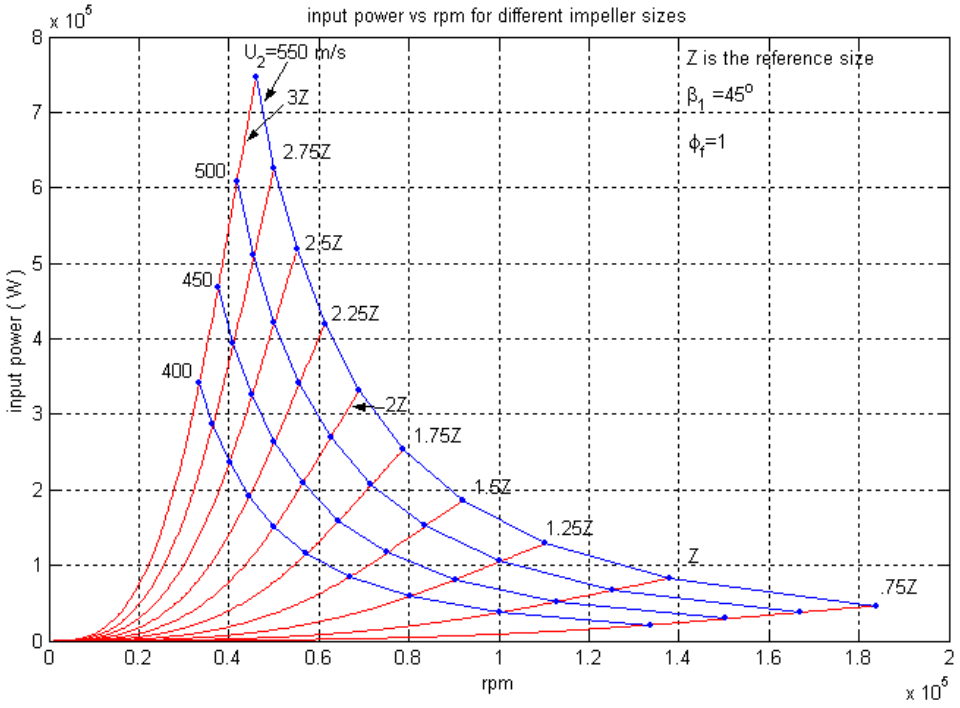

Figure 2.7.c Input power vs. rpm for different impeller sizes and exit tangential velocities where $\beta_1 = 45^0$ and $\phi_f = 1$.

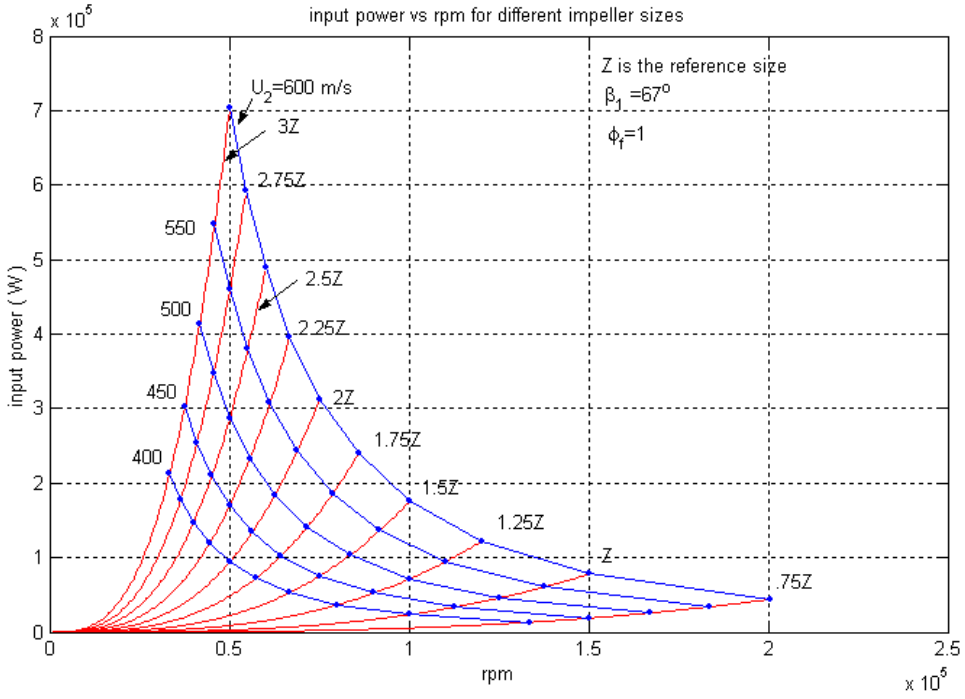

Figure 2.7.d Input power vs. rpm for different impeller sizes and exit tangential velocities where $\beta_1 = 67^0$ and $\phi_f = 1$.

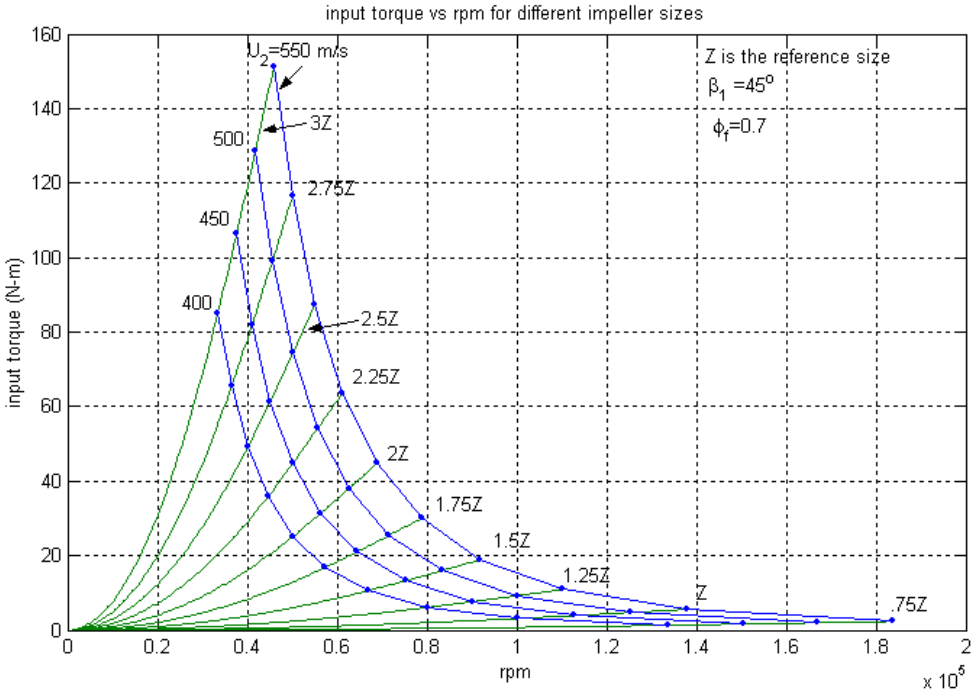

Figure 2.8.a Input torque vs. rpm for different impeller sizes and impeller exit tangential velocities where $\beta_1 = 45^0$ and $\phi_f = 0.7$.

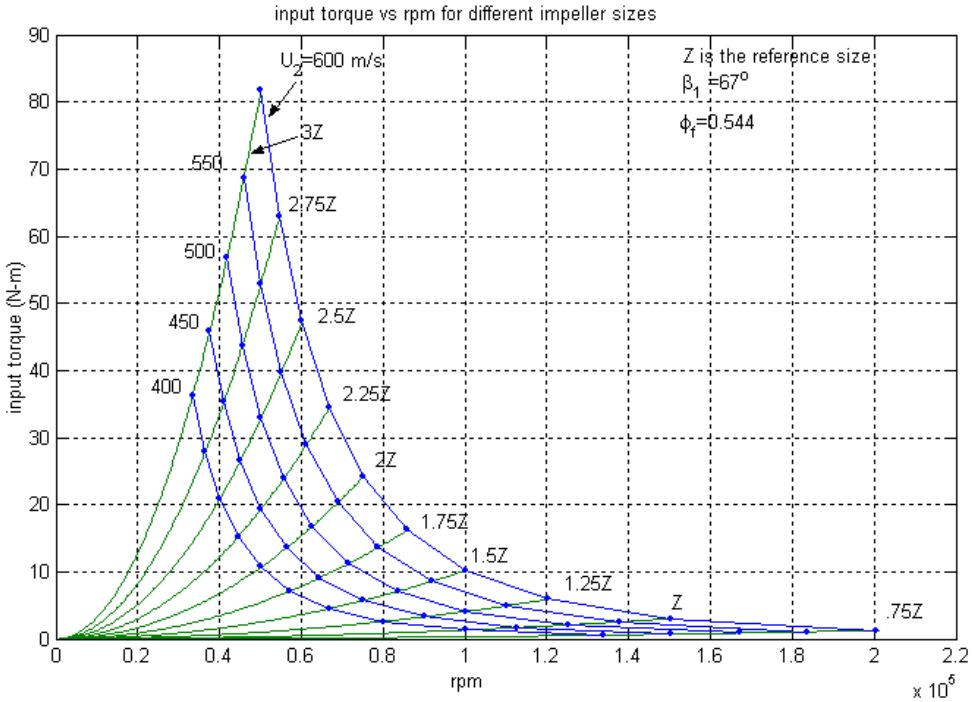

Figure 2.8.b Input torque vs. rpm for different impeller sizes and impeller exit tangential velocities where $\beta_1 = 67^0$ and $\phi_f = 0.544$.

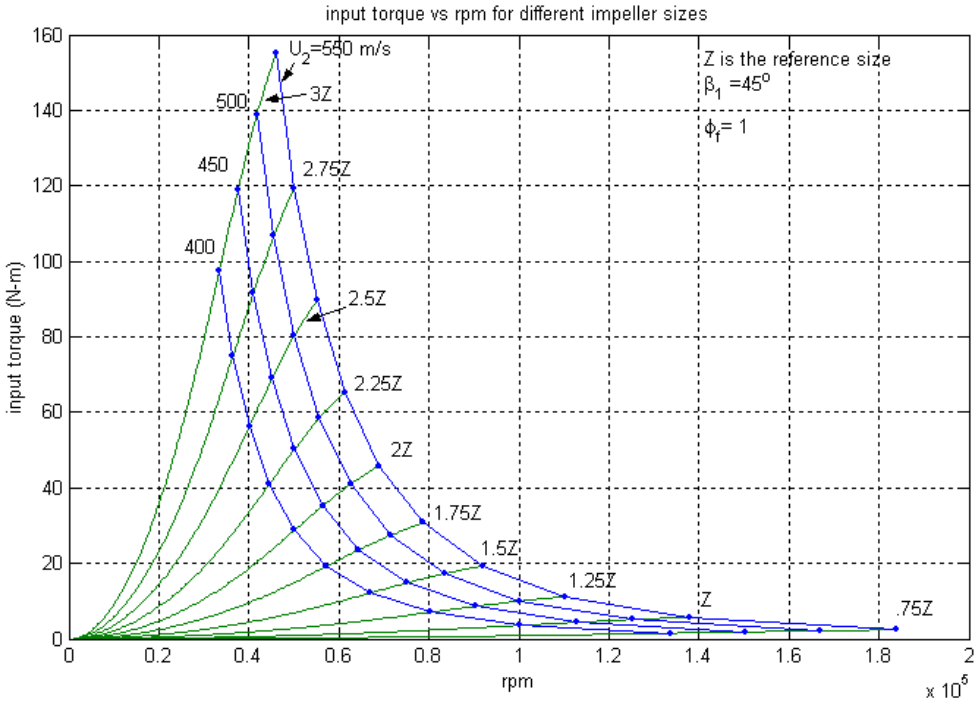

Figure 2.8.c Input torque vs. rpm for different impeller sizes and impeller exit tangential velocities where $\beta_1 = 45^0$ and $\phi_f = 1$.

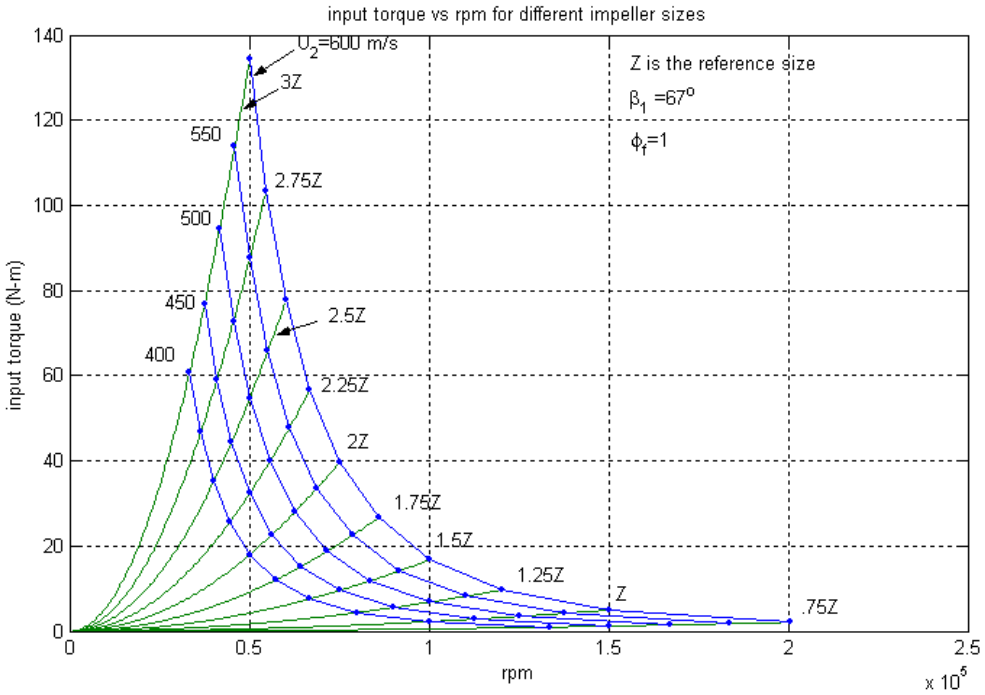

Figure 2.8.d Input torque vs. rpm for different impeller sizes and impeller exit tangential velocities where $\beta_1 = 67^0$ and $\phi_f = 1$.

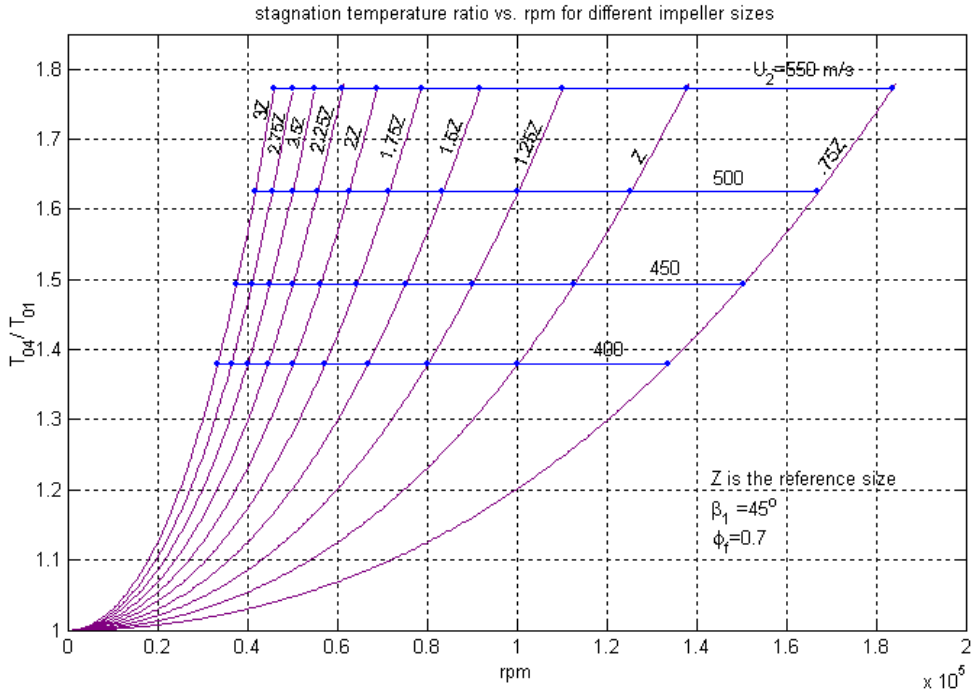

Figure 2.9.a Stagnation Temperature ratio vs. rpm for different impeller sizes and impeller exit tangential velocities where $\beta_1 = 45^0$ and $\phi_f = 0.7$.

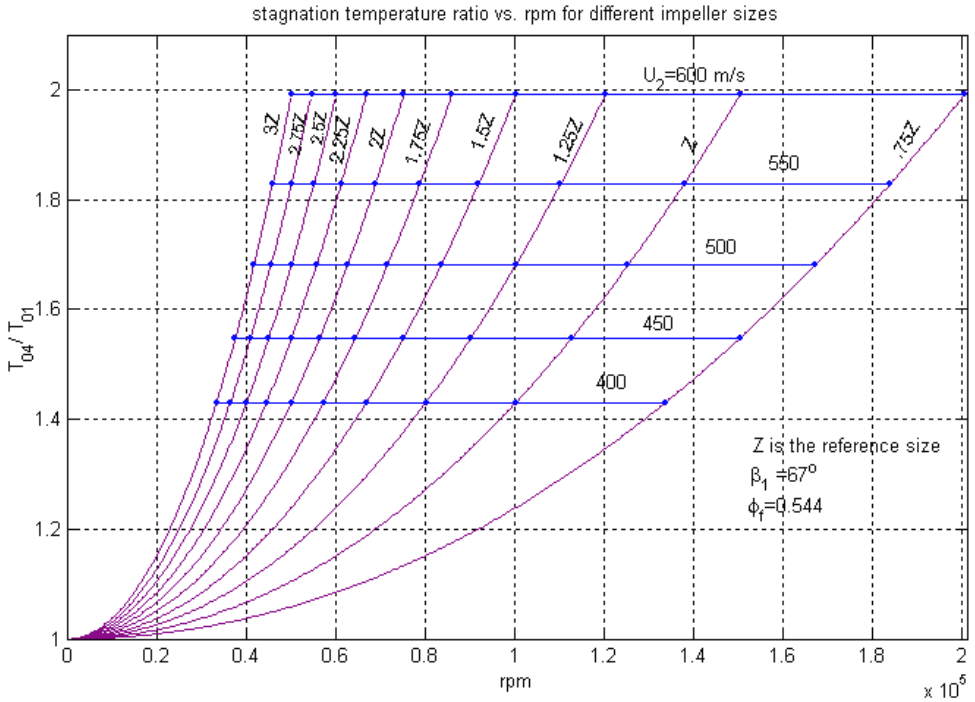

Figure 2.9.b Stagnation Temperature ratio vs. rpm for different impeller sizes and impeller exit tangential velocities where $\beta_1 = 67^0$ and $\phi_f = 0.544$.

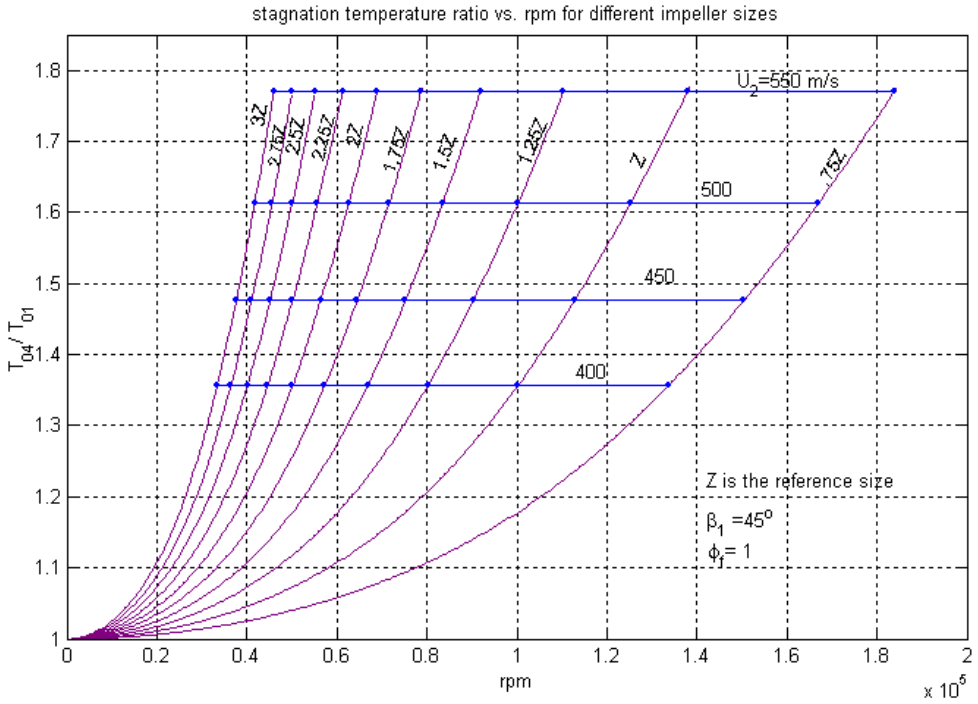

Figure 2.9.c Stagnation Temperature ratio vs. rpm for different impeller sizes and impeller exit tangential velocities where $\beta_1 = 45^0$ and $\phi_f = 1$.

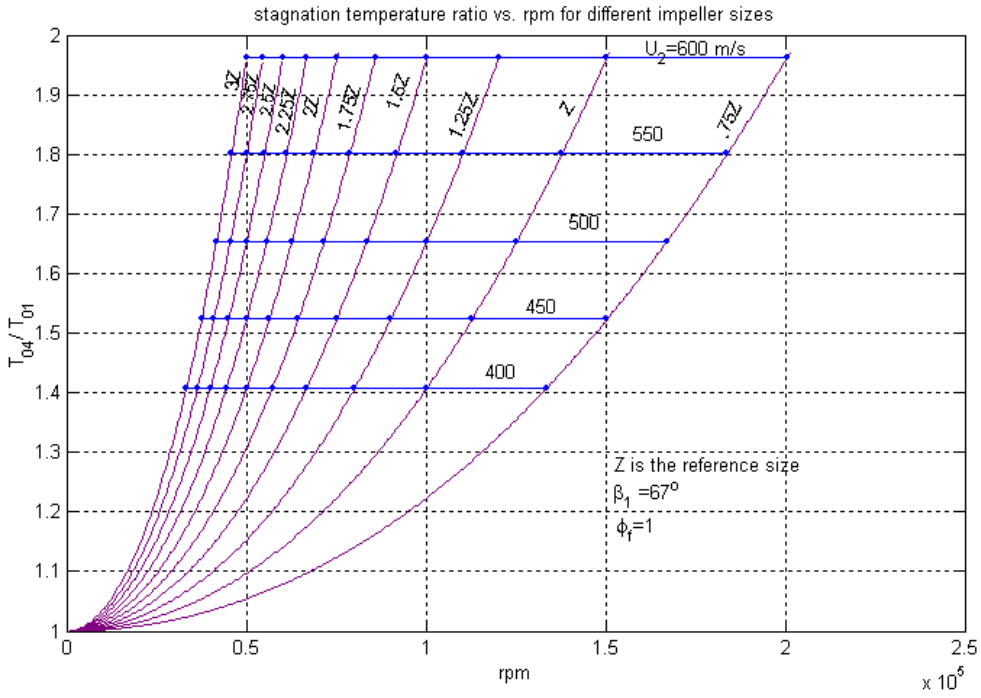

Figure 2.9.d Stagnation Temperature ratio vs. rpm for different impeller sizes and impeller exit tangential velocities where $\beta_1 = 67^0$ and $\phi_f = 1$.

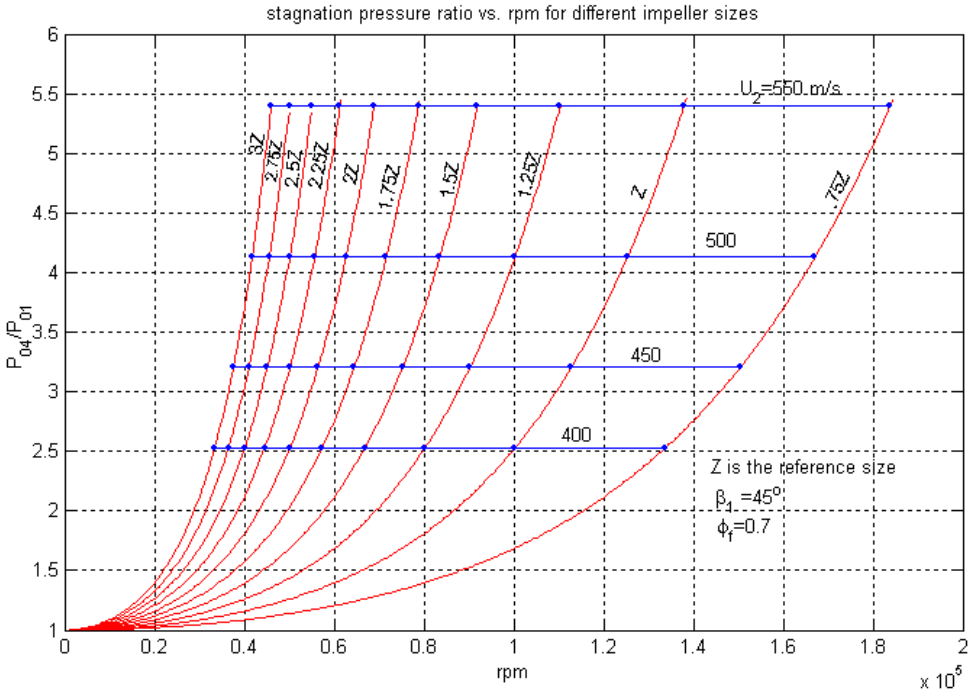

Figure 2.10.a Stagnation pressure ratio vs. rpm for different impeller sizes and impeller exit tangential velocities where $\beta_1 = 45^0$ and $\phi_f = 0.7$.

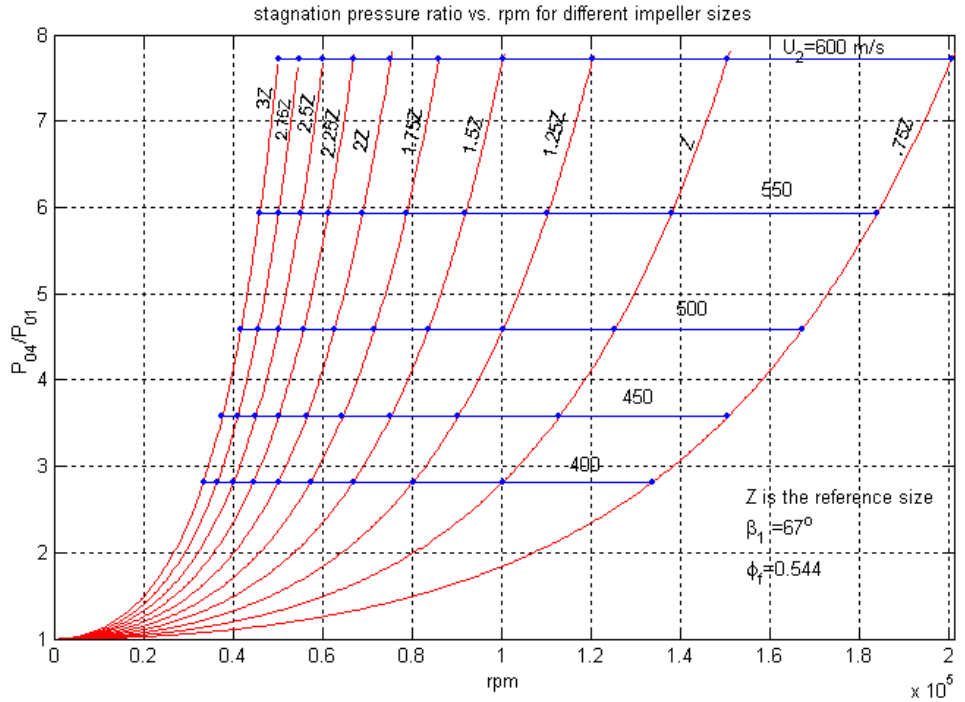

Figure 2.10.b Stagnation pressure ratio vs. rpm for different impeller sizes and impeller exit tangential velocities where $\beta_1 = 67^0$ and $\phi_f = 0.544$.

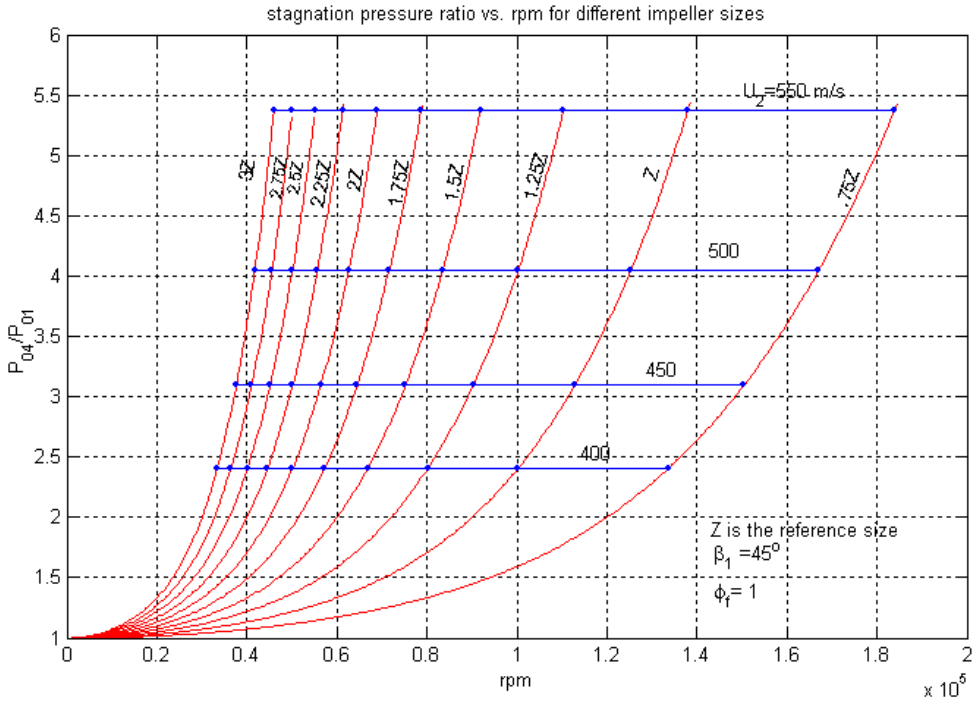

Figure 2.10.c Stagnation pressure ratio vs. rpm for different impeller sizes and impeller exit tangential velocities where $\beta_1 = 45^0$ and $\phi_f = 1$

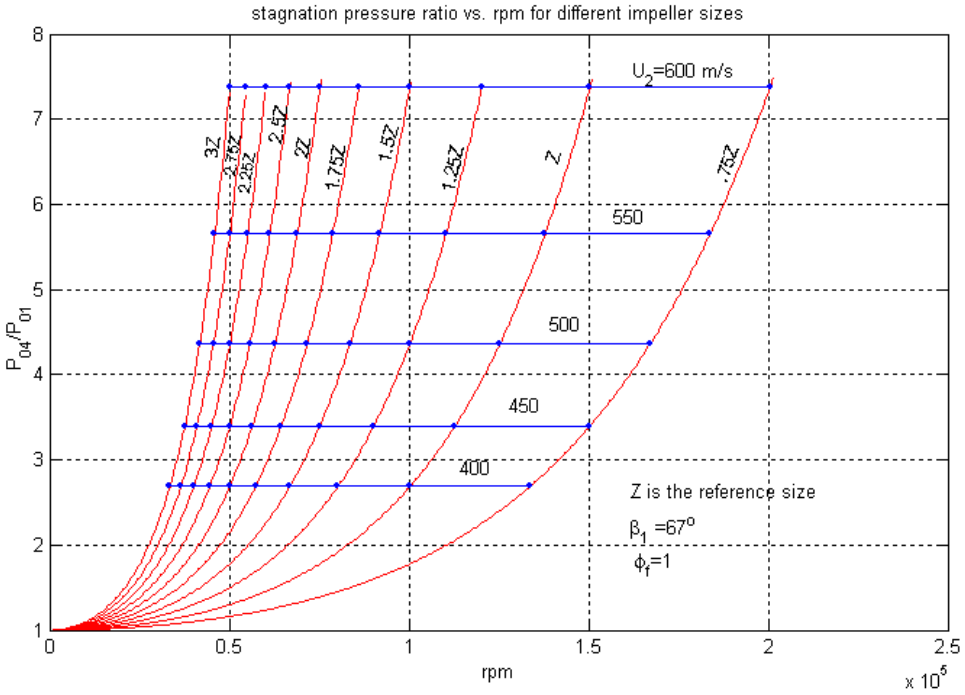

Figure 2.10.d Stagnation pressure ratio vs. rpm for different impeller sizes and impeller exit tangential velocities where $\beta_1 = 67^0$ and $\phi_f = 1$.

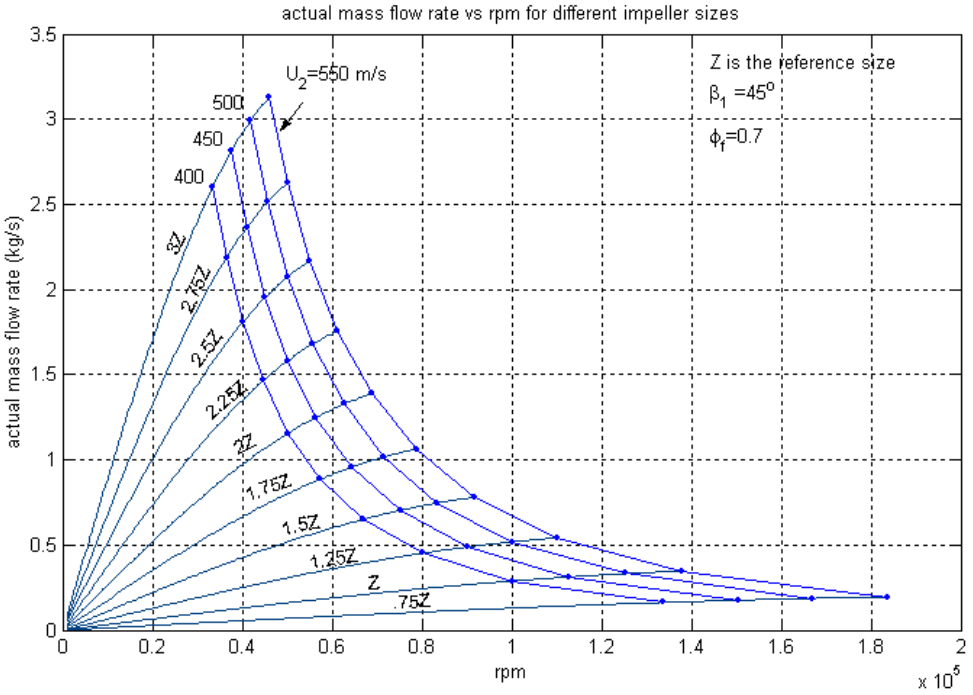

Figure 2.11.a Actual mass flow rate vs. rpm for different impeller sizes and impeller exit tangential velocities where $\beta_1 = 45^0$ and $\phi_f = 0.7$.

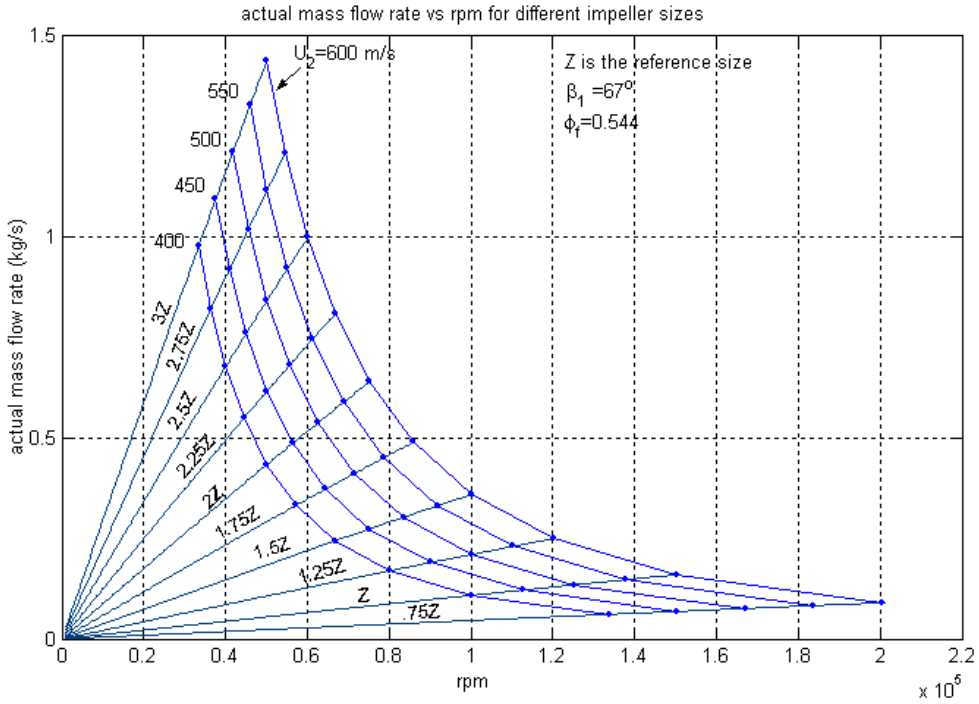

Figure 2.11.b Actual mass flow rate vs. rpm for different impeller sizes and impeller exit tangential velocities where $\beta_1 = 67^0$ and $\phi_f = 0.544$.

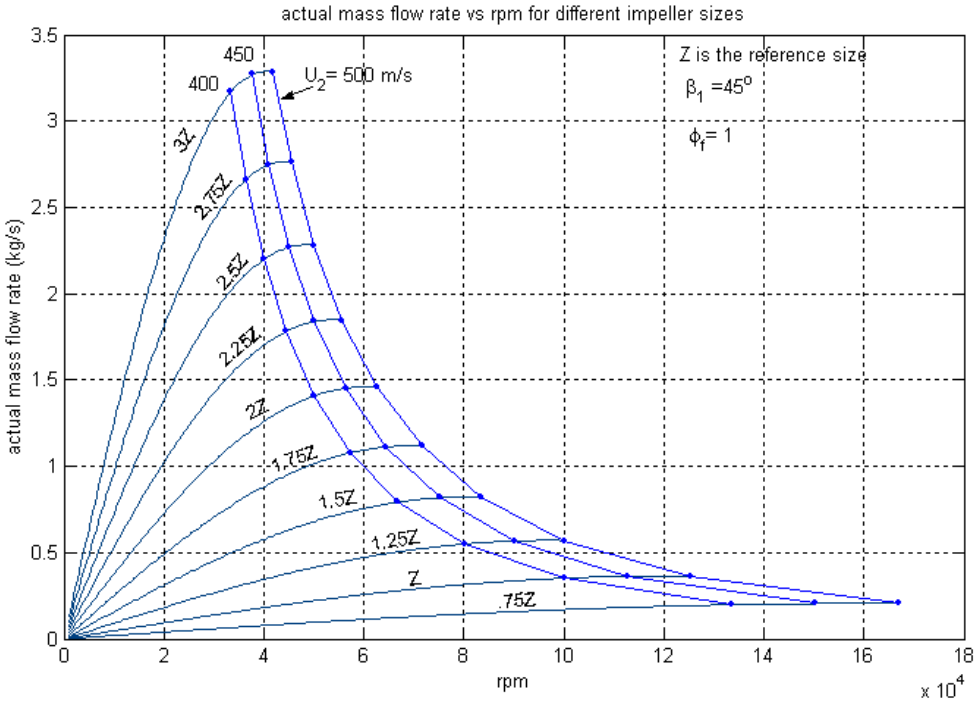

Figure 2.11.c Actual mass flow rate vs. rpm for different impeller sizes and impeller exit tangential velocities where $\beta_1 = 45^0$ and $\phi_f = 1$

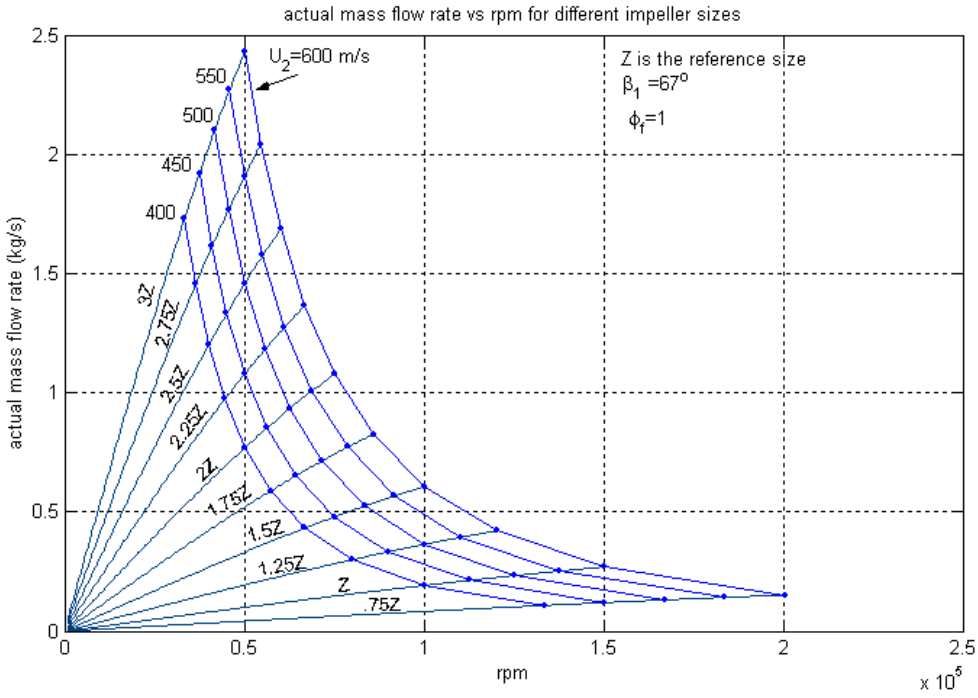

Figure 2.11.d Actual mass flow rate vs. rpm for different impeller sizes and impeller exit tangential velocities where $\beta_1 = 67^0$ and $\phi_f = 1$.

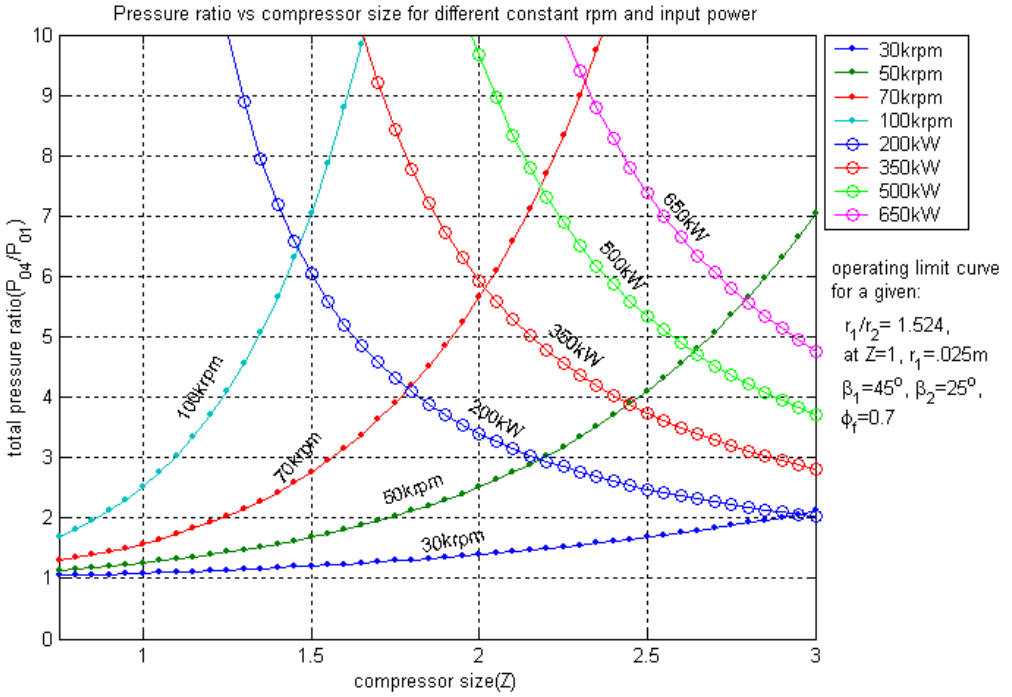

Figure 2.12.a Pressure ratio versus compressor size for different rotational speed and input power where $\beta_1 = 45^0$ and $\phi_f = 0.7$.

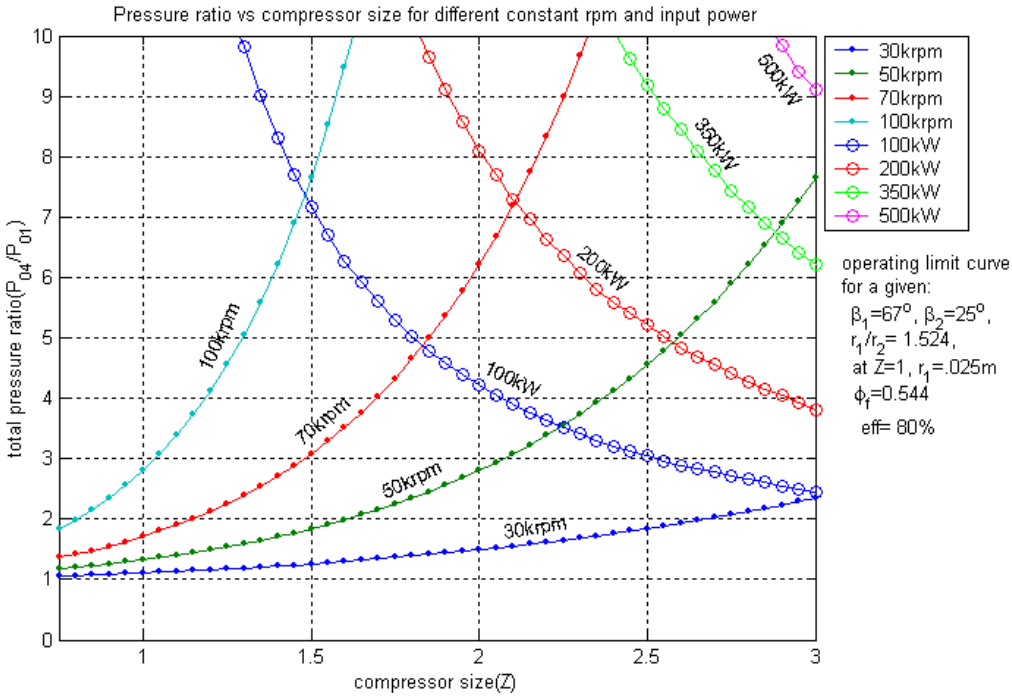

Figure 2.12.b Pressure ratio versus compressor size for different rotational speed and input power where $\beta_1 = 67^0$ and $\phi_f = 0.544$.

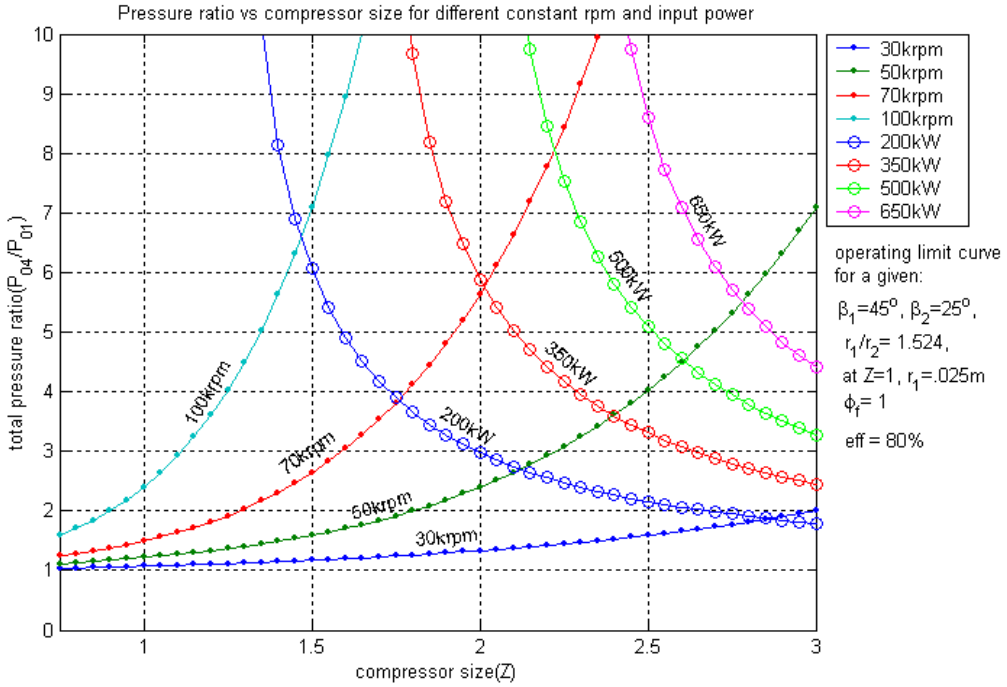

Figure 2.12.c Pressure ratio versus compressor size for different rotational speed and input power where $\beta_1 = 45^0$ and $\phi_f = 1$.

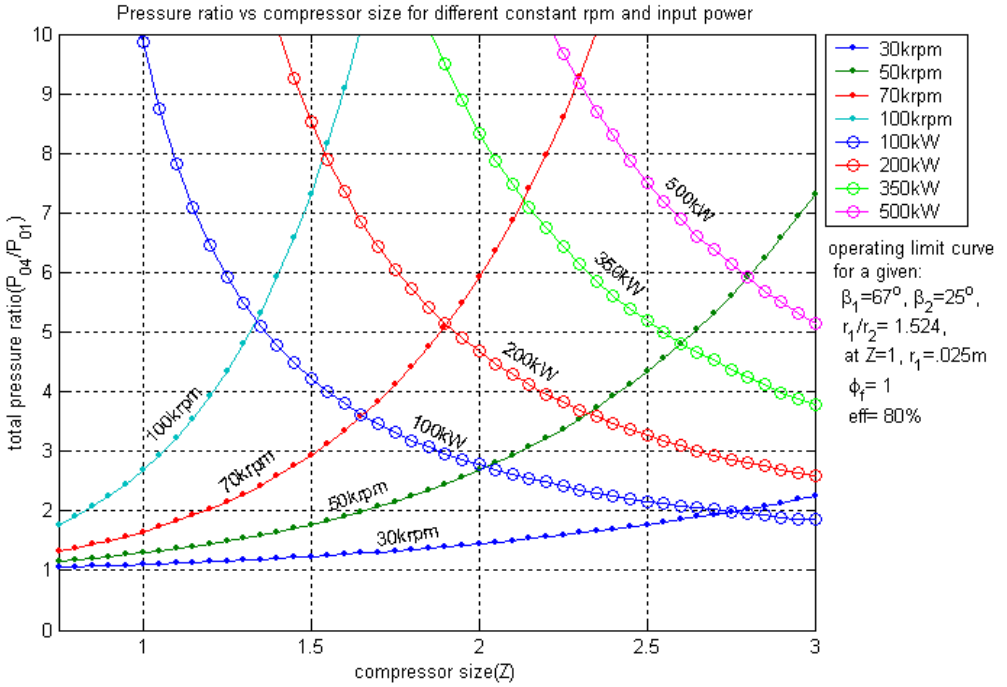

Figure 2.12.d Pressure ratio versus compressor size for different rotational speed and input power where $\beta_1 = 67^0$ and $\phi_f = 1$.

2.4 RESULTS AND DISCUSSION

To validate the codes, their outputs are needed to be compared with some other experimental results, as well as other similar codes. But in open literature, the experimental results usually investigate the total pressure ratio vs. mass flow rate with different rotational speeds. This represents only one output of the codes. Similar situation is for the commercial codes. This will increase the importance of this code but further research is needed to validate the code completely. This can be done in the next step during the experimental testing. Also, one thing that will increase the difficulties in codes validation is deficiency in the information given about the impeller configuration in many experimental investigations. The first code was validated with Krain et al. (1995). The output of the first code gives very good results for the pressure ratio and mass flow rate, as well as choke limit, see figure 2.13.b and table 2.1. The code does not have the capability to predict the surge limit correctly which is the usual case for many others commercially codes. The errors for the pressure ratio for most of points are less than 10%.

Each compressor has a limited range of operation due to the choke and surge phenomena. One of the main requirements of the centrifugal compressors deign is to know the mass flow limits. From this the importance to find a program that can estimate the operation range is increased and this what is done in the first code. The plots of the input power, input torque, stagnation temperature and pressure ratios vs. mass flow rate

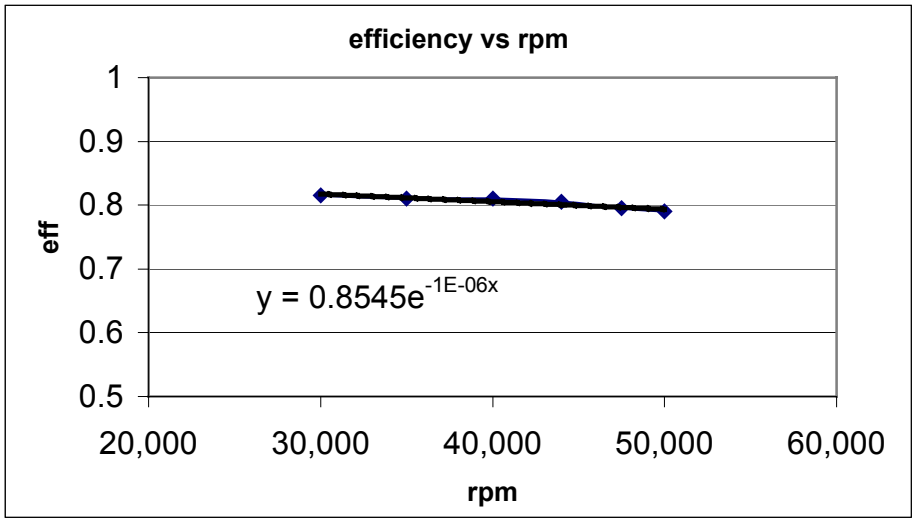

Figure 2.13.a Efficiency modeling validation, Comparison with Krain et al. (1995).

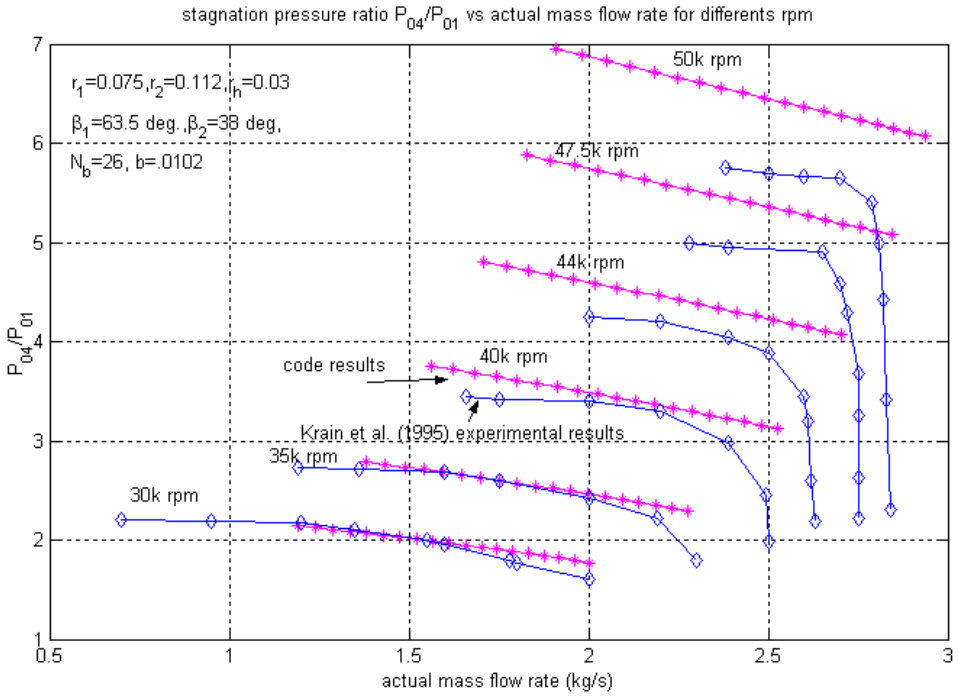

Figure 2. 13.b Total pressure ratio vs. flow rate for different rotational speeds, first code output compared with Krain et al. (1995).

Table 2.1 Impeller characteristics of Krain et al. (1995).

Impeller characteristics	**Value**
Inlet impeller raduis r_1 (m)	0.078
Hup impeller raduis r_h (m)	.03
Exit impeller raduis r_2 (m)	.112
Impeller width (m)	.0102
Impeller inlet angle (deg)	63.5
Impeller exit angle (deg)	38
Number of the impeller blades	26

for different rpms, impeller sizes and inlet angles were obtained from the first code, see figures 2.3-2.6. The results of these figures are valuable. For example, if it is needed a compressor that can accommodate the mass flow rate from 0.23-0.27 kg/s with stagnation pressure ratio around 1.5, it is recommended to choose an impeller reference size equal to one, and impeller inlet angle equals 45^{o}, as well as to operate the compressor with 70,000 rpm, see figure 2.3-2.6. In this case, the compressor needs an approximate input power of 14 kW and 1.8 N-m torque. Also, it is expected to have 1.17 stagnation temperature ratio. These information help to choose the proper instrumentations to measure the compressor perfomance. For instance, to measure the total pressure at the exit a probe that can cover the range of 1.3-1.6 of the inlet total pressure is required, see figure 2.6.

In the compressor test rig design process, it is needed to see the effect of changing the size of the compressor on the input power and torque requirement, as well as the expected mass flow rate and total temperature and pressure ratios. These can be achieved from the plots in figures 2.7-2.11, which were obtained from the second code.

Compressor driver map is important to predict the needed input power and rotational speed from the driver. This map, which helps to choose the proper driver unit, can be obtained from the third code as shown in figures 2.12.

In conclusion, the present codes are valid for purpose of setting the test facility requirement. This includes power and rpm requirement for driving compressor impeller, as well as different instrumentation operating range, such as rpm, temperature, flow rate, etc.

CHAPTER 3

DRIVER UNIT SELECTION

3.1 INTRODUCTION

This chapter will discuss the selection of the compressor driver based on criterion set by the objective of this work. The type of the driver unit used to drive a compressor is very important due to many reasons. For instance, the driver has to be flexible to test different types of compressors with good control system on the rotational speed, especially near the surge line. In general, the driver has to be:

a) Flexible (can accumulates several sizes of compressor),

b) Reliable,

c) Excellent control on the rpm and torque,

d) Safe,

e) Easy to use,

f) Environment friendly,

g) Economical.

3.2 COMPARISON BETWEEN THE ELECTRIC MOTOR, THE COMBUSTION GAS TURBINE AND THE BLOW DOWN FACILITY WITH A TURBOCHARGER

Based on literature survey, there are three major types of drivers: electrical motor, gas turbine and blow-down facility with a turbocharger. Each one of them has its advantages and disadvantages, such as cost, size, and power requirement. To reach to the proper operation of the compressor some considerations must be taken into account. The main considerations are (Chevron Co. 1988):

- Starting or breakaway torque,
- Speed-torque characteristics,
- Torsional and lateral of the critical speed and vibration,
- Coupling,
- Weight,
- Control,
- Gearbox if needed to harmonize speeds,
- Space,
- Energy costs,
- Energy source reliability and
- Supporting systems, i.e. cooling, filtration, etc.

The first four considerations have no direct effect on the results of the test since they are depended on the design of the driver.

In most practical use, such as gas plants and refinery, compressors are driven more by electrical motors than all the other driver types combined where the motors have many advantages and limited disadvantages, Saudi Armco (2001). The reasons behind that are the possibilities of providing economically the electrical power, as well as, the proper electrical distribution systems for the plants. In addition to that, the motor can be operated in a safe manner for different industrial environments. Furthermore, torque and rotational speed can be well controlled. In general, the electrical motors:

- Run for long time without considerable mechanical or performance weakening,
- Require low maintenance costs,
- Have quicker startup and slightly higher equipment reliability comparing to the other drivers and
- Uncomplicated operation and controlling with minimal monitoring.

On the other hand, the main disadvantage comes from the electrical source due to the high-energy costs and their possibility of discontinuity and price unsteadiness, which does not apply locally. Previous points represent the general characteristics of the electrical motors. Each motor type has special characteristics, for example, some of them can rotate in both directions, movable, small and flexible to test different compressor sizes.

The choice of the motor type depends on the applications. One of the examples, which discuss this point, was done by Clarkson et al. (1998). In case of a motor driver for

a high-speed centrifugal compressor, where the speed can be over 30,000rpm, usually a gearbox is used since majority of motors in the market cannot reach a very high speed especially in the case of high power requirements (>250 hp). Recently, considerable efforts are made to overcome this problem for the case of the low power. For example, Soong et al (2000) discussed the design, construction, and testing of an electrical motor that can be used to derive a small centrifugal compressor which has an output of 28 hp at 50,000 rpm. Also, there are research efforts to overcome high rotational speed problems produce for large power units. For example, Kim et al., (2001), tested a centrifugal compressor for high power and rotational speed, which is driven by an electrical motor, see figure 3.1. The main components of this test facility are motor (300 hp & 2688 r/min), gearbox (speed transmission ratio 14.5), compressor, inlet and discharge pipe, throttling valves and settling chamber and filter. The test was done for two different inlet geometries where the performance range was from choke to mild surge for each one. This shows the flexibility of this type of driver. Also, Yun and Smith, (1996) investigated the application of a novel, electric motor-driven, variable speed centrifugal compressor for automotive A/C with design rotational speed 75,000 rpm and the maximum cooling capacity 5,275 Watts.

As a drive unit for centrifugal compressors, gas turbines have many drawbacks compared to electric motors. In general, the efficiency of the gas turbine is low, except at its design operation point. Normally, the gas turbine is affected by the change in the ambient temperature, operation at partial loads, filtration of inlet air and blade fouling of the compressor, Saxena (2000). It is also difficult to control the turbine especially if it is

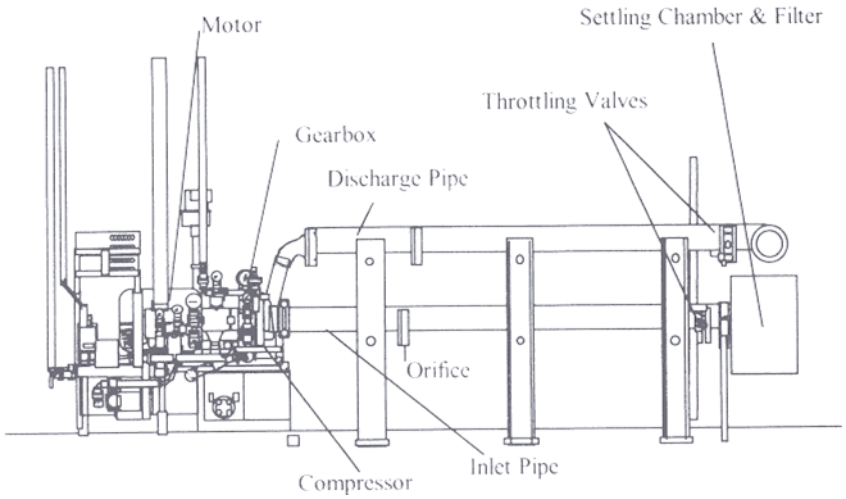

Figure 3.1 A test facility of a centrifugal compressor driven by a motor (Kim, Y. et al., 2001).

operated away from the design speed and this will affect the turbine efficiency. Actually, the control unit of the turbine engine alone needs speed, temperature, flame detection and vibration inputs. These inputs are important to control the turbine engine during startup and shutdown, steady state operation and for the turbine protection, Boyce (2002). Moreover, gas turbines require a number of auxiliaries, such as, the electrical starter, the main oil pump and the fuel pump. All of these auxiliaries require control. These supplementary devices increase the maintenance difficulty and price, as will as, difficulty in controlling. The flexibility to test many different sizes of compressors is also reduced due to performance characteristics of gas turbines. In addition, special type of fuel and filtration need to be used to decrease the gas turbine pollution to the air. Because of the combustion process that may result in pollution and or explosion, the combustion gas turbines are considered to be unsafe machine. Sometimes the available turbine needs some development before it can be used to derive the centrifugal compressor for the purpose of testing; see Turner et al, (2000) as an example. In their case, the turbine engine has a two-stage centrifugal compressor. This engine was used to drive a two-stage centrifugal compressor, which was coupled directly with the engine as shown in figure 3.2. The engine has a power of over 1790 kW at a rotational speed equal to 15,000 rpm. The compressor has 3.3:1 pressure ratio and supplied 10.5 kg/s of air. Any change in compressor size and characteristics may require some modifications, such as, a special gearbox. This means that this type of drive is not flexible to test many different compressors configurations.

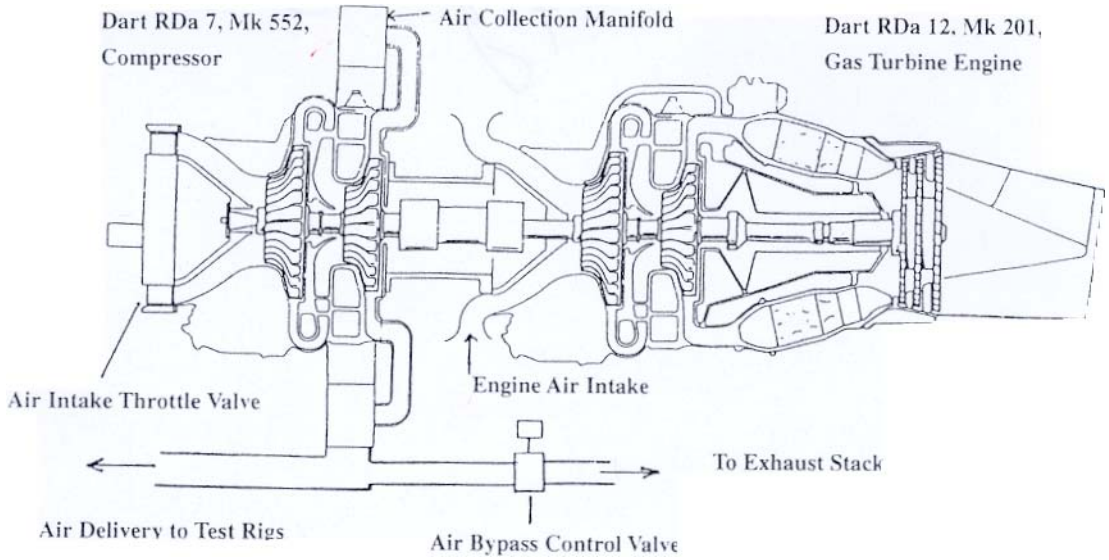

Figure 3.2 A test facility of a centrifugal compressor driven by a combustion gas turbine
(Turner, A. B. et al., 2000).

The third possible driver is the cold air turbine, such as in turbochargers. Blow-down facility is usually required to provide compressed air to the turbocharger to rotate the radial turbine that is coupled directly with the centrifugal compressor through a common shaft. This type of experiment is not expensive especially if the blow-down facility is available. However, it needs some auxiliaries for the purpose of control, which leads to larger size and more complexity in construction and maintenance compared to the electric motor. The facility is considered to be safe, has no negative effect on the environment but its drawback is the limited flexibility for the purpose of testing different sizes of compressors. Capece (1982) and Fink (1984) worked on the development of a turbocharger test rig to investigate the centrifugal compressor stall and surge. Fink (1988), also, used the same facility later to investigate the surge dynamics and unsteady flow phenomena for the centrifugal compressor, see figure 3.3. Air ejector was used for driving the turbocharger turbine. Supporting systems, such as, cooling and filtrations systems were used for the bearing lubrication.

The main objective of this study is to develop a test facility that can be used to test different compressor sizes with a good controlling system. Table 3.1 compares the characteristics of the three driver units discussed. From this table the selection of the electrical motor as a driver unit is the best choice. The main reasons of that are the simplicity of control and flexibility to test different compressor sizes. In addition, it is easier to maintain and the overall system is smaller compared to the other two drive systems.

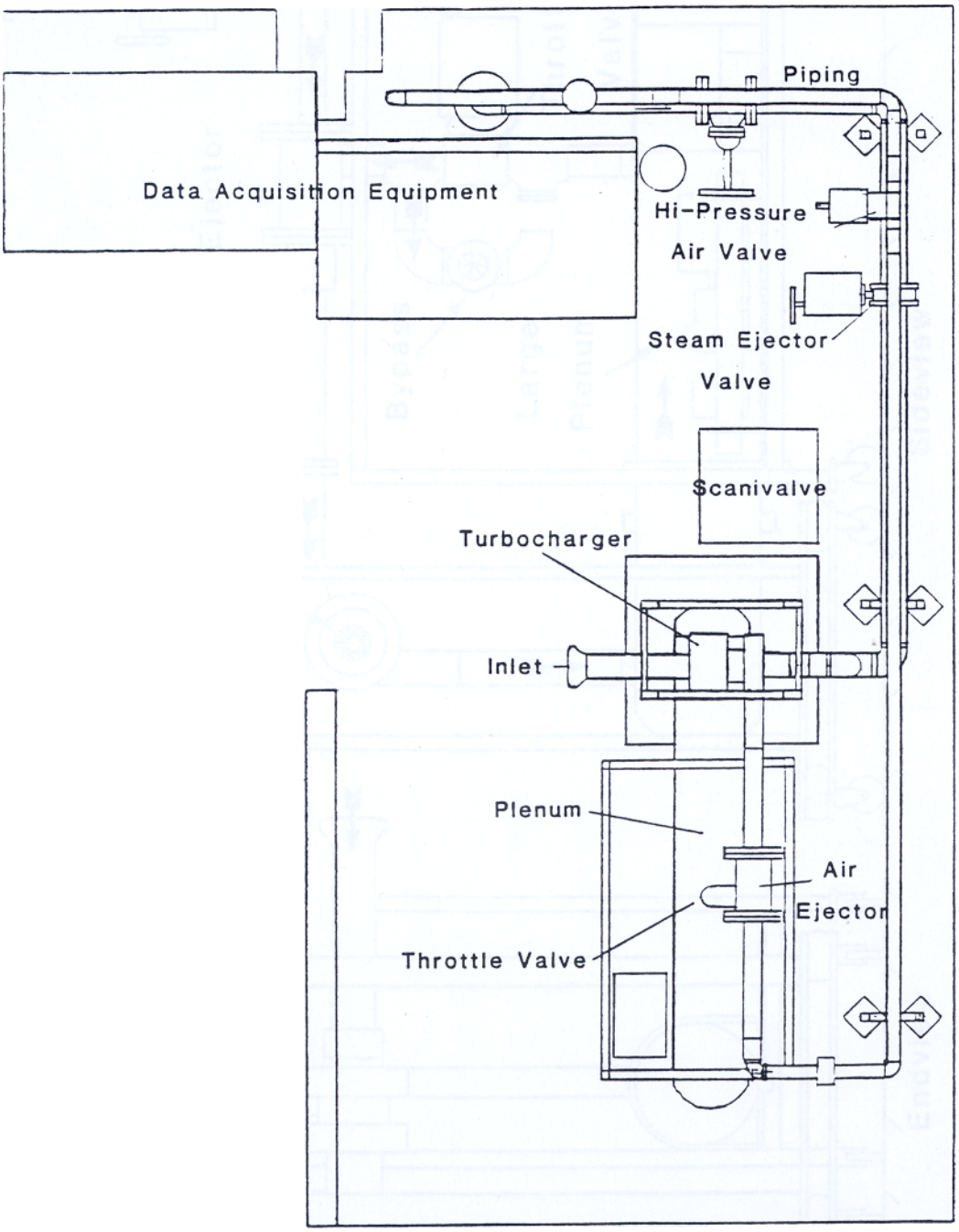

Figure 3.3 A test facility of a centrifugal compressor driven by turbocharger (Fink, D. A., 1988).

Table 3.1 Characteristics of the electric motor, gas turbine and bow down facility with a turbocharger as driver units.

Drive / Characteristics	Motor (without a vacuum system)	Motor (with a vacuum system)	Gas Turbine	Blow Down Facility (with turbocharger)
Cost	Expensive	Expensive	V. Expensive	Medium
Size	Medium	Medium	Medium	Large
Specification of location requirement	Isolated base	-Larger space -Isolated space	Extra ventilation	Extra blow down facility
Movement of the test section	Difficult	V. difficult	Possible	Possible
Power requirement	High electrical supply	Relatively low electrical supply compared to electrical motor	Fuel	Compressed air
Technology:	Gearbox Possible to get	Advanced sealing system, possible to get	Too high	Possible to get
Control (rpm, power)	Excellent	Excellent (rpm) Difficult (flow conditions)	Difficult especially at the surge line of the compressor	Difficult especially at the surge line
Maintenance	Easy	Difficult	Difficult	Medium
Environmental issue	Excellent	Excellent	Poor	Excellent
Bi-directional	OK	OK	Need special gearbox	OK
Safety	High	High	Low	High
Flexibility of testing different compressors sizes	V. good	Excellent	Not flexible	Low flexibility

3.3 COMPARISON BETWEEN TWO ELECTRICAL MOTORS, WITH AND WITHOUT VACUUM SYSTEM

There are two methods commonly used to satisfy dynamic similarity when testing centrifugal compressor driven by electric motors. First method includes a vacuum environment system and the second one is without vacuum. By using the vacuum system almost all practical conditions can be tested and this is done mainly by simulating the pressure to match the Reynolds number while maintaining low rpm. However, this type of driving system is relatively complex. It requires an advanced sealing system; a closed loop that needs a heat exchanger to cool the output air from the compressor; and flow straightener and equalizer to improve the flow quality at the compressor inlet, Shirley (1998), see figure 3.4. Also, the test section of the vacuumed type is more difficult to move, maintain, control (inlet conditions) and has larger size compared to non-vacuum one. However, it has lower power requirement for the motor due to low rpm and vacuum. On the other hand, driving the impeller without the vacuum system is relatively simple compared to the vacuum assisted system. It does not need a closed loop or advanced sealing system but requires higher power and rpm drive unit, which might require a gearbox in some cases, see figure 3.1. Table 3.1 shows the characteristics of the two type of electrical system. **In conclusion, the non-vacuumed type is the most suitable to meet the objectives of the present design.**

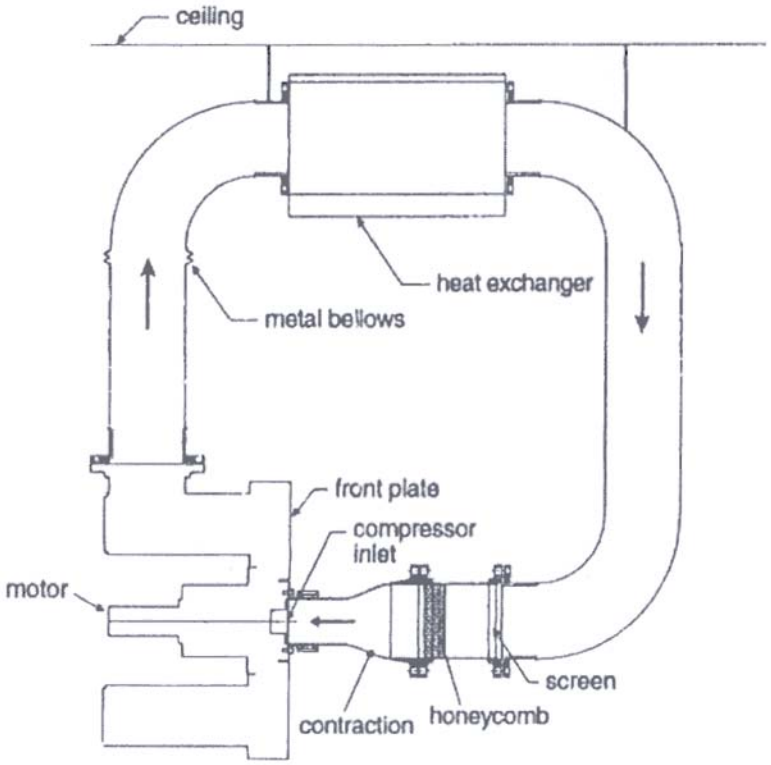

Figure 3.4 A simplified sketch of a centrifugal compressor test facility driven by an electric motor with vacuum system
Shirley, G. (1998).

3.4 COUPLING CONFIGURATION FOR THE COMPRESSOR TEST FACILITY

There are two coupling configurations to drive the compressor. One configuration is driving the compressor from its inlet and the other from the diffuser side. The general layouts of these options are shown in figures 3.5. a & b. In these figures, two possible methods of coupling location are shown. The easier way to test the compressor is to drive it from the diffuser side. However, when the diffuser is a radial-axial type, it is recommended to drive the impeller from the inlet which imposes technical difficulty. The reason behind that is due to flow restriction by the coupling.

The main effect of coupling configuration is the instrumentation set up for mass flow measurement and controlling inlet flow condition. Front coupling is expected to pose some challenges in this regard. However, other set up and measuring devices are expected not to be effected by coupling configuration.

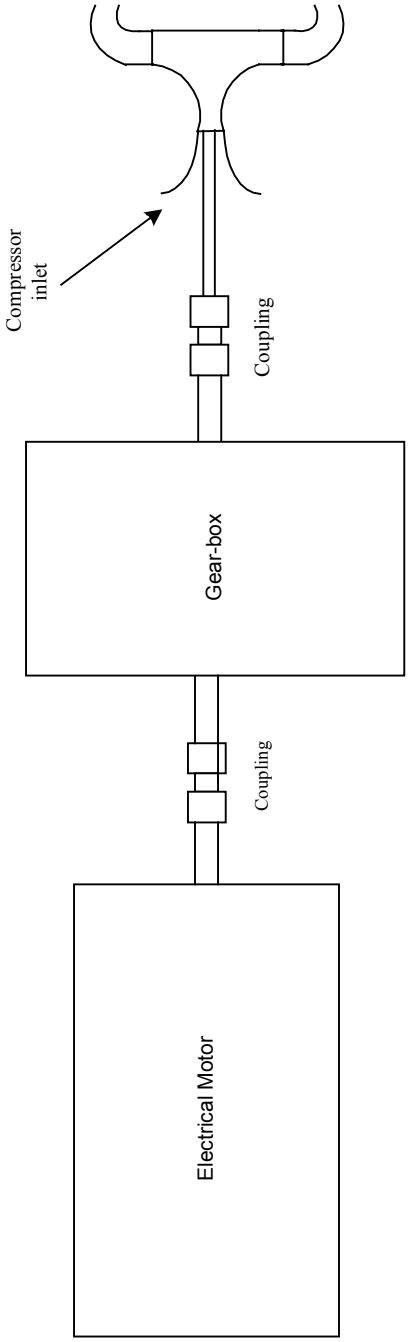

Figure 3.5. a. General facility layout of the centrifugal compressor where the driver is from the compressor inlet.

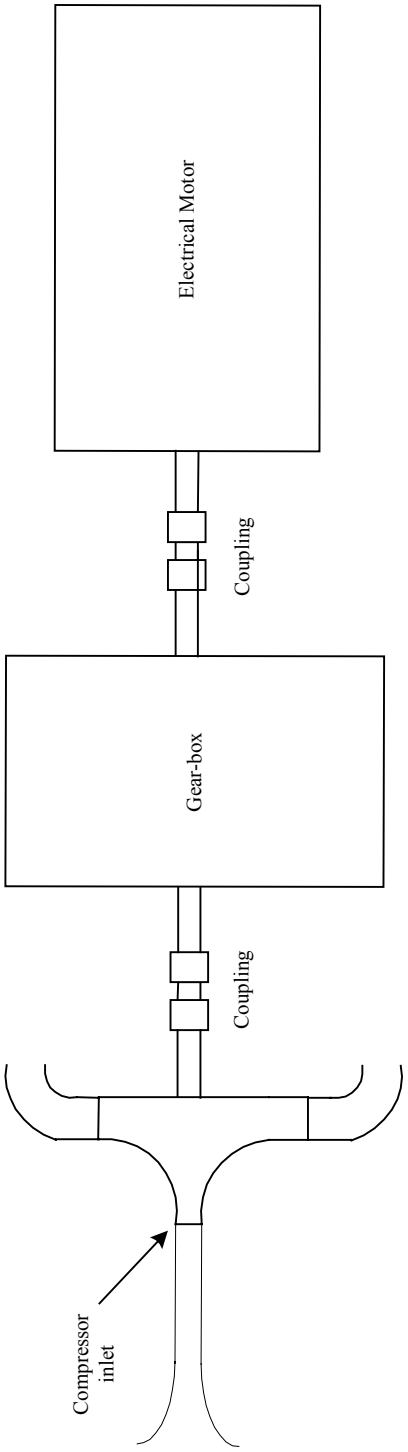

Figure 3.5. b. General facility layout of the centrifugal compressor where the driver is from diffuser side.

CHAPTER 4

MEASUREMENTS AND INSTRUMENTATION

4.1 INTRODUCTION

The aim of designing high performance compressors is to get high-pressure ratio with high efficiency and large flow rate. The performance map of a compressor is the plot of the pressure ratio and efficiency versus mass flow rate for different rotational speeds. The first three parameters cannot be measured directly and need combination of instrumentations, while the rotational speed can be measured directly. These parameters are function of several variables, such as compressor geometry and operating conditions. In actual case, the geometry for a tested compressor and piping arrangement, inlet and exit, remain constant during test.

The four parameters that represent the compressor map are:

- Rotational speed: usually it is measured directly in revolution per minutes, *rpm*, and so no specific data reduction equation for it.
- Mass flow rate: its unit is in kilogram per second, $\dot{m}$. It can be measured by several techniques, such as the venturi and orifice meters.

$$\dot{m} = f(T_f, P_f, \Delta P). \quad (4.1)$$

where T_f is the static temperature, P_f is static pressure and ΔP is the static differential pressure. The subscript *f* refers to the condition at the flow meter.

- Pressure ratio: it is a dimensionless quantity, *Pr*. Usually; it is the measured total pressure at the compressor exit divided by the total pressure at the compressor inlet. In this case,

$$Pr \text{ or } Pr_{tt} = f(P_{04}, P_{01}). \quad (4.2)$$

Where the subscript tt refers to total conditions and 01 and 04 refer to the inlet and exit of the compressor, respectively.

- Isentropic efficiency: dimensionless quantity, η_s. It is equal to the isentropic work divided by the actual work. In the experiment the efficiency of the compressor is a function of several measured variables. In the case where the restriction flow passage meter (pressure differential meter) at the exit or away from the inlet:

$$\eta_s = f_\eta(P_f, T_f, \Delta P, T_{01}, P_{01}, P_{04}, \tau, rpm). \quad (4.3.a)$$

Here the subscript f indicates the value at flow meter. If the flow meter is at the inlet opening:

$$\eta_s = f_\eta(P_I, T_I, \Delta P, T_{01}, P_{01}, P_{04}, \tau, rpm). \quad (4.3.b)$$

Each one of these four parameters is analyzed keeping into consideration American Society of Mechanical Engineering, Perfomance Test Code 10 (ASME PTC 10) regulations. The analysis will help in choosing which instrumentation techniques are suitable to test the compressor performance.

4.2 THE FOUR PARAMETERS THAT DETERMINE THE PERFOMANCE MAP OF THE CENTRIFUGAL COMPRESSOR

4.2.1 Rotational Speed

Regarding the rotational speed of the compressor shaft, it can be measured directly through an electric transducer. For example, an inductive system may be used, which provides electrical signals of 60 equally spaced slots on the rotor shaft, such as in the case of Krain and Hoffmann (1998). A gearbox was used to increase the speed, so the rotational speed of the motor must be multiplied by the gear ratio to get the actual rotational speed of the impeller. Also, the rotational speed was controlled by a computer to insure the reliability of the measurement. Shirley (1998) installed a probe in the side of the motor-mount that functioned as steel setscrew in the coupling passes over the sensing head of the probe; an electrical signal is generated once per shaft revolution. ASME PTC 10 paragraph 4.10 requires from the rotational speed instrument to have the ability to provide a continuous speed indication without restriction to specific type of instrument. For details on speed measurement see ASME PTC19.13.

In conclusion, the measurement of the impeller speed has flexibility in terms of instrumentation type for the rotational speed of the shaft and several types are available in

the market. So, its selection depends on the accuracy requirement for compressor testing, range of reading and its compatibility with controlling system of the compressor. The permissible fluctuation of speed-readings must be within $\leq \pm 0.5\%$, according to ASME PTC 10. So, it is recommended to have rpm indication with accuracy of $\leq \pm 0.25\%$ of readings.

4.2.2 Mass Flow Rate

Mass flow rate is the multiplication of the static density and flow rate. That is:

$$\dot{m} = \rho Q \,. \tag{4.4}$$

where ρ is the density and Q is the flow rate.

Here the density cannot be measured directly, so static temperature and static pressure measurements are used to calculate it. Pressure tabs and temperature probe(s) can be used to measure the static pressure and temperature. Temperature probes are discussed below under the isotropic efficiency. In most flow meter devices, the static pressure and static pressure difference are measured to calculate the flow rate, which also can be used to find the density. Several types of flow meter devices are available in the market. The choice of the metering device depends mainly on the size, accuracy, cost, pressure losses and compatibility with the fluid, Figliola and Beasley (2001), as well as the operating range. Mainly, there are two suitable kinds of flow measurement methods for compressor, either the restriction flow passage meter (pressure differential meter) or insertion volume flow meter method. The most practical devices to find the mass flow rate and widely used

in experimental testing, are the restriction flow passage meters. There are mainly three types of them: orifice plate, flow nozzle and venturi meter. Some of their characteristics are shown in figures 4.1a, b and c. Comparing the three types, the head loss of the venturi is low but it is expensive while in orifice is high but it is cheep. The flow nozzle is in between, both the cost and head loss, Figliola and Beasley (2000). Roduner et al. (1999) compared the results of mass flow measurements from three types of probes (insertion volume flow meter) with a standard orifice as the reference for comparison and they stated, "Certainly, measuring the mass flow with a standard orifice is a more suitable method". The main drawback of these probes comes from highly mass flow measurement sensitivity to the uncertainty of the flow angle. On the other hand, the venturi meter and flow nozzle are more accurate than the orifice plate, which means they are much more suitable than the three probes tested by Roduner et al. This is due to the fact that the calculated flow rate from the orifice depends on the estimated value of the smaller diameter where static pressure probe is located while in the other two types, this diameter is exact, see figure 4.1. In addition to that, the flow range, which can be handled by the venturi meters and flow nozzles, is typically 60% larger than the orifice plates with varied pressure losses, Boyce (2003), for a given diameter of a pipe. A quick approve of that comes from the study of the geometry of the three meters, see figure 4.1. The proper choice of the flow meters is important otherwise it may cause undesirable large pressure drop. For example, Whitefield et al. (1993) tested the perfomance of a turbocharger compressor and used a small nozzle to measure the low flow rates near surge but at high flow rate it generated a large drop in pressure. Due to this reason the small nozzle was replaced with a larger one. The

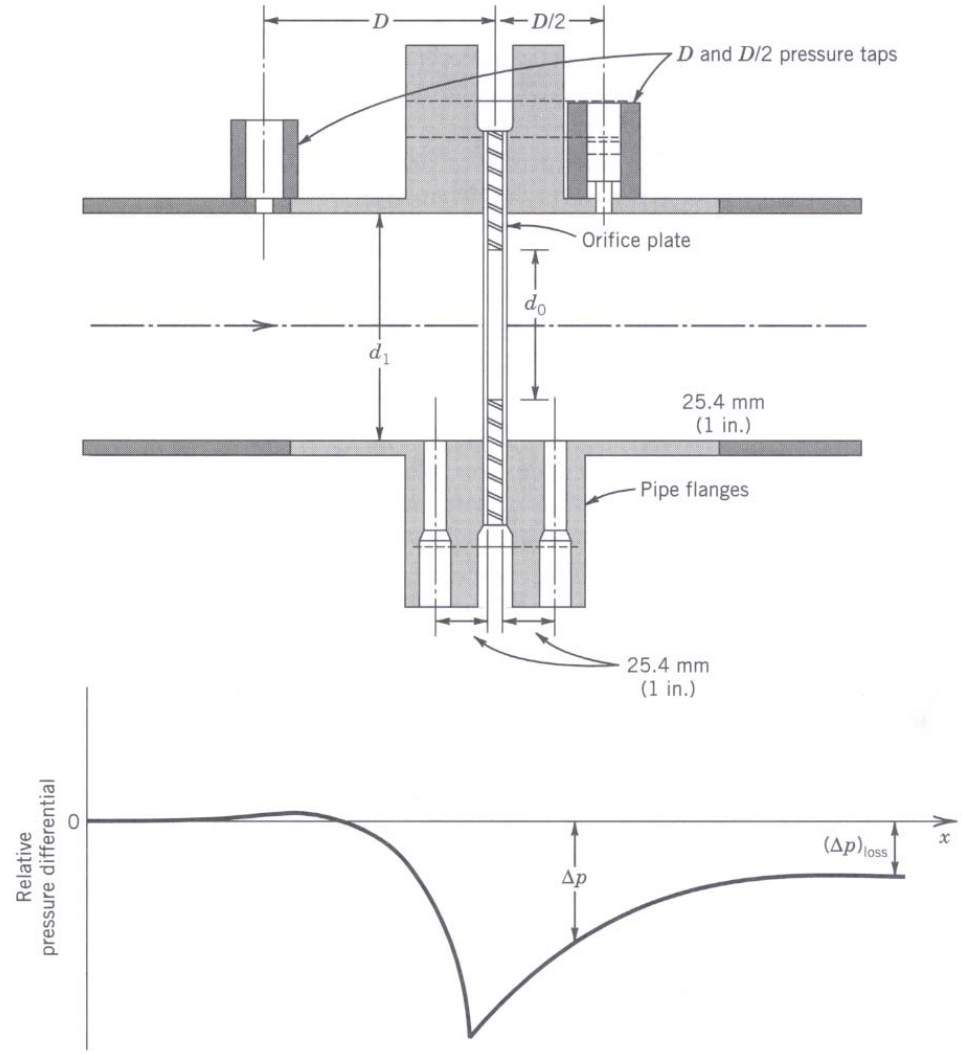

Figure 4.1.a Schematic daigram of squared-edge orifice meter with its relative pressure drop along the pipe axis
(Figliola, R. S. and Beasley, 2001).

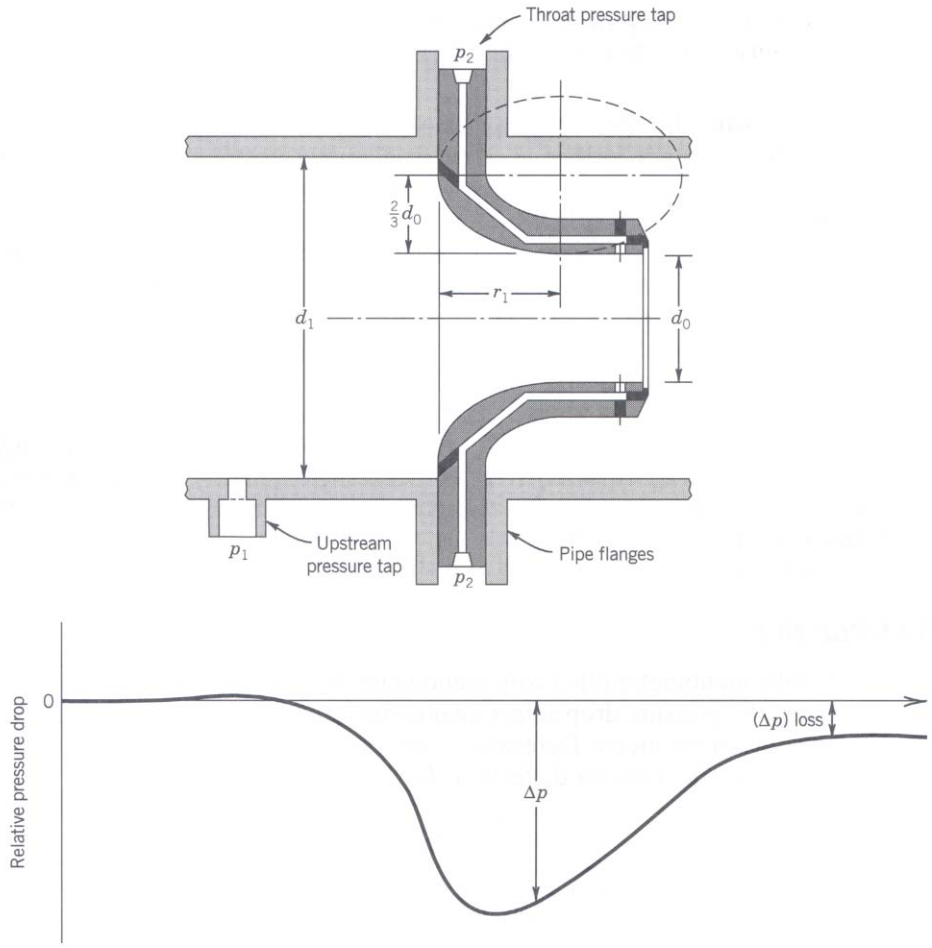

Figure 4.1.b. Flow nozzle meter
Figliola, R. S. and Beasley, D. E. (2000).

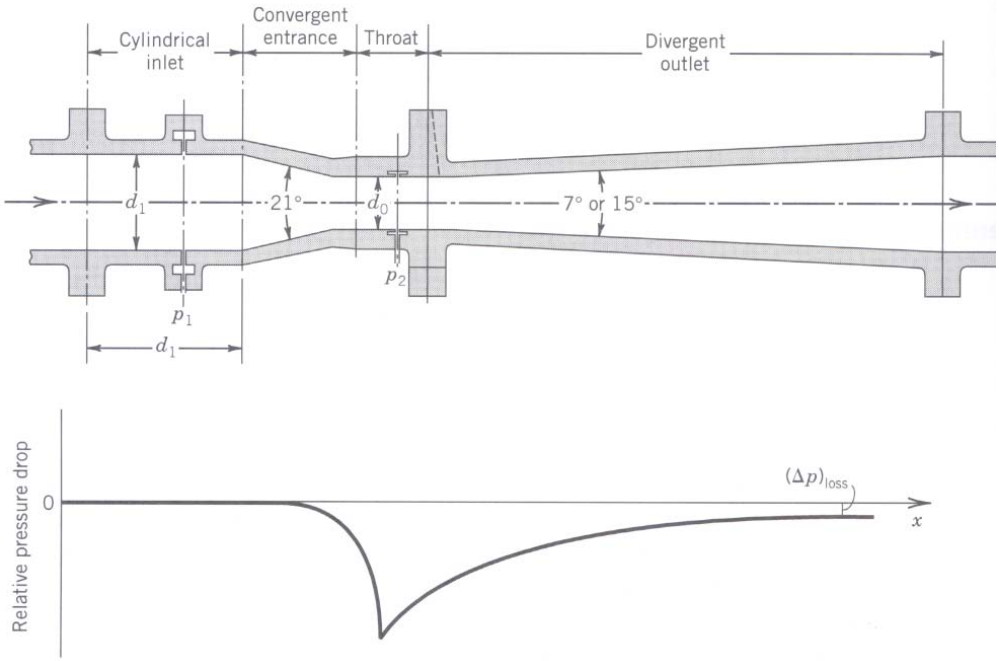

Figure 4.1.c Venturi meter and its relative pressure drop along the pipe axis (Figliola, R. S. and Beasley, 2001).

compressor test facility is shown in figure 4.2. Another example was the failure of the venturi meter at the inlet of a compressor piping, Colantuoni and Colella (1993), see figure 4.3. However, since there was an orifice at the outlet piping, the mass flow rate was measured and the mass of the leaked flow was estimated. Regarding the ASME PTC 10, paragraph 4.8, all the three mentioned types of the insertion volume flow meter are acceptable and can be installed in either the inlet or the exit piping. Each one of them has special requirements, such as the location of the flow meter device.

Piping arrangement is one of the main requirements that affect the choice of restriction flow passage meter. If the metering device has to be located close to the compressor, then the venturi meter is the best choice since its head loss is the lowest and flow disturbance is minimum. For example, Rodgers (1997) and Krain et al. (1998) used a ventruri meter to find the mass flow rate at the inlet of the compressor, see figure 4.4. Since orifice plate flow meter produces grater flow disturbance and pressure losses, it is required to be located much further from compressor (upstream or downstream), such as the arrangement used by Roduner et al. (1999), see figure 4.5.

If this method is not practical to utilize, insertion volume flow meter can be used. For example, when nozzles or orifice plates cannot be installed owing to the configurations of the piping, velocity traverse technique can be used. Care must be taken where the measured pressure must represent the average value; otherwise an estimated correction factor or calibration is needed. Also, the prediction of the right flow angle is important to reduce the uncertainty in the mass flow measurement. There are many references in literature, which discuss the flow measurement, such as, Figliola and Beasley, (2000)

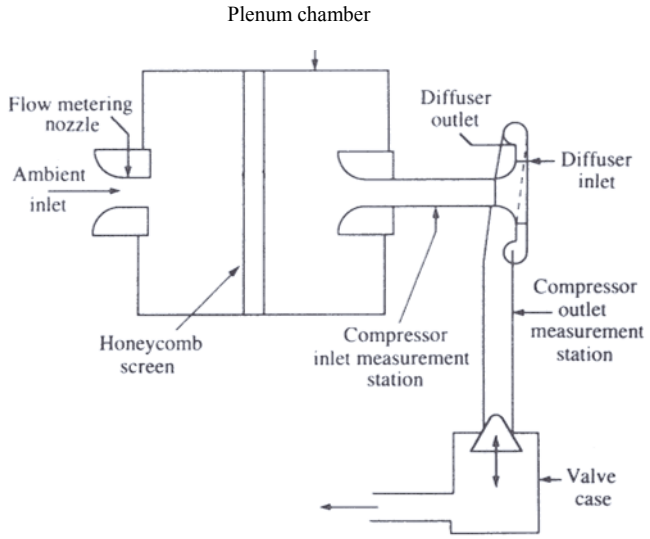

Figure 4.2 Compressor test facility
(Whitefield, A et al., 1993).

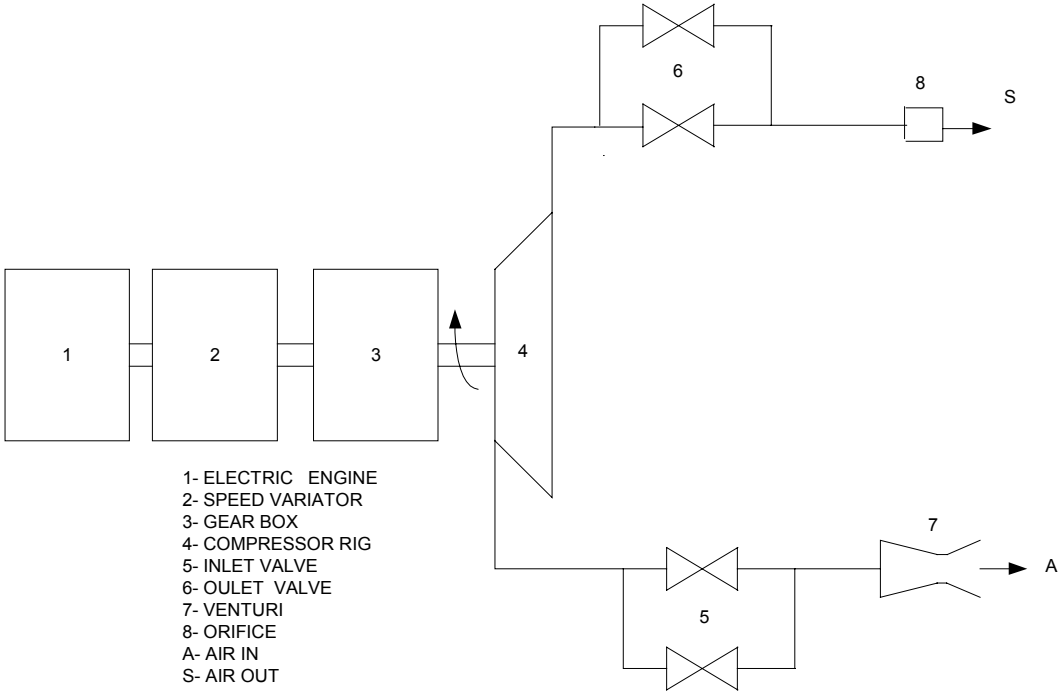

Figure 4.3 Compressor test facility that includes both orifice and venturi meter.
Colantuoni, S and Colella, A. (1993).

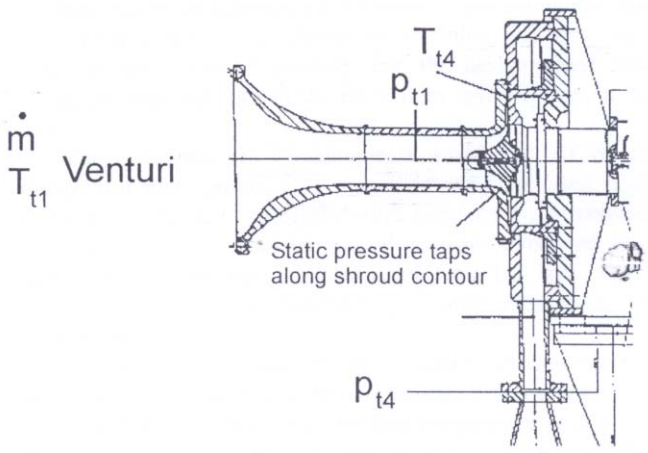

Figure 4.4 Compressor test facility that has a venturi meter at the inlet
Krain et al. (1998).

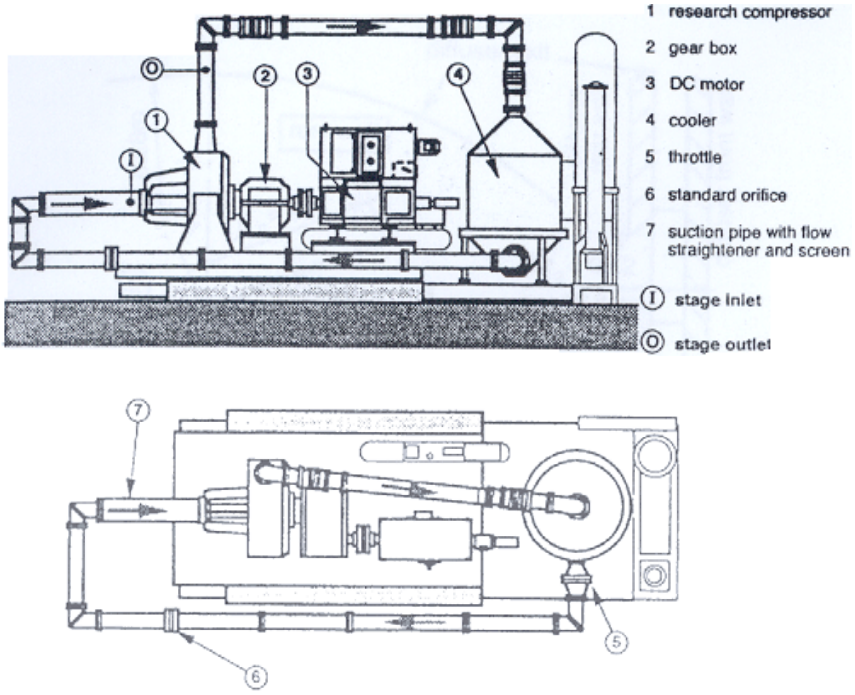

Figure 4.5 General view with centrifugal compressor test rig where the orifice is far from the compressor inlet
(Roduner, C. et al., 1999).

Ower and Pankhurst (1977) and Goldstein (1996), as well as, the ASME PTC 10 for general information on performance test code of compressor and ASME PTC19.5 for more details on flow measurement.

In conclusion, since the accuracy of the mass flow value is important, the restriction flow passage meter is more suitable than insertion volume flow meter method. To test the performance of a compressor, especially near the surge limit, there must be no disturbing element next to the compressor openings as much as possible. In case of using the restriction flow passage meter, there has to be enough pipe length to overcome their disturbance on the flow. The flow straightener is an important element that can reduce this disturbance but will not eliminate it. Also, as the flow meter can read for larger range and higher accuracy as it better. So, the orifice plate is not appropriate since it has lower range and accuracy. The proposed test facility is an open loop with an electric motor driver and in this case the piping, inlet and exit, is usually short. This means there is a need for a device, which has low-pressure loss and minimum disturbance. So, the best available choice is the **venturi meter**. According to ASME PTC10 the allowable differential pressure fluctuation for the nozzle, which can be used for the venturi, is $\leq \pm 2\%$. To comply with this requirement, the maximum allowable uncertainty of differential pressure measurement should be is $\leq \pm 1\%$.

4.2.3 Pressure Ratio

Pressure ratio of the compressor, which is used to find its performance, is the ratio of the total pressure at the compressor exit over the total pressure at compressor inlet, Pr_{tt} or Pr. Also, it is sometimes called total pressure ratio.

$$Pr = P_{04},/P_{01}. \tag{4.5}$$

Two methods can be used to find the total pressure, either direct measurement with total pressure probes or combination of static pressure measurements and flow rate.

Three types of probes are widely used in literature the pitot, the Kiel and the multi-hole probes, see figures 4.6.a and b. Figliola and Beasley (2000) explained briefly the characteristics of the first two probes. The pitot probe is capable of measuring the total pressure with high accuracy if the flow angle is aligned within $\pm 7^0$ from the probe's opening. On the other hand, Kiel probes can measure, with high accuracy, the total pressure even with flow misalignment up to $\pm 40^0$. The reason behind the higher capability of the Kiel probe to measure the pressure with high flow angle misalignment comes from the shroud around the probe. This shroud helps to straighten the flow to be parallel to probe's opening. Krain and Hoffmann (1998) used pitot probes while Rodgers (1997) used Kiel probes. Both types were used at the inlet and exit of the centrifugal compressor. A combination of stagnation pressure measuring technique may be used, for example Shirley (1998) used the pitot probe at the inlet where the flow almost was non-disturbed and the Kiel probe at exit of the compressor where the flow was disturbed.

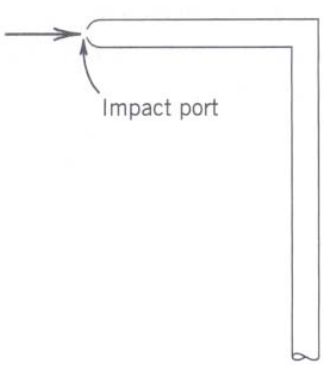

(a) Pitot probe

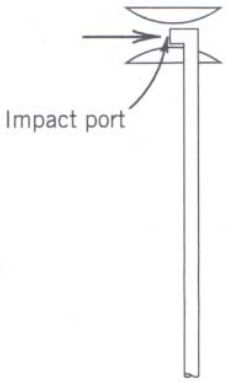

(b) Kiel probe

Figures 4.6 Total pressure measurement devices
(Figliola, R. S. and Beasley, D. E. 2000).

The multi-hole probe: three, four, five or seven holes proved to have reliable measurement results. Reunanen (2001) used three-hole Cobra-probe, developed by Concepts ETI, to measure the static pressure and total pressure, as well as flow direction on a plane at the diffuser exit of a centrifugal compressor, see figure 4.7. This type of probes can be used also for turbulence measurement. Chen (1998) validated the four-hole probe (Cobra probe) through turbulence measurement in a fully developed pipe flow. A schematic diagram of the cobra probe is shown in figure 4.8. This type of probes can also measure the high misalignment of the flow angle. For example, Dantec Dynamics Inc. developed five and seven-hole probes that can measure the misalignment of flow up to 60^{o} and 70^{o}, respectively from the probe axis.

Another method, which can be used to find the pressure ratio, is by calculating the total pressure from some measured values. The total pressure is function of static pressure and velocity. The static pressure is measured with a probe. The velocity is calculated from the measured mass flow rate, as well as the calculated density and area. Whitefield (1993) used a similar method to find the total pressure.

In conclusion, within each measurement there is an upper limit of accuracy. That is, as the series of a calculated value need more measured values as the accuracy decreases. This means the method of finding the total pressure from some other measured values is not suitable as long as the direct method of measurement is possible with high accuracy. So, this method is not recommended for the proposed compressor test facility.

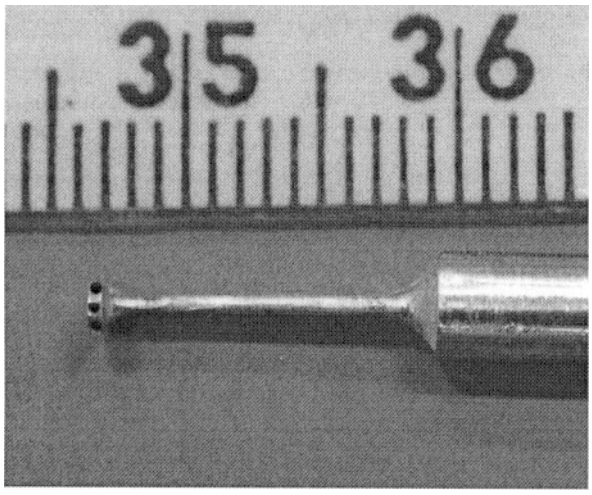

Figure 4.7 Three-hole cobra-probe
(Reunanen, Arttu; 2001).

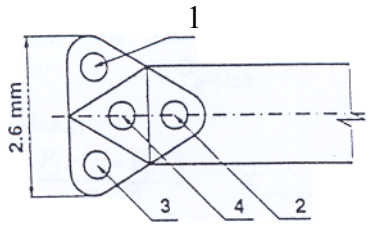

Figure 4.8 Schematic diagram of the cobra probe
(Hooper, John D., 1998).

The direct measurement of the total pressure is widely done by a pitot, a Kiel or multi-hole probe. The proposed test rig will be used for different compressors geometries with high rotational speeds. Also, these compressors will be tested for perfomance. This means they will operate around surge line, where separation and back flow take place. With these operating conditions the pitot probe is not recommended, especially at the compressor exit since it is relatively sensitive to the flow angle comparing to the Kiel and multi-hole probes. The main drawback of the Kiel probe comes from the blockage that build up inside its shroud. However, clean air is the working fluid and the operation time is relatively short. In addition, pretest run will be done to insure that all the instrumentations function properly, as required by ASME PTC 10 paragraph 3.10. Also, the pressure transducers will be calibrated before and after each measurement, following ASME PTC 10 paragraph 4.6.5. So, the problem of uncertainty in the accuracy of Kiel probe due to blockage is eliminated. On the other hand, the multi-hole probe does not have the problem of the blockage and can measure the misalignment of the flow angle up to high limit, 70^{o} for seven hole probe as claimed by Dantec Dynamics Inc. Adding to that it can measure the velocity vector and static pressure. The permissible fluctuation of test reading of the total pressure according to ASME PTC10 is $\leq \pm 2\%$. So, the maximum allowable uncertainty in pressure measurement is $\leq \pm 1\%$.

The aim of the proposed test rig for the time being is to investigate the performance of the compressor that needs the value of the total pressure ratio without the need for the turbulent measurement. Both the Kiel and multi-hole probes provide the value of the total pressure ratio with high accuracy. On the other hand, Kiel probe is considered to be

cheaper than the multi-hole type. Therefore, it is recommended to choose the Kiel probe over the multi-hole probe, as long as there is no need to measure the turbulent flow fields.

4.2.4 Isentropic Efficiency

The efficiency of the compressor is the ability to compress the gas ideally comparing to actual case. That is:

$$\eta_s = \frac{W_{ideal}}{H_d - H_i} \tag{4.6}$$

at test condition. Where the ideal work (isentropic work) is:

$$W_{ideal} = \dot{m} C_p T_{01} \left((\frac{P_{04}}{P_{01}})^{\frac{\gamma-1}{\gamma}} - 1 \right) \quad \text{or} \quad W_{ideal} = \frac{P_f}{RT_f} Q_f C_p T_{01} \left((\frac{P_{04}}{P_{01}})^{\frac{\gamma-1}{\gamma}} - 1 \right)$$

If the flow meter at the pipe inlet, then the data reduction equation is:

$$W_{ideal} = \frac{P_I}{RT_I} Q_f C_p T_{01} \left((\frac{P_{04}}{P_{01}})^{\frac{\gamma-1}{\gamma}} - 1 \right)$$

The calculation of $P_f, T_f, Q_f, P_{04}, P_{01}$ and rpm were explained above. The static pressure, P_I, and static temperature, T_I, at the pipe inlet are measured with static pressure tab and static temperature probe, respectively.

The total temperature at the inlet of the compressor can be directly measured by a probe. Two types of probes are widely used in literature, the thermocouples and resistance temperature detectors (RTD), see figure 4.9. Colantuoni and Colella (1993) and Shirley (1998) used thermocouples whereas Krain and Hoffmann (1998) and Whitefield et al.

(1993) used the resistance temperature devices, Platinum (Pt) type. Nicholas and White (2001) discussed the characteristics of both types of the probes. Platinum resistance thermometers are a non-expensive type that can operate over wide range of temperature, -260 C^o to 960 C^o, with accuracy reach to 1 mK. For these reasons they are used in many applications and preferred comparing to other thermometers types. On the other hand, the thermocouples are mainly used in low-accuracy or high temperature applications, over than 1400^{o}C. On other point of view, the Pt-RTD is delicate while the thermocouple is robust, Walsh and Fletcher (1998) and Omega Engineering Inc. Some Company, such as Omega Engineering Inc., has thermocouples that can measure the temperatures range from –270 to 2300^{0}C, as well as relatively inexpensive and robust but not accurate as RTD.

In conclusion, since the Pt-RTD has high accuracy and wide range of temperature measurement, as well as, the test environment is undisturbed, it is recommended to use it as a total temperature instrument. If a thermocouple is accurate enough for the measurement, it can be used. The permissible fluctuation of the nozzle temperature, which can be used also for venturi, as well as the total temperature test readings according to ASME PTC10 are $\leq \pm 0.5\%$. So, the maximum allowable uncertainty in temperature probes is $\leq \pm 0.25\%$.

Calculating the actual work from the total temperature measurement, where adiabatic condition is assumed, is not practical in the proposed compressor test facility. The reason behind that is the possibility of having the heat loses through the compressor casing and

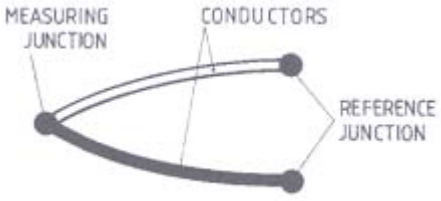

Figure 4.9.a. the physical structure and notation of the thermocouple

(Michalski, L. et al., 2001).

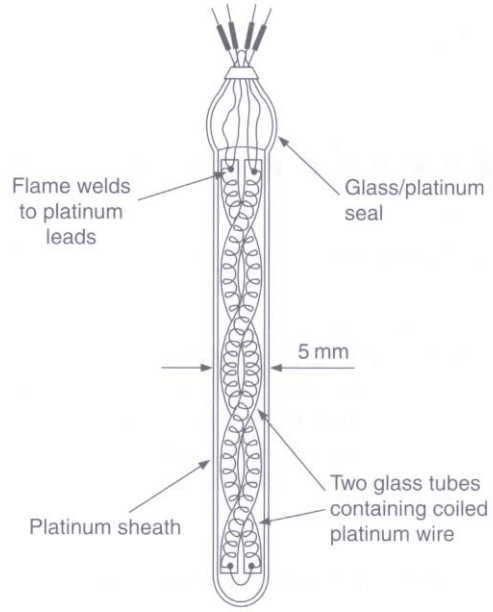

Figure 4.9.b. Platinum resistance thermometer, the platinum sheath is 5 mm in diameter and 50 mm long
(Nicholas, J. V. and White, D. R., 2001).

the impeller if no insulation is used. Thus, the assumption of adiabatic condition is not realistic and there has to be another way to find the actual work.

Two different methods may be used to find the actual work of the compressor through power calculation. The power of the compressor can be calculated from either measurement of electrical input to a driving motor or torquemeters. Both methods are used in literature and comply with ASME PTC 10, paragraph 4.12.

With consideration that the mechanical losses of the transmission system are low and well estimated by the manufacturer, the actual work can be calculated from the power of the motor. On other words, the impeller power can be calculated by subtracting the losses from the input power, which is known as calorimetric technique. That is:

$H_d - H_i$ =impeller's power = η_{mech} motor's mechanical power =

mechanical input power- power lost.

This method has simplicity in construction and compressor mount and effective in many cases as long as it can satisfy uncertainty limits.

Using the other method, the impeller's power can be calculated from the torque and the rotational speed. That is:

impeller's power = $\tau\ \Omega = \tau(\frac{2\pi}{60} rpm)$

Where τ and Ω are the torque and angular velocity of the impeller, respectively. Torque can be measured through several measuring techniques. A brief review of some torquemeters, with concentration on laser torquemeter, was done by Tullis (2000). The ideal torque meter is:

- Accurate,

- Safe,
- Robust,
- Easy to use,
- Not affected by environment conditions,
- Does not require the stopping of the machine to insert a shaft or instrument into the drive shaft and
- Has negligible time for the torquemeter setup.

A brief survey for some torque transduction methodologies for industrial applications (excluding laser technique) was discussed by Beihoff (1996).

Several torque measurement devices are used in practical applications but each has advantages and disadvantages. For example, torque can be measured through a free structure around the compressor assembly that is attached to torque measurement device. In this case, proper alignment with the transmission axis is required. This method minimizes uncertainty from the measurement techniques but requires complex structure. New two similar techniques are starting to spread, one is using laser and the other is using photoelectric technique.

Siemens' Corporate Technology Department in Erlangen developed a laser technique which operates as follow:

- Two small concave mirrors (normally one centimeter in diameter) are attached to the rotating shaft or to a disc at its side,
- Two laser diodes are mounted a few centimeters from the shaft,
- The light emitted by each diode directly hits one of the concave mirrors,

- For each rotation the mirrors reflect the incident light in the direction of the detectors,
- The difference in time interval between the two detectors is used to find the degree of torsion and thus the torque, see figure 4.10.

The advantages of this torquemeter are:

- Inexpensive,
- *Can work independently of fluctuations in light intensity. Thus its accuracy is not affected by the dirt on the optical system*
- Easy to install,
- Withstand shaft temperature up to 700 ^{0}C,
- Overload proof,
- Inexpensive to operate,
- It can provide information about the rotational speed and backlash,
- It can be used almost in all rotating machines to measure and control torque or power distribution,
- The resolution in torsion reach to 10^{-4} deg,
- Maintenance free since it depends on standard laser technique,
- Very robust system.

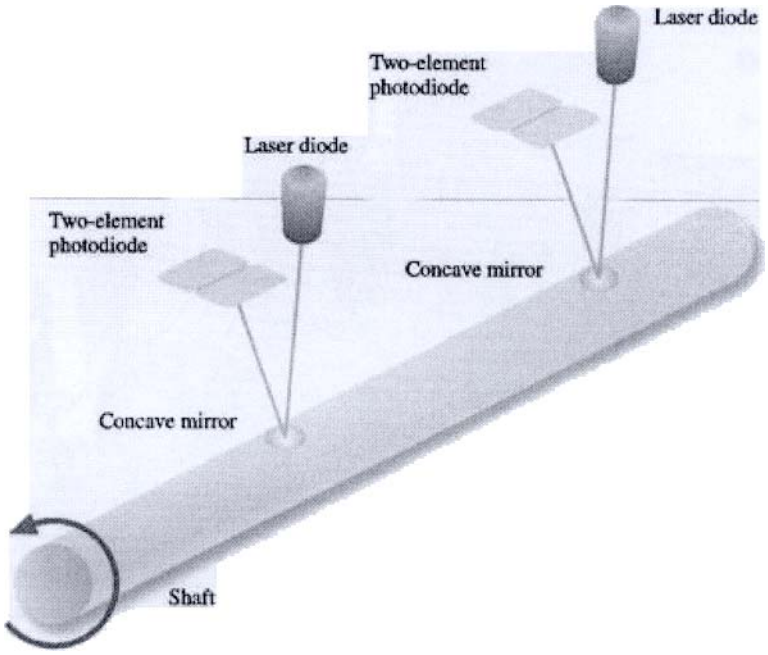

Figure 4.10. Torque measurement through using laser technique (Siemens' Corporate Technology Dept. in Erlangen, Germany, 2000).

Ebi et al., (1999), investigated a similar system where they worked on an integrated-optical, non-contact torque measurement micro-system. This type of torquemeter is also based on calculating torsional angle and thus the torque. In other words, the torque:

$$\tau = \frac{\phi JG}{L} \tag{4.7}$$

ϕ is the angular torsion, J is the moment of inertia, G is the modulus of rigidity and L is the shaft length.

This type of torquemeter is attractive to use but there are some questions need to be answered before it can be recommended.

- For which range of torque it can measure,
- For which rpm range it can work,
- Up to which centrifugal force does it work,
- Is there a limitation for shaft material,
- For which shaft length and diameter it can be used,
- Can it measure the dynamic torque effectively,
- Does it need software modification for different test setup,
- Does the accuracy change with the shaft deflection,
- Does it cause imbalance in system.

For the time being the measurement of power from the electrical input to a driving motor is chosen as long as the questions about the laser torquemeter are not answered positively. According to ASME PTC10, the allowable fluctuation of the torque reading is $\leq \pm 1\%$. So, the maximum allowable uncertainty of the torque meter should be $\leq \pm 0.5\%$.

4.3 GENERAL LAYOUT OF THE COMPRESSOR TEST FACILITY WITH RECOMMENDED INSTRUMENTATION

Four parameters are needed to find the performance map of the compressor. That is the rotational speed, mass flow rate, pressure ratio and compressor isentropic efficiency. Each one of them should be found directly or indirectly through measurement. On the other hand, the centrifugal compressor can be driven from either the front or back. Thus, there are two general setups for the test rig. The instrumentations for both of them are shown in figure 4.11.a & b.

4.3.1 Rotational Speed Instrumentation

As mentioned earlier there is flexibility in rotational speed instrumentation, as long as it can provide a continuous indication of speed fluctuation as required by ASME PTC 10, paragraph 4.10.1 The proper location of the rotational speed instrument to get a high accurate measurement by eliminating any further calculation is to mount it on the impeller shaft, see figure 4.11 a & b. If it is not possible, it can be installed on the shaft of the motor. In this case, the measured speed must be multiply by the gear ratio to get the rotational speed of the impeller if the gearbox is used. The outputs of the codes as discussed in chapter 2 help to know the needed range of the rotational speed instrument.

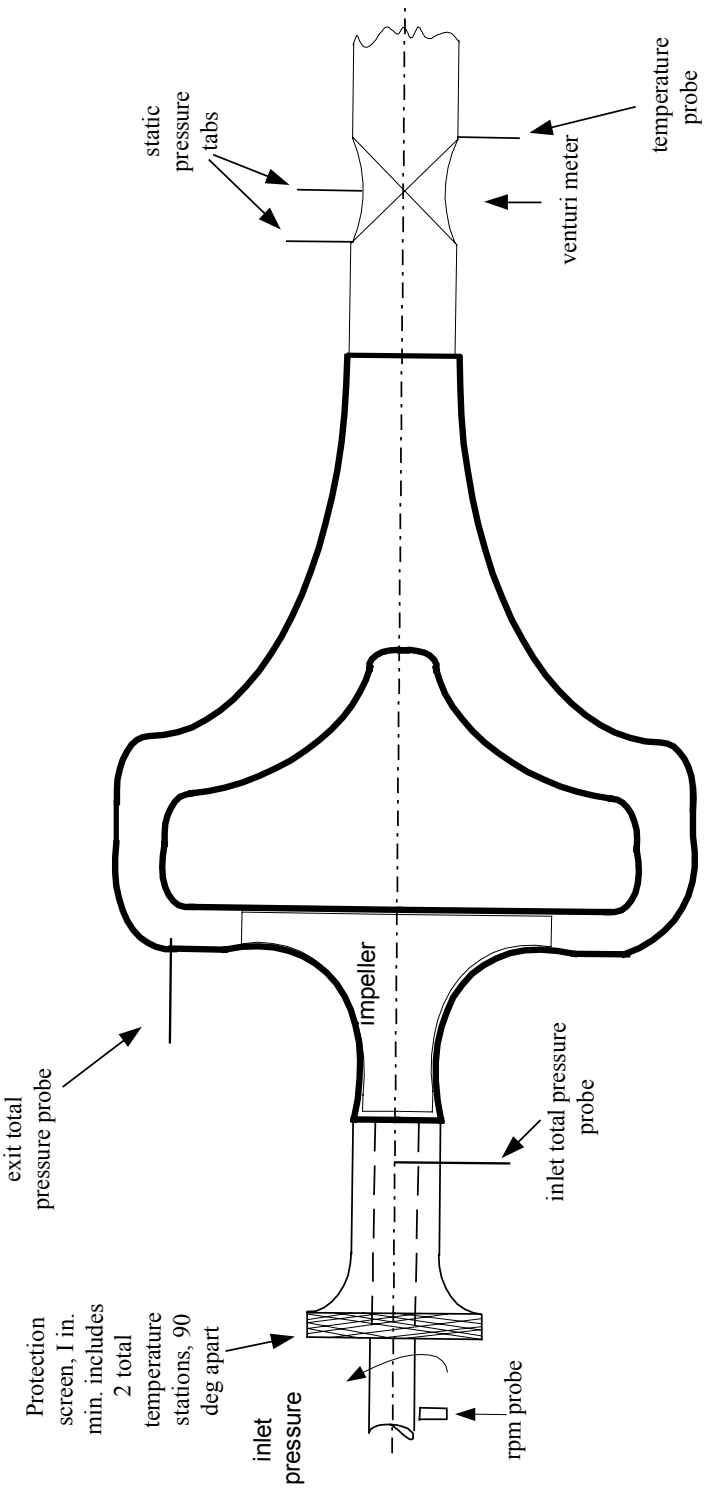

Figure 4.11. a. General layout of the centrifugal compressor test rig, driver from the compressor inlet

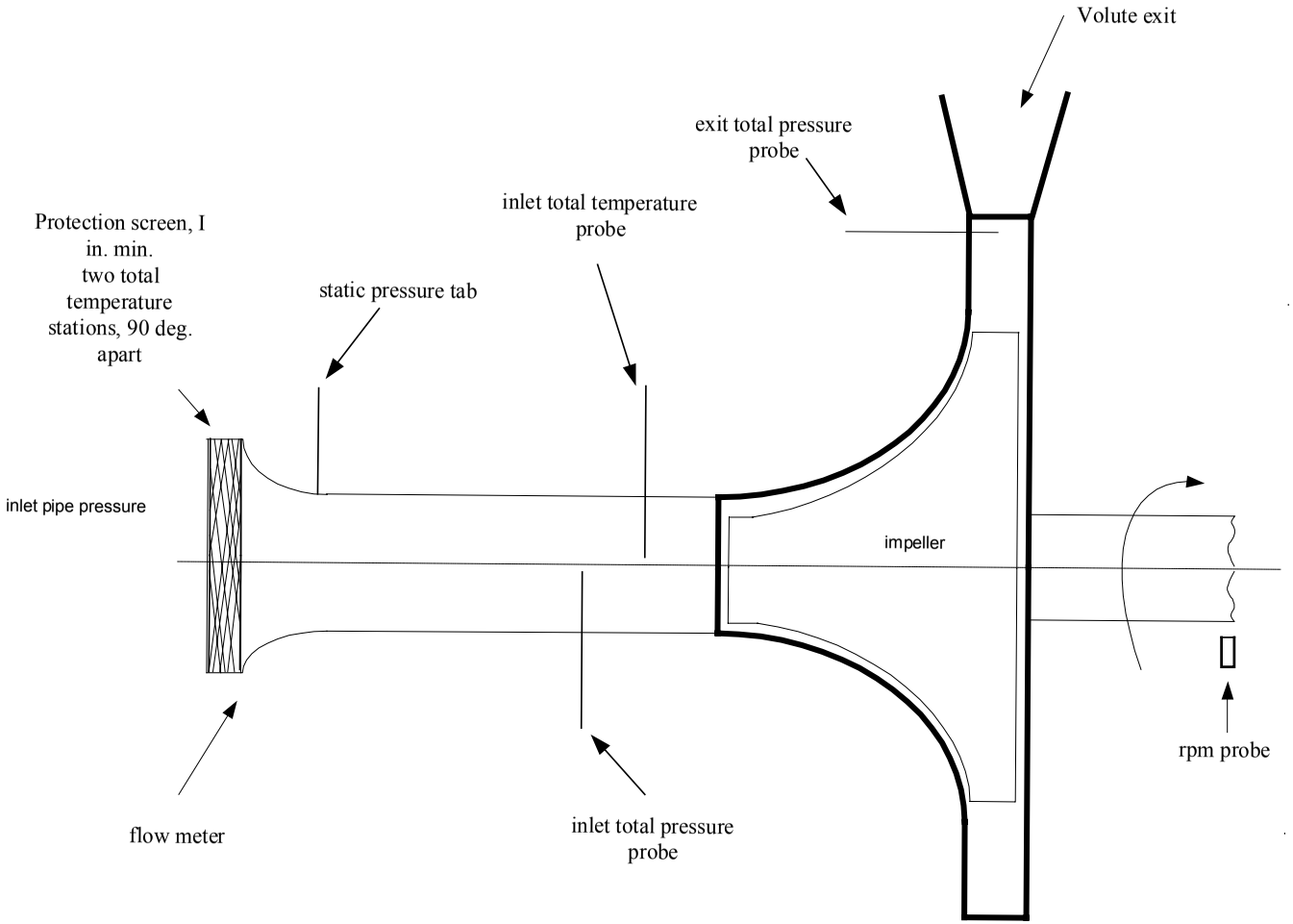

4.11.b. General layout of the centrifugal compressor test rig, driven from the diffuser side.

For example, from figure 2.7, the range of the rotational speed that covers all the compressor sizes (0.75Z to 3Z) is from 0 to 200,000 rpm. So, it is needed a rotational speed instrument(s) that can measure the speed from 0 to 200,000 rpm. Here Z is the reference size as defined in Chapter 2.

4.3.2 Mass Flow Rate Instrumentation

Mass flow rate can be measured by several types of devices. The recommended type is the venturi meter. It can be installed on either the inlet or discharge side of the compressor as mentioned by ASME PTC 10, paragraph 4.8.2, see figure 4.11 a & b. In the case if the venturi meter install at the exit, it should include two static pressure tabs to calculate the velocity. Also, a temperature probe needs to be installed at the inlet or exit of the venturi to get with the measured static pressure, the density of the flow. To improve accuracy of temperature measurement, the average of two temperature probes reading, at the inlet and exit of the venturi, can be used. When the venturi is at the pipe inlet, one static pressure tab is required and the second static pressure is almost equal to the atmospheric pressure. Similar temperature probe(s) arrangement, as in the case when the venturi is at the exit, is applicable here where the inlet stagnation temperature is equal to the atmospheric temperature. The output of the codes can be used to select the proper flow rate meter. For instance, from figures 2.3-2.6 the range of the mass flow rate is from .095 to 0.36 kg/s for Z equals 1 and β_2 equals 45^0. That is, after dividing mass flow rate by the density the proper flow meter device(s) can be chosen.

4.3.3 Pressure Ratio Instrumentation

Either Kiel or multi-hole probes can be used to find the total pressure. The inlet total pressure probe is fitted just upstream of the impeller inlet while the exit total pressure probe is mounted at the diffuser exit, see figure 4.11.a & b. The results of the codes help to choose the suitable pressure probe that can cover the required range. For example, for a given compressor size, Z=1 as shown in figures 2.10, it is recommended to choose a total pressure probe at the exit that can measure the range of 1 – 8 of the inlet total pressure.

4.3.4 Isentropic Efficiency Instrumentation

The isentropic efficiency is a function of several variables, as shown in equation 4.3. It can be found from the mass flow rate, pressure ratio, inlet temperature and impeller power. The requirements for mass flow rate and pressure ratio calculations are explained above.

The inlet total temperature, as explained earlier, can be measured by either a RTD-Pt, or a thermocouple if it has an acceptable accuracy. Its instrumentation is mounted at the compressor inlet, as shown in figure 4.11. Regarding impeller power calculation, the measurement of motor power and the system losses can be used as in ASME PTC10. The other way is to measure the torque and the rotational speed, see figure 4.10. If it is needed to know the required range of the temperature measurement device(s) to test different

compressor sizes, figure 2.9s help to predict the proper device(s). Similarly, figures 2.8 can help to predict the proper torque instrument.

A summary for instrumentations needed to find the four parameters that determine the performance map of the compressor is shown in table 4.1.

Table 4.1 Summary of the instrumentations design.

Needed parameters	**Measured parameter(s)**	**Recommended instrument type**	**Permissible fluctuation of test reading according to ASME PTC 10**	**Comment**
Rotational speed	Rotational speed	--------	0.5 %	There is flexibility on its type as long as it can provide continuous indication of speed fluctuation
Mass flow rate	If the flow meter is at the inlet:			Venturi meter is recommended.
	T_I	RTD, platinum type	0.5%	Thermocouple can be used if it has acceptable accuracy.
	P_I P_f	Pressure probe Static pressure tab	ΔP= 2%	Allowable nozzle differential pressure, can be used for the venturi.
	If the flow meter is at the exit:			Venturi meter is recommended.
	P_{f1} and P_{f2}	Static pressure tab	ΔP= 2%	Allowable nozzle differential pressure, can be used for the venturi
	T_f	RTD, platinum type	0.5%	Limitations for nozzle temperature, can be used for the venturi (Thermocouple can be used if it has acceptable accuracy)
Pressure ratio	P_{01} and P_{04}	Kiel probe	2%	Multi-hole probe can be used also
Isentropic efficiency	T_{01}	RTD, platinum type	0.5%	Thermocouple can be used if it has acceptable accuracy
	Power: Electric motor input Line voltage Torque	------ ------ ------	 1% 2% 1%	

4.4 INSTRUMENTATIONS UNCERTAINTY ANALYSIS

4.4.1 Introduction

Uncertainty is an estimation of the measurement or experimental errors. In other words, it is the degree of goodness of a measurement or experimental result, Coleman and Glenn Steele (1989). Decreasing in the range of the uncertainty means a more accurate result. Uncertainty results from two types of errors: precision and bias errors, which are also known as random and fixed errors, respectively. Figliola and Beasley (2000) defined the precision error as the measurement of the random variation originated during repeated measurements. Also, they defined the bias error as the difference between the average value of the measurements and the true value, see figures 4.12 and 4.13. The uncertainty analysis may be used below to find the uncertainty in the four parameters that determined the compressor performance map. That is, the rotational speed, mass flow rate, total pressure ratio and isentropic efficiency. The instrumentation uncertainty analysis done below is based on single sample measurement.

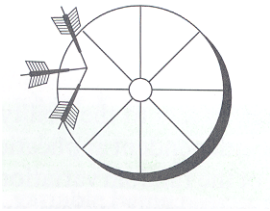

Figure 4.12.a High repeatability gives low precision error but no direct indication of accuracy.

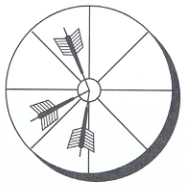

Figure 4.12.b High accuracy means low precision and bias errors.

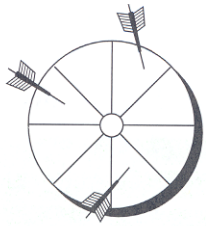

Figure 4.12.c Bias and precision errors lead to poor accuracy.

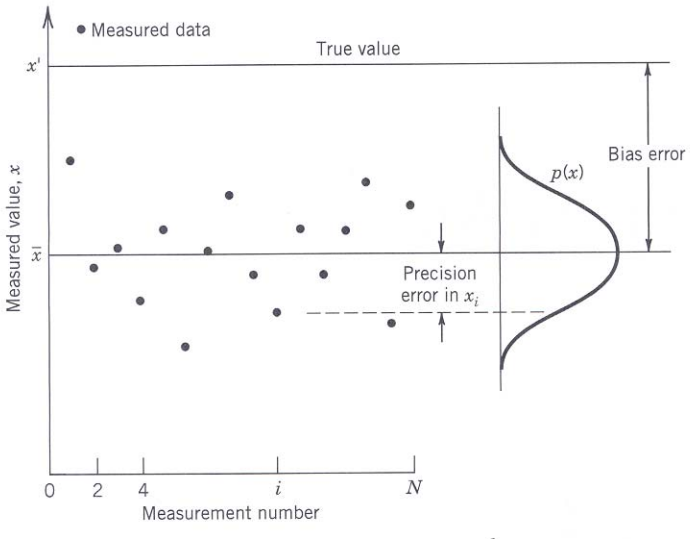

Figure 4.13 Distribution of errors upon repeated measurements (Figliola, R.S. and Beasley, D. E., 2000).

4.4.2 Analysis

General uncertainty analysis equations, precision, bias, and resultant uncertainty, can be found in Coleman and Glenn Steele (1989). These equations with some modifications are applied on the four parameters that determined the compressor performance map as shown below.

4.4.2.1 Precision Uncertainty:

The general dimensionless precision uncertainty equation is:

$$\left(\frac{U_p}{R}\right)^2 = \sum_{i=1}^{J} \left(\frac{1}{R}\frac{\partial R}{\partial x_i} U_{p,x_i}\right)^2 \tag{4.8.a}$$

which can be expanded to

$$\left(\frac{U_p}{R}\right)^2 = \left(\frac{1}{R}\frac{\partial R}{\partial x_1} U_{p,x_1}\right)^2 + \left(\frac{1}{R}\frac{\partial R}{\partial x_2} U_{p,x_2}\right)^2 + \ldots\ldots\ldots + \left(\frac{1}{R}\frac{\partial R}{\partial x_J} U_{p,x_J}\right)^2 \tag{4.8.b}$$

in which U_p is the precision uncertainty, R is the experimental result, U_{p,x_i} are the precision uncertainties in the measured variables x_i.

4.4.2.2 Bias Uncertainty:

The general dimensionless bias uncertainty equations is:

$$\left(\frac{U_B}{R}\right)^2 = \sum_{i=1}^{J} \left(\frac{1}{R}\frac{\partial R}{\partial x_i} U_{B,x_i}\right)^2 + \sum_{i=1}^{J}\sum_{k=1}^{J} \frac{1}{R}\frac{\partial R}{\partial x_i}\frac{1}{R}\frac{\partial R}{\partial x_k} \zeta_{ik} U_{B,x_i} U_{B,x_k} (1-\delta_{ik}) \tag{4.9.a}$$

Here the subscript B refers to the bias error. The second term on the right hand side of equation 4.9.a is known as the bias correlation term. This term is equal to zero unless the bias limits in the measurements of different individual variables are dependent on each other. The kronecker delta is defined as:

$$\delta_{ik}\begin{cases}=1 & i=k\\ =0 & i\neq k\end{cases}$$

and ζ_{ik} is the correlation coefficient of the bias limit and its range from zero to one, depending on the degree of correlation. Equation 4.9.a can be expanded to:

$$\begin{aligned}\left(\frac{U_B}{R}\right)^2 &= \left(\frac{1}{R}\frac{\partial R}{\partial x_1}U_{B,x_1}\right)^2+\left(\frac{1}{R}\frac{\partial R}{\partial x_2}U_{B,x_2}\right)^2+.....+\left(\frac{1}{R}\frac{\partial R}{\partial x_J}U_{B,x_J}\right)^2\\ &+2\frac{1}{R}\frac{\partial R}{\partial x_1}\frac{1}{R}\frac{\partial R}{\partial x_2}\zeta_{12}U_{B,x_1}U_{B,x_2}+2\frac{1}{R}\frac{\partial R}{\partial x_1}\frac{1}{R}\frac{\partial R}{\partial x_3}\zeta_{13}U_{B,x_1}U_{B,x_3}\\ &+2\frac{1}{R}\frac{\partial R}{\partial x_1}\frac{1}{R}\frac{\partial R}{\partial x_4}\zeta_{14}U_{B,x_1}U_{B,x_4}+.....+2\frac{1}{R}\frac{\partial R}{\partial x_2}\frac{1}{R}\frac{\partial R}{\partial x_3}\zeta_{23}U_{B,x_2}U_{B,x_3}+...\end{aligned} \qquad (4.\ 9.b)$$

4.4.2.3 Resultant Uncertainty

The resultant uncertainty is the square root summation of equations 4.8 and 4.9. That is:

$$\left(\frac{U_R}{R}\right)=\sqrt{\left(\frac{U_p}{R}\right)^2+\left(\frac{U_B}{R}\right)^2} \qquad (4.10)$$

The uncertainty analysis equations can be used to find the uncertainties in the measured values. In other words, the uncertainty in the four parameters, which represent the compressor perfomance map, can be calculated. Uncertainties in the rotational speed, mass flow rate, pressure ratio and isentropic efficiency are explained below. Table 4.2 shows the values of the derivative used to find the uncertainty.

4.4.2.4 Uncertainty In The Rotational Speed

The rotational speed is function of the measured rpm. That is:

Rotational speed = rpm (4.11)

To find the resultant of the rotational speed uncertainty apply equation 4.11 on equation 4.10 to get:

$$\left(\frac{U_{rot.sp.}}{rot.sp.}\right) = \sqrt{\left(\frac{U_{p,rot.sp}}{rot.pd}\right)^2 + \left(\frac{U_{B,rot.sp}}{rot.sp}\right)^2} \tag{4.12}$$

Since the rotational speed is measured directly from rotational speed device, it depends on the specification of the device, which is usually provided with it.

Table 4.2 The derived parameters used to find the uncertainty.

Parameter	Derivative result
$\frac{\partial \dot{m}}{\partial c_d}$	$\sqrt{2}\, A_{2f} \sqrt{\frac{\Delta P\, P_{2f}}{R(1-\frac{A_{2f}^2}{A_{1f}^2})T_{2f}}}$
$\frac{\partial \dot{m}}{\partial P_{2f}}$	$\frac{\Delta P\, A_{2f}\, C_d}{\sqrt{2}\, R\left(1-\frac{A_{2f}^2}{A_{1f}^2}\right)\sqrt{\frac{\Delta P\, P_{2f}}{R(1-\frac{A_{2f}^2}{A_{1f}^2})T_{2f}}\, T_{2f}}}$
$\frac{\partial \dot{m}}{\partial T_{2f}}$	$-\frac{\Delta P\, A_{2f}\, C_d\, P_{2f}}{\sqrt{2}\, R\left(1-\frac{A_{2f}^2}{A_{1f}^2}\right)\sqrt{\frac{\Delta P\, P_{2f}}{R(1-\frac{A_{2f}^2}{A_{1f}^2})T_{2f}}\, T_{2f}^2}}$
$\frac{\partial \dot{m}}{\partial \Delta P}$	$\frac{A_{2f}\, C_d\, P_{2f}}{\sqrt{2}\, R\left(1-\frac{A_{2f}^2}{A_{1f}^2}\right)\sqrt{\frac{\Delta P\, P_{2f}}{R(1-\frac{A_{2f}^2}{A_{1f}^2})T_{2f}}\, T_{2f}}}$
$\frac{\partial Pr}{\partial P_{01}}$	$-\frac{P_{04}}{P_{01}^2}$
$\frac{\partial Pr}{\partial P_{04}}$	$\frac{1}{P_{01}}$
$\frac{\partial \eta}{\partial c_d}$	$\frac{\sqrt{2} A_{2f}\, C_p \left(-1+(\frac{P_{04}}{P_{01}})^{\frac{-1+\gamma}{\gamma}}\right) T_{01} \sqrt{\frac{\Delta P\, P_{2f}}{R(1-\frac{A_{2f}^2}{A_{1f}^2})T_{2f}}}}{\tau\, \Omega}$

$\frac{\partial \eta}{\partial P_{2f}}$	$\frac{\Delta P A_{2f} C_d C_p (-1+(\frac{P_{04}}{P_{01}})^{\frac{-1+\gamma}{\gamma}}) T_{01}}{\sqrt{2} R \tau \Omega (1-\frac{A_{2f}^2}{A_{1f}^2}) \sqrt{\frac{\Delta P P_{2f}}{R(1-\frac{A_{2f}^2}{A_{1f}^2}) T_{2f}} T_{2f}}}$
$\frac{\partial \eta}{\partial T_{2f}}$	$-\frac{\Delta P A_{2f} C_d C_p (-1+(\frac{P_{04}}{P_{01}})^{\frac{-1+\gamma}{\gamma}}) P_{2f} T_{01}}{\sqrt{2} R \tau \Omega (1-\frac{A_{2f}^2}{A_{1f}^2}) \sqrt{\frac{\Delta P P_{2f}}{R(1-\frac{A_{2f}^2}{A_{1f}^2}) T_{2f}} T_{2f}^2}}$
$\frac{\partial \eta}{\partial \Delta P}$	$\frac{A_{2f} C_d C_p (-1+(\frac{P_{04}}{P_{01}})^{\frac{-1+\gamma}{\gamma}}) P_{2f} T_{01}}{\sqrt{2} R \tau \Omega (1-\frac{A_{2f}^2}{A_{1f}^2}) \sqrt{\frac{\Delta P P_{2f}}{R(1-\frac{A_{2f}^2}{A_{1f}^2}) T_{2f}} T_{2f}}}$
$\frac{\partial \eta}{\partial T_{01}}$	$\frac{\sqrt{2} A_{2f} C_d C_p (-1+(\frac{P_{04}}{P_{01}})^{\frac{-1+\gamma}{\gamma}}) \sqrt{\frac{\Delta P P_{2f}}{R(1-\frac{A_{2f}^2}{A_{1f}^2}) T_{2f}}}}{\tau \Omega}$
$\frac{\partial \eta}{\partial P_{01}}$	$-\frac{\sqrt{2}(-1+\gamma) A_{2f} C_d C_p P_{04} (\frac{P_{04}}{P_{01}})^{-1+\frac{-1+\gamma}{\gamma}} T_{01} \sqrt{\frac{\Delta P P_{2f}}{R(1-\frac{A_{2f}^2}{A_{1f}^2}) T_{2f}}}}{\gamma \tau \Omega P_{01}^2}$
$\frac{\partial \eta}{\partial P_{04}}$	$\frac{\sqrt{2}(-1+\gamma) A_{2f} C_d C_p (\frac{P_{04}}{P_{01}})^{-1+\frac{-1+\gamma}{\gamma}} T_{01} \sqrt{\frac{\Delta P P_{2f}}{R(1-\frac{A_{2f}^2}{A_{1f}^2}) T_{2f}}}}{\gamma \tau \Omega P_{01}}$

$\frac{\partial \eta}{\partial \tau}$	$-\frac{\sqrt{2} A_{2f} C_d C_p (-1+(\frac{P_{04}}{P_{01}})^{-1+\frac{-1+\gamma}{\gamma}}) T_{01} \sqrt{\frac{\Delta P P_{2f}}{R(1-\frac{A_{2f}^2}{A_{1f}^2}) T_{2f}}}}{\tau^2 \Omega}$
$\frac{\partial \eta}{\partial \Omega}$	$-\frac{\sqrt{2} A_{2f} C_d C_p (-1+(\frac{P_{04}}{P_{01}})^{-1+\frac{-1+\gamma}{\gamma}}) T_{01} \sqrt{\frac{\Delta P P_{2f}}{R(1-\frac{A_{2f}^2}{A_{1f}^2}) T_{2f}}}}{\tau \Omega^2}$

4.4.2.5 Uncertainty in Mass Flow Rate

The mass flow rate is a function of the static density and the flow rate. That is:

$$\dot{m} = \rho Q = \rho A_{2f} C_d \sqrt{\frac{2\Delta P}{\rho(1-(\frac{A_{2f}}{A_{1f}})^2)}} = A_{2f} C_d \sqrt{\frac{P_{2f}}{RT_{2f}} \frac{2\Delta P}{(1-(\frac{A_{2f}}{A_{1f}})^2)}} \tag{4.13}$$

Taking into consideration only the measured values, which have significant uncertainty, the mass flow rate is a function of:

$\dot{m} = f(C_d, P_{2f}, T_{2f}, \Delta P)$.

Flow area is not included in the measured variables since it has negligible error in the diameter. Now substitute equation 4.13 into equations 4.8 to get:

$$\left(\frac{U_{p,\dot{m}}}{\dot{m}}\right)^2 = \left(\frac{1}{\dot{m}}\frac{\partial \dot{m}}{\partial c_d}U_{p,c_d}\right)^2 + \left(\frac{1}{\dot{m}}\frac{\partial \dot{m}}{\partial P_{2f}}U_{p,P_{2f}}\right)^2 + \left(\frac{1}{\dot{m}}\frac{\partial \dot{m}}{\partial T_{2f}}U_{p,T_{2f}}\right)^2 + \left(\frac{1}{\dot{m}}\frac{\partial \dot{m}}{\partial \Delta P}U_{p,\Delta P}\right)^2$$

Substitute for the mass flow rate, see table 4.2, to get

$$\left(\frac{U_{p,\dot{m}}}{\dot{m}}\right)^2 = \left(\frac{U_{p,c_d}}{C_d}\right)^2 + \left(\frac{U_{p,P_{2f}}}{2P_{2f}}\right)^2 + \left(\frac{U_{p,T_{2f}}}{-2T_{2f}}\right)^2 + \left(\frac{U_{p,\Delta P}}{2\Delta P}\right)^2 \tag{4.14}$$

Similarly, as done in equation 4.14, substitute equation 4.13 into 4.9 to get:

$$\left(\frac{U_{\dot{m}}}{\dot{m}}\right)^2 =$$

$$\left(\frac{1}{\dot{m}}\frac{\partial \dot{m}}{\partial c_d}U_{B,c_d}\right)^2 + \left(\frac{1}{\dot{m}}\frac{\partial \dot{m}}{\partial P_{2f}}U_{B,P_{2f}}\right)^2 + \left(\frac{1}{\dot{m}}\frac{\partial \dot{m}}{\partial T_{2f}}U_{B,T_{2f}}\right)^2 + \left(\frac{1}{\dot{m}}\frac{\partial \dot{m}}{\partial \Delta P}U_{B,\Delta P}\right)^2$$

$$2\frac{1}{\dot{m}}\frac{\partial \dot{m}}{\partial P_{2f}}\frac{1}{\dot{m}}\frac{\partial \dot{m}}{\partial \Delta P}\zeta_{p_{2f},\Delta P}U_{B,p_{2f}}U_{B,\Delta P}$$

Now, substitute for the mass flow rate derivative, see table 4.2 to get:

$$\left(\frac{U_{\dot{m}}}{\dot{m}}\right)^2 =$$

$$\left(\frac{U_{B,c_d}}{C_d}\right)^2 + \left(\frac{U_{B,P_{2f}}}{2P_{2f}}\right)^2 + \left(\frac{U_{B,T_{2f}}}{-2T_{2f}}\right)^2 + \left(\frac{U_{B,\Delta P}}{2\Delta P}\right)^2 + 2\zeta_{p_{2f},\Delta P}\frac{U_{B,P_{2f}}}{2P_{2f}}\frac{U_{B,\Delta P}}{2\Delta P} \tag{4.15}$$

In case P_{2f} and ΔP are correlated, such as when using the same device to calibrate them, the correlation coefficient of the bias limit, in equation 4.15, $\zeta_{p_{2f},\Delta P}$, needs to be minimized since their derivatives are positive. The resultant uncertainty in mass flow rate is:

$$\left(\frac{U_{\dot{m}}}{\dot{m}}\right) = \sqrt{\left(\frac{U_{p,\dot{m}}}{\dot{m}}\right)^2 + \left(\frac{U_{B,\dot{m}}}{\dot{m}}\right)^2} \tag{4.16}$$

4.4.2.6 Uncertainty in Pressure Ratio

The pressure ratio is defined as compressor exit stagnation pressure divided by the compressor inlet stagnation pressure. That is:

$$Pr = \frac{P_{04}}{P_{01}} \tag{4.17}$$

or

$$Pr = \Pr(P_{01}, P_{04})$$

As done in the mass flow rate, substitute equation 4.17 into equations 4.8 and 4.9 to get:

$$\left(\frac{U_{p,Pr}}{Pr}\right)^2 = \left(\frac{1}{Pr}\frac{\partial Pr}{\partial P_{01}}U_{p,P_{01}}\right)^2 + \left(\frac{1}{Pr}\frac{\partial Pr}{\partial P_{04}}U_{p,P_{04}}\right)^2$$

$$\left(\frac{U_{p,Pr}}{Pr}\right)^2 = \left(-\frac{U_{p,P_{01}}}{p_{01}}\right)^2 + \left(\frac{U_{p,P_{04}}}{P_{04}}\right)^2 \tag{4.18}$$

$$\left(\frac{U_{B,Pr}}{Pr}\right)^2 = \left(\frac{1}{Pr}\frac{\partial Pr}{\partial P_{01}}U_{B,P_{01}}\right)^2 + \left(\frac{1}{Pr}\frac{\partial Pr}{\partial P_{04}}U_{B,P_{04}}\right)^2 + 2\frac{1}{Pr}\frac{\partial Pr}{\partial P_{01}}\frac{1}{Pr}\frac{\partial Pr}{\partial P_{04}}\zeta_{P_{01},P_{04}}U_{B,P_{01}}U_{B,P_{04}}$$

$$\left(\frac{U_{B,Pr}}{Pr}\right)^2 = \left(-\frac{U_{B,P_{01}}}{p_{01}}\right)^2 + \left(\frac{U_{B,P_{04}}}{P_{04}}\right)^2 + 2\zeta_{P_{01},P_{04}}\left(-\frac{U_{B,P_{01}}}{p_{01}}\frac{U_{B,P_{04}}}{P_{04}}\right) \tag{4.19}$$

The derivatives of the stagnation pressures are available in table 4.2. The derivative of P_{01} has negative sign while the derivative of P_{04} has positive sign. So, their multiplication is negative and due to that it is recommended to have a maximized correlation coefficient between the two stagnation pressures to decrease the bias uncertainty. The resultant uncertainty in the pressure ratio is:

$$\left(\frac{U_{Pr}}{Pr}\right)=\sqrt{\left(\frac{U_{p,Pr}}{Pr}\right)^2+\left(\frac{U_{B,Pr}}{Pr}\right)^2} \tag{4.20}$$

4.4.2.7 Uncertainty in Isentropic Efficiency

The equation of the isentropic efficiency is:

$$\eta=\left(A_{2f}C_d\sqrt{\frac{P_{2f}}{RT_{2f}}\frac{2\Delta P}{(1-(\frac{A_{2f}}{A_{1f}})^2)}}C_pT_{01}\left((\frac{P_{04}}{P_{01}})^{\frac{(\gamma-1)}{\gamma}}-1\right)\right)/(\tau\Omega) \tag{4.21}$$

Taking into consideration there is no uncertainty in the flow meter area the efficiency is function of

$$\eta=\eta(C_d,P_{2f},T_{2f},\Delta P,T_{01},P_{01},P_{04},\tau,\Omega)$$

Now substitute equation 4.21 into equations 4.8 and 4.9 to get:

$$\left(\frac{U_{p,\eta}}{\eta}\right)^2=\left(\frac{1}{\eta}\frac{\partial\eta}{\partial c_d}U_{p,c_d}\right)^2+\left(\frac{1}{\eta}\frac{\partial\eta}{\partial P_{2f}}U_{p,P_{2f}}\right)^2+\left(\frac{1}{\eta}\frac{\partial\eta}{\partial T_{2f}}U_{p,T_{2f}}\right)^2+\left(\frac{1}{\eta}\frac{\partial\eta}{\partial\Delta P}U_{p,\Delta P}\right)^2$$
$$+\left(\frac{1}{\eta}\frac{\partial\eta}{\partial T_{01}}U_{p,T_{01}}\right)^2+\left(\frac{1}{\eta}\frac{\partial\eta}{\partial P_{01}}U_{p,P_{01}}\right)^2+\left(\frac{1}{\eta}\frac{\partial\eta}{\partial P_{04}}U_{p,P_{04}}\right)^2+\left(\frac{1}{\eta}\frac{\partial\eta}{\partial\tau}U_{p,\tau}\right)^2+\left(\frac{1}{\eta}\frac{\partial\eta}{\partial\Omega}U_{p,\Omega}\right)^2$$

Substitute the efficiency derivatives to get:

$$\left(\frac{U_{p,\eta}}{\eta}\right)^2 =$$

$$\left(\frac{U_{p,c_d}}{C_d}\right)^2+\left(\frac{U_{p,P_{2f}}}{2P_{2f}}\right)^2+\left(\frac{U_{p,T_{2f}}}{-2T_{2f}}\right)^2+\left(\frac{U_{p,\Delta P}}{2\Delta P}\right)^2+\left(\frac{U_{p,T_{01}}}{T_{01}}\right)^2+\left(\frac{U_{p,p_{01}}}{-\frac{(-1+\gamma)P_{04}(\frac{P_{04}}{P_{01}})^{(-1+(\frac{-1+\gamma}{\gamma}))}}{\gamma P_{01}^2(-1+(\frac{P_{04}}{P_{01}})^{(\frac{-1+\gamma}{\gamma})})}}\right)^2$$

$$+\left(\frac{U_{p,P_{04}}}{\frac{(-1+\gamma)(\frac{P_{04}}{P_{01}})^{(-1+(\frac{-1+\gamma}{\gamma}))}}{\gamma P_{01}(-1+(\frac{P_{04}}{P_{01}})^{(\frac{-1+\gamma}{\gamma})})}}\right)^2+\left(-\frac{U_{p,\tau}}{\tau}\right)^2+\left(-\frac{U_{p,\Omega}}{\Omega}\right)^2 \qquad (4.22)$$

$$\left(\frac{U_{B,\eta}}{\eta}\right)^2 = \left(\frac{1}{\eta}\frac{\partial\eta}{\partial c_d}U_{B,c_d}\right)^2 + \left(\frac{1}{\eta}\frac{\partial\eta}{\partial P_{2f}}U_{B,P_{2f}}\right)^2 + \left(\frac{1}{\eta}\frac{\partial\eta}{\partial T_{2f}}U_{B,T_{2f}}\right)^2 + \left(\frac{1}{\eta}\frac{\partial\eta}{\partial \Delta P}U_{B,\Delta P}\right)^2$$

$$+\left(\frac{1}{\eta}\frac{\partial\eta}{\partial T_{01}}U_{B,T_{01}}\right)^2 + \left(\frac{1}{\eta}\frac{\partial\eta}{\partial P_{01}}U_{B,P_{01}}\right)^2 + \left(\frac{1}{\eta}\frac{\partial\eta}{\partial P_{04}}U_{B,P_{04}}\right)^2 + \left(\frac{1}{\eta}\frac{\partial\eta}{\partial \tau}U_{B,\tau}\right)^2 + \left(\frac{1}{\eta}\frac{\partial\eta}{\partial \Omega}U_{B,\Omega}\right)^2$$

$$+2\frac{1}{\eta}\frac{\partial\eta}{\partial P_{01}}\frac{1}{\eta}\frac{\partial\eta}{\partial P_{04}}\zeta_{P_{01},P_{04}}U_{B,P_{01}}U_{B,P_{04}} + 2\frac{1}{\eta}\frac{\partial\eta}{\partial P_{01}}\frac{1}{\eta}\frac{\partial\eta}{\partial P_{2f}}\zeta_{P_{01},P_{2f}}U_{B,P_{01}}U_{B,P_{2f}}$$

$$+2\frac{1}{\eta}\frac{\partial\eta}{\partial P_{01}}\frac{1}{\eta}\frac{\partial\eta}{\partial \Delta P}\zeta_{P_{01},\Delta P}U_{B,P_{01}}U_{B,\Delta P} + 2\frac{1}{\eta}\frac{\partial\eta}{\partial P_{04}}\frac{1}{\eta}\frac{\partial\eta}{\partial P_{2f}}\zeta_{P_{04},P_{2f}}U_{B,P_{04}}U_{B,P_{2f}}$$

$$+2\frac{1}{\eta}\frac{\partial\eta}{\partial P_{04}}\frac{1}{\eta}\frac{\partial\eta}{\partial \Delta P}\zeta_{P_{04},\Delta P}U_{B,P_{04}}U_{B,\Delta P} + 2\frac{1}{\eta}\frac{\partial\eta}{\partial P_{2f}}\frac{1}{\eta}\frac{\partial\eta}{\partial \Delta P}\zeta_{P_{2f},\Delta P}U_{B,P_{2f}}U_{B,\Delta P}$$

$$+2\frac{1}{\eta}\frac{\partial\eta}{\partial T_{01}}\frac{1}{\eta}\frac{\partial\eta}{\partial T_{2f}}\zeta_{T_{01},T_{2f}}U_{B,T_{01}}U_{B,T_{2f}}$$

Again substitute the efficiency derivatives to get:

$$\left(\frac{U_{B,\eta}}{\eta}\right)^2=\left(\frac{U_{B,C_d}}{C_d}\right)^2+\left(\frac{U_{B,P_{2f}}}{2P_{2f}}\right)^2+\left(\frac{U_{B,T_{2f}}}{-2T_{2f}}\right)^2+\left(\frac{U_{B,\Delta P}}{2\Delta P}\right)^2+\left(\frac{U_{B,T_{01}}}{T_{01}}\right)^2+$$

$$\left(\frac{\frac{U_{B,P_{01}}}{-\frac{(-1+\gamma)P_{04}(\frac{P_{04}}{P_{01}})^{(-1+(\frac{-1+\gamma}{\gamma}))}}{\gamma P_{01}^2(-1+(\frac{P_{04}}{P_{01}})^{(\frac{-1+\gamma}{\gamma})})}}}{}\right)^2+\left(\frac{\frac{U_{B,P_{04}}}{\frac{(-1+\gamma)(\frac{P_{04}}{P_{01}})^{(-1+(\frac{-1+\gamma}{\gamma}))}}{\gamma P_{01}(-1+(\frac{P_{04}}{P_{01}})^{(\frac{-1+\gamma}{\gamma})})}}}{}\right)^2+\left(-\frac{U_{B,\tau}}{\tau}\right)^2+\left(-\frac{U_{B,\Omega}}{\Omega}\right)^2$$

$$+2\zeta_{P_{01},P_{04}}\left[\frac{\frac{U_{B,P_{01}}}{-\frac{(-1+\gamma)P_{04}(\frac{P_{04}}{P_{01}})^{(-1+(\frac{-1+\gamma}{\gamma}))}}{\gamma P_{01}^2(-1+(\frac{P_{04}}{P_{01}})^{(\frac{-1+\gamma}{\gamma})})}}\frac{U_{B,P_{04}}}{\frac{(-1+\gamma)(\frac{P_{04}}{P_{01}})^{(-1+(\frac{-1+\gamma}{\gamma}))}}{\gamma P_{01}(-1+(\frac{P_{04}}{P_{01}})^{(\frac{-1+\gamma}{\gamma})})}}}{}\right]+2\zeta_{P_{01},P_{2f}}\left[\frac{\frac{U_{B,P_{01}}}{-\frac{(-1+\gamma)P_{04}(\frac{P_{04}}{P_{01}})^{(-1+(\frac{-1+\gamma}{\gamma}))}}{\gamma P_{01}^2(-1+(\frac{P_{04}}{P_{01}})^{(\frac{-1+\gamma}{\gamma})})}}\frac{U_{B,P_{2f}}}{2P_{2f}}}{}\right]$$

$$+2\zeta_{P_{01},\Delta P}\left[\frac{\frac{U_{B,P_{01}}}{-\frac{(-1+\gamma)P_{04}(\frac{P_{04}}{P_{01}})^{(-1+(\frac{-1+\gamma}{\gamma}))}}{\gamma P_{01}^2(-1+(\frac{P_{04}}{P_{01}})^{(\frac{-1+\gamma}{\gamma})})}}\frac{U_{B,\Delta P}}{2\Delta P}}{}\right]+2\zeta_{P_{04},P_{2f}}\left[\frac{\frac{U_{B,P_{04}}}{\frac{(-1+\gamma)(\frac{P_{04}}{P_{01}})^{(-1+(\frac{-1+\gamma}{\gamma}))}}{\gamma P_{01}(-1+(\frac{P_{04}}{P_{01}})^{(\frac{-1+\gamma}{\gamma})})}}\frac{U_{B,P_{2f}}}{2P_{2f}}}{}\right]$$

$$+2\zeta_{P_{04},\Delta P}\left[\frac{\frac{U_{B,P_{04}}}{\frac{(-1+\gamma)(\frac{P_{04}}{P_{01}})^{(-1+(\frac{-1+\gamma}{\gamma}))}}{\gamma P_{01}(-1+(\frac{P_{04}}{P_{01}})^{(\frac{-1+\gamma}{\gamma})})}}\frac{U_{B,\Delta P}}{2\Delta P}}{}\right]+2\zeta_{P_{2f},\Delta P}\left(\frac{U_{B,P_{2f}}}{2P_{2f}}\frac{U_{B,\Delta P}}{2\Delta P}\right)+2\zeta_{T_{01},T_{2f}}\left(\frac{U_{B,T_{01}}}{T_{01}}\frac{U_{B,T_{2f}}}{-2T_{2f}}\right) \tag{4.23}$$

Since the derivative of the inlet stagnation pressure has a negative sign, it is recommended to correlate it with the other pressure terms, as shown in equation 4.23. Thus they need to be correlated with maximized correlation coefficients to decrease the bias uncertainty in the efficiency. For the other pressure correlation terms it is recommended to correlate them with minimized correlation coefficients. Due to the same reason for the inlet stagnation pressure bias correlation terms, the two temperature terms are correlated with maximized correlation coefficient. The resultant uncertainty in the isentropic efficiency is:

$$\left(\frac{U_{Pr}}{\eta}\right)=\sqrt{\left(\frac{U_{p,Pr}}{\eta}\right)^2+\left(\frac{U_{B,Pr}}{\eta}\right)^2} \tag{2.24}$$

The values of the uncertainties in the calculated parameters are important since they help to predict the accuracy in the result. In other words, they explain which instrument needs to have more care during the measurement and calibration.

CHAPTER 5

GENERAL SAFETY REQUIREMENTS

Safety is one of the main requirements of designing a centrifugal compressor test facility. When the compressor is deviated from its safe operation range or any part of the test facility, there must be a monitoring system that can indicate this case and solve it automatically if possible. There are many regulations for the safe operation of the compressor test facility, some of them are explained below.

Overcoming the compressor facility deviation from the safe limits, can be done by using a standby device or if it is not applicable the system need to be shutdown. Erhard and Gehrer (2000) summarized the signals safety requirements for the operation of the transonic turbine test facility which is applicable to centrifugal compressor test facility as discussed below. There has to be a fast automatic emergency shutdown of the machine if any of the following subsystems indicate a deviation from the safe operating range:

- Electric circuit interruption to emergency supply,
- 2 channel over-speed system at compressor shaft coupling,
- Miss-displacement of the bearings,

- Over temperature reading in bearing,
- Inlet pressure for the bearing supply pipes,
- Pressure of the main and the auxiliary electrical oil pump,
- Temperature and oil level of the oil tank,
- Over-pressure of the compressor exit casing,
- Over vibration reading for each part of the test rig.

In addition to the above signals safety subsystems, there are some other requirements related to emergency mechanical failure for any part of the test facility:

- Steel case for couplings,
- Protection for compressor impeller,
- Steel frame for the whole unit with proper fixed rubber mounts to isolate vibration,
- Bricks walls surround the whole test rig,
- Isolated concrete floor slap to minimize the effect on sensitive equipments in the lab.

CHAPTER 6

CONCLUSION AND RECOMMENDATION

The experimental investigations are the core of any practical design because the numerical analysis is based on many assumptions. On the other hand, the accuracy of experimental results depends on the experimental facility. That is, it depends on the types of the instrumentations used for the measurement, as well as the setup of the experiment. The design requirements for these two factors were investigated in this project.

The main investigated points in this study are summarized below:

1. Aero-thermodynamics analysis of the impeller was done which can help to estimate the power requirement for a given compressor geometry. Also, this analysis can help to predict the input torque, total pressure and temperature ratios, as well as mass flow rate for a given rotational speed and impeller size. These represent the guide-lines for the proper selection of driver unit and the needed range of instrumentations for the measurements. The results of the codes indicate the need for a driver with 500 kW to run the compressor for a given impeller tip radius ranged from .0286 to 0.1143 m to satisfy the objective. Also, the maximum expected total pressure ratio is over 8 and the maximum expected mass flow rate is 3.35 kg/s.

2. Critical review of the driver units used in the literature was completed. The types of drivers used in the literature are: electrical motors, combustions gas turbines and turbochargers. This review showed that the electrical motors are the best drivers for the centrifugal compressors. This is mainly because they have better control and more flexibility to test several compressor configurations.
3. Instrumentations setup and deciding types as well as specification of sensors were achieved in this study. Critical review on the instrumentations used to find the performance of the compressor was completed. This review showed that there is a flexibility to choose the rotational speed instrument as long as it can provide continuous accurate reading as required by ASME PTC 10, paragraph 4.10.1. It is recommended to install it on the impeller shaft if it is possible; otherwise it can be installed in motor shaft. This review showed that the proper flow measurement device is the venturi meter. The mains reasons behind that are its capability to accommodate large flow range, has low-pressure drop and high accuracy compared to the orifice and the nozzle meters. Three types of pressure probes are widely used in the experimental investigation: pitot , Kiel and multi-hole probes. Since the pitot probe has limited capability to measure the misalignment of the flow from the probe opening, it is not recommended, especially at compressor exit. On the other hand, the other two types of the probes have much higher capability to measure the flow misalignment. Since the Kiel probe is cheaper, it is recommended as long as there is no need to measure the turbulent flow fields. Inlet stagnation temperature is important parameter to predict the isentropic efficiency of the compressor. Two types of temperature instrumentations are widely used in

the literature: resistance temperature detectors, platinum type, and thermocouples. It is recommended to use the Pt-RTD probe as long as the thermocouples do not have enough accurate measurement.

4. Uncertainty analysis can predict the accuracy of the results. Instrumentations uncertainty analysis showed the importance to correlate the static pressure tabs with minimized correlation factor to decrease the bias uncertainty for the flow measurement. Also, it showed that stagnation probes need to be correlated with maximized correlation factor to decrease the bias uncertainty for the stagnation pressure ratio measurement. Similar case is for the stagnation pressure. In addition, for the isentropic efficiency all the pressure probes need to be correlated with the inlet stagnation probe with maximized correlation factor to decrease the bias uncertainty and the others pressure probes need to be correlated to minimize bias uncertainty. The temperature probes need to be minimized by using maximized correlation factor, similar to the pressure stagnation probes.
5. General safety requirements in case when any parts of the compressor test facility are deviate from the safe range.

Further improvements of the three codes are needed. They need some advanced empirical formulas to have high accurate predicted efficiency and surge. Also, they need to be improved to take into account the changing of diffuser configuration. On the other hand, further investigations on torque measurement devices are recommended. In addition, uncertainty analysis based on multiple samples is proposed.

Appendix A.1

First Code

```
% MATLAB SOFTWARE
% this program is written to find the pressure ratio, input power,
% input torque, pressure ratio and temperature ratio
% for a centrifugal compressor vs. different mass flow rate for
% different rpms and impeller sizes.
% NOTE : SI units are used

%------------------------------ starting the program -------------------------------%

 clear all % clear all statement in the memory of MATLAB command window
 close all % clear statement for the figure(s)

% GIVEN
% rpm, flow factor (PHIf) , impeller size and configuration and
% inlet stagnation conditions
% ASSUMPTIONS
% ideal gas and bulk flow

%ANALYSIS

% IMPELLER SIZE
r1 =.025 ;  % inlet tip radius (for the inducer) : r1
r2 =.0381 ; % exit tip radius (for the impeller) : r2
rh =.008 ;  % hub raduis: rh

% IMPELLER CONFIGURATION
beta1 =45*pi/180 ; % inlet tip angles : Beta1 (in radian)
beta2 =25*pi/180 ; % exit tip angles : Beta2 (in radian )
Nb =14 ; % number of the blades : Nb
b=.005 ; % impeller width :b

% GAS PROPERTIES : air
gama = 1.4 ; % specific ratio : gama ,constant
R = 287 ;  % gas constant : R
Cp = 1004 ; % constant pressure specific heat : Cp

% INLET CONDITIONS
T01 =300 ; % stagnation inlet temperature : T01
P01 = 101000 ;% stagnation inlet pressure : P01
Ro01 =1.2 ;% stagnation inlet density : Ro01

% SPECIAL ASSUMPTIONS
MC=.86;%Mass flow rate correction for the assumption of the bulk flow (MC)
alpha=10*pi/180;
```

```
%---------------------------------- calculations ---------------------------------%

% to find the power, torque, pressure ratio and temperature ratio for different sizes, q is
used
% for bbeta1=45:22:67;
%     beta1 = bbeta1*pi/180 ;
q1=1; q2=3;
for q= q1:q2
   % r11,r22,rhh and bb are used to refer for different geometries and
   % their definitions are the same as r1,r2,rh and b, respectively
   r11 = (.75+ .25*(q-1))*r1 ; r22 = ( .75 + .25*(q-1))*r2 ;
   rhh = (.75 + .25*(q-1))*rh ; bb  = (.75+ .25*(q-1))*b ;

   rpm = [30000 50000 70000 100000];  % rotational speed :rpm
   for  n = 1:length(rpm);
      % eff : is the efficiency of the compressor
      eff= 0.8;

      PHIf =tan(beta1)/tan(beta1+alpha):.025:1.05; % flow factor :PHIf
      for m = 1:length(PHIf)

         for s = 1:50;
            w(s,m,n,q)= rpm(n)*2*pi/60;  % angular velocity : w
            if ((PHIf(m)*w(s,m,n,q)*r11/tan(beta1))^2/(2*Cp))> (T01-10)
            disp('(PHIf*w*r11/tan(beta1))^2/(2*Cp))> T01, so you will get imaginary
number, so stop calculations for this loop')
            break ,  end
            U2(s,m,n,q)= w(s,m,n,q)*r22 ; % blade velocity at the impeller tip :U2
            % the static density at location 1 (inlet of the impeller):Ro1
            Ro1 = Ro01*(1+(gama-1)/2*(PHIf(m)*w(s,m,n,q)*r11/tan(beta1))^2/...
               (gama*R*(T01-((PHIf(m)*w(s,m,n,q)*r11/tan(beta1))^2/(2*Cp)))))^(-
1/(gama-1));
            % the static density at location 2 (exit of the impeller):Ro2 ,
            % first guess for the iteration
            Ro2(1,m,n,q) = Ro1;
            % actual mass flow rate : Mract
            Mract(s,m,n,q) = Ro1*pi*(r11^2-rhh^2)*(PHIf(m)*w(s,m,n,q)*r11/tan(beta1));
            Mractc(s,m,n,q) = MC*Mract(s,m,n,q); % corrected actual mass flow rate :
Mractc
            % slip factor : Slipf
            Slipf(s,m,n,q) = (1-(2/Nb*sqrt(cos(beta2))))*...
               (1-Mractc(s,m,n,q)/(Ro2(s,m,n,q)*pi^2*r22^2*bb*2*rpm(n)/30)*tan(beta2));
            if  Slipf(s,m,n,q)<= 0.1
            disp('Slip factor very small, so you will get imaginary number, so stop
calculations for this loop')
```

```
            break ,  end
            % exit radial relative velocity of the impeller : Wr2
            Wr2(s,m,n,q)= Mractc(s,m,n,q)/(2*pi*r22*bb*Ro2(s,m,n,q));
           % absolute tangential velocity at the impeller exit : Cth2
            Cth2(s,m,n,q)= Slipf(s,m,n,q)*U2(s,m,n,q);
            % input power : Pm (this value of the power for the iteration inside the s  loop
and
            % does not represent the actual power which are used for the pressure ratio
calculation)
            % this distinguishing between the two power (Pm  and P, below) is important to
get the
            % rigth plot
            Pm(s,m,n,q) = Mractc(s,m,n,q)*(U2(s,m,n,q)*Cth2(s,m,n,q)) ;
            % input torque : Tm (see the comment on Pm)
            Tm(s,m,n,q) = Pm(s,m,n,q)/w(s,m,n,q);
            % stagnation temperature at the impeller output : T02
            T02(s,m,n,q) = Pm(s,m,n,q)/(Mractc(s,m,n,q)*Cp) + T01;
            % resultant speed at the impeller exit: C2
            C2(s,m,n,q)=sqrt((U2(s,m,n,q)-Wr2(s,m,n,q)*tan(beta2))^2+Wr2(s,m,n,q)^2);
            % Mach no.(1)squared :M12
            M12(s,m,n,q)=((PHIf(m)*w(s,m,n,q)*r11/tan(beta1))^2)/...
               (gama*R*((T01-(((PHIf(m)*w(s,m,n,q)*r11/tan(beta1))^2)/(2*Cp)))));
            % Mach no.(2)squared : M22
            M22(s,m,n,q)=C2(s,m,n,q)^2/(gama*R*(T02(s,m,n,q)-
(C2(s,m,n,q)^2)/(2*Cp)));
            Ro2(s+1,m,n,q) = Ro1*((1+(gama-1)/(2)*M22(s,m,n,q))/(1+(gama-
1)/(2)*M12(s,m,n,q)))...
               ^(-1/(gama-1))*((1+((1+eff)/2)*((gama-
1)/gama)*(U2(s,m,n,q)/sqrt(R*T01))^2*Slipf(s,m,n,q)))...
               ^(1/(gama-1));

            if  (abs((Ro2(s+1,m,n,q)-Ro2(s,m,n,q))./Ro2(s,m,n,q))) <=0.000001 , break ,
end
         end
         if  Slipf(s,m,n,q)<= 0.1
            disp('Slip factor very small, so you will get imaginary number, so stop
calculations for this loop')
            break ,  end
         % input power : P
         P(s,m,n,q) = Mractc(s,m,n,q)*(U2(s,m,n,q)*Cth2(s,m,n,q)) ;
         % input torque : T
         T(s,m,n,q) = P(s,m,n,q)/w(s,m,n,q);
         % stagnation temperature of the impeller output :T02
         T02(s,m,n,q) = P(s,m,n,q)/(Mractc(s,m,n,q)*Cp) + T01;
         % stagnation temperature ratio of the impeller out put to the input : T0201r
```

```
            T0201r(s,m,n,q) = T02(s,m,n,q)/T01;
            % isentropic stagnation temperature of the compressor exit : T04s
            T04s(s,m,n,q) = eff*(T02(s,m,n,q)-T01) + T01;
            % stagnation pressure ratio : P04P01r
            P04P01r(s,m,n,q) =(T04s(s,m,n,q)/T01)^(gama/(gama-1)) ;
            % to plot Mract, new Mract (Mractn) is written in the below line
            Mractn(s,m,n,q) = Mractc(s,m,n,q);
        end
    end
end
for  n = 1:length(rpm)

    MMractn1 = nonzeros(Mractn(:,:,n,2));
        % MMractn2 = nonzeros(Mractn(:,:,n,3));
    %     MMractn3 = nonzeros(Mractn(:,:,n,6));
    %     MMractn4 = nonzeros(Mractn(:,:,n,8));
    %     MMractn5 = nonzeros(Mractn(:,:,n,9));
    %
    PP1 = nonzeros(P(:,:,n,2));
        % PP2 = nonzeros(P(:,:,n,3));
    %     PP3 = nonzeros(P(:,:,n,6));
    %     PP4 = nonzeros(P(:,:,n,8));
    %     PP5 = nonzeros(P(:,:,n,9));

    TT1 = nonzeros(T(:,:,n,2));
        % TT2 = nonzeros(T(:,:,n,3));
    %     TT3 = nonzeros(T(:,:,n,6));
    %     TT4 = nonzeros(T(:,:,n,8));
    %     TT5 = nonzeros(T(:,:,n,9));

    TT0201r1 = nonzeros(T0201r(:,:,n,2));
        % TT0201r2 = nonzeros(T0201r(:,:,n,3));
    %     TT0201r3 = nonzeros(T0201r(:,:,n,6));
    %     TT0201r4 = nonzeros(T0201r(:,:,n,8));
    %     TT0201r5 = nonzeros(T0201r(:,:,n,9));

    PP04P01r1 = nonzeros(P04P01r(:,:,n,2));
       % PP04P01r2 = nonzeros(P04P01r(:,:,n,3));
    %      PP04P01r3 = nonzeros(P04P01r(:,:,n,6));
    %      PP04P01r4 = nonzeros(P04P01r(:,:,n,8));
    %      PP04P01r5 = nonzeros(P04P01r(:,:,n,9));

    %end
    figure(1)
```

```
   plot(MMractn1,PP1,'rd-')%,MMractn2,PP2,'ro-')%,MMractn3,PP3,'g*-
',MMractn4,PP4,'ms-',MMractn5,PP5,'cd-');
   hold on
   figure(2)
   plot(MMractn1,TT1,'rd-')%,MMractn2,TT2,'ro-')%,MMractn3,TT3,'g*-
',MMractn4,TT4,'ms-',MMractn5,TT5,'cd-');
   hold on
   figure(3)
   plot(MMractn1,TT0201r1,'rd-')%,MMractn2,TT0201r2,'ro-
')%,MMractn3,TT0201r3,'g*-',MMractn4,TT0201r4,'ms-',MMractn5,TT0201r5,'cd-' );
   hold on
   figure(4)
   plot(MMractn1,PP04P01r1,'rd-')%,MMractn2,PP04P01r2,'ro-
')%,MMractn3,PP04P01r3,'g*-',MMractn4,PP04P01r4,'ms-',MMractn5,PP04P01r5,'cd-');
   hold on

end
hold off
figure(1);grid on
xlabel('actual mass flow rate (kg/s)'); ylabel(' input power ( W )')
title('input power vs actual mass flow rate for different rpm')
gtext('Z is the reference size')
% gtext('r1 =.025,r2 =.0381,rh =.008')
gtext('\beta_1 =67^o')%, \beta_2 =25')
% gtext('Nb =14, b=.005')
gtext('30k rpm');gtext('50k rpm');gtext('70k rpm');gtext('100k rpm')
%legend('Z=1',' Z=1.25',-1)

figure(2); grid on
xlabel('actual mass flow rate (kg/s)');ylabel('input torque (N-m)')
title('input torque vs actual mass flow rate for different rpm')
gtext('Z is the reference size')
% gtext('r1 =.025,r2 =.0381,rh =.008')
gtext('\beta_1 =67^o')%, \beta_2 =25')
% gtext('Nb =14, b=.005')
gtext('30k rpm');gtext('50k rpm');gtext('70k rpm');gtext('100k rpm')
%legend('Z=1',' Z=1.25',-1)

figure(3); grid on
xlabel('actual mass flow rate (kg/s)')
ylabel('stagnation Tempreture ratio T_0_4/T_0_1 ')
title('stagnation temperature ratio vs. actual mass flow rate for different rpm')
gtext('Z is the reference size')
% gtext('r1 =.025,r2 =.0381,rh =.008')
gtext('\beta_1 =67^o')%, \beta_2 =25')
```

```
% gtext('Nb =14, b=.005')
gtext('30k rpm');gtext('50k rpm');gtext('70k rpm');gtext('100k rpm')
%legend('Z=1',' Z=1.25',-1)

figure(4); grid on
xlabel('actual mass flow rate (kg/s)')
ylabel(' stagnation pressure ratio P_0_4/P_0_1 ')
title('stagnation pressure ratio vs actual mass flow rate for different rpm')
gtext('Z is the reference size')
%gtext('r1 =.025,r2 =.0381,rh =.008')
gtext('\beta_1 =67^o')%, \beta_2 =25')
%gtext('Nb =14, b=.005')
gtext('30k rpm');gtext('50k rpm');gtext('70k rpm');gtext('100k rpm')
%legend('Z=1',' Z=1.25',-1)
```

Appendix A. 2

Second Code

```
% MATLAB SOFTWARE
% this program is written to find the required input power, input torque,
% stagnation temperature ratio, stagnation pressure ratio and
% actual mass flow rate for
% different rpm, flow factor(PHIf) and impeller configuration
% NOTE : SI units are used

%------------------------------ starting the program -------------------------------%

clear all % clear statement for the text
close all % clear statement for the figure(s)

% GIVEN
% rpm, flow factor (PHIf) , impeller size and configuration, inlet stagnation conditions
% and gas properties

% MAIN ASSUMPTIONS
% ideal gas and bulk flow

%ANALYSIS

% IMPELLER SIZE
r1 =.025 ;  % inlet tip radius (for the inducer) : r1
r2 =.0381 ; % e xit tip radius (for the impeller) : r2
rh =.008 ;  % hub raduis: rh

% IMPELLER CONFIGURATION
beta1 =67*pi/180 ; % inlet tip angles : Beta1 (in radian)
beta2 =25*pi/180 ; % exit tip angles : Beta2 (in radian )
Nb =14 ; % number of the blades : Nb
b=.005 ; % impeller width :b

% GAS PROPERTIES: air
gama = 1.4 ; % specific ratio : gama ,constant
R = 287 ;  % gas constant : R
Cp = 1004 ; % constant pressure specific heat : Cp

% INLET CONDITIONS
T01 =300 ; % stagnation inlet temperature : T01
P01 = 101000 ;% stagnation inlet pressure : P01
Ro01 =1.2 ;% stagnation inlet density : Ro01

% SPECIAL ASSUMPTIONS
MC=.86;% Mass flow rate correction for the assumption of the bulk flow (MC)
alpha= 10*3.1416/180;
```

```
%---------------------------------- calculations ----------------------------------%

for q= 1:10 % to find the power for different sizes q is used
   % r11,r22,rhh and bb are used to refer for different geometries and...
   % their definitions are the same as r1,r2,rh and b, respectively
   r11 = (.75 + .25*(q-1))*r1 ; r22 = ( .75 + .25*(q-1))*r2 ;
   rhh = (.75 + .25*(q-1))*rh ; bb  = (.75+ .25*(q-1))*b ;
   % the max angle of the flow just before stall is alpha
   PHIf = tan(beta1)/tan(beta1+alpha);
   for m = 1:length(PHIf)
       maxrpm= 603*60/(2*pi*r22);
      rpm =1000:500:maxrpm;% rotational speed :rpm

      for  n = 1:length(rpm);
        % eff : is the efficiency of the compressor(stage adiabatic efficiency)
        eff= .8;

         for s = 1:20; % to consider the iteration of the density and the slip factor, use s

            w(s,m,n,q)= rpm(n)*2*pi/60; % angular velocity : w
            if ((PHIf(m)*w(s,m,n,q)*r11/tan(beta1))^2/(2*Cp))> (T01-10)
            disp('(PHIf*w*r11/tan(beta1))^2/(2*Cp))> T01, so you will get imaginary
number, so stop calculations for this loop')
            break ,  end
            U2(s,m,n,q)= w(s,m,n,q)*r22 ;% blade velocity at the impeller tip :U2
            % the static density at location 1 (inlet of the impeller):Ro1
            Ro1(s,m,n,q) = Ro01*(1+(gama-
1)/2*(PHIf(m)*w(s,m,n,q)*r11/tan(beta1))^2/...
               (gama*R*(T01-((PHIf(m)*w(s,m,n,q)*r11/tan(beta1))^2/(2*Cp)))))^(-
1/(gama-1));
            % the static density at location 2 (exit of the impeller):Ro2, first
            % guess for the iteration
            Ro2(1,m,n,q) = Ro1(1,m,n,q);
            % actual mass flow rate :Mract
            Mract(s,m,n,q)= Ro1(s,m,n,q)*pi*(r11^2-
rhh^2)*(PHIf(m)*w(s,m,n,q)*r11/tan(beta1));
            Mractc(s,m,n,q) = MC*Mract(s,m,n,q);% corrected actual mass flow rate :
Mractc
            % slip factor : Slipf
            Slipf(s,m,n,q) = (1-(2/Nb*sqrt(cos(beta2))))*...
               (1-Mractc(s,m,n,q)/(Ro2(s,m,n,q)*pi^2*r22^2*bb*2*rpm(n)/30)*tan(beta2));
            if  Slipf(s,m,n,q)<= 0.1
            break ,  end
            % exit radial relative velocity of the impeller : Wr2
            Wr2(s,m,n,q)= Mractc(s,m,n,q)/(2*pi*r22*bb*Ro2(s,m,n,q));
```

```
            % absolute tangential velocity at the impeller exit : Cth2
            Cth2(s,m,n,q)= Slipf(s,m,n,q)*U2(s,m,n,q);
            % input power : Pm (this value of the power for the iteration inside the s  loop
and
            % does not represent the actual power which are used for the pressure ratio
calculation)
            % this distinguishing between the two power (Pm and P, below) is important to
get the
            % right plot
            Pm(s,m,n,q) = Mractc(s,m,n,q)*(U2(s,m,n,q)*Cth2(s,m,n,q)) ;
            % input torque : Tm (see the comment on Pm)
            Tm(s,m,n,q) = Pm(s,m,n,q)/w(s,m,n,q);
            %stagnation temperature at the impeller output : T02
            T02(s,m,n,q) = Pm(s,m,n,q)/(Mractc(s,m,n,q)*Cp) + T01;
            % resultant speed at the impeller exit: C2
            C2(s,m,n,q)=sqrt((U2(s,m,n,q)-Wr2(s,m,n,q)*tan(beta2))^2+Wr2(s,m,n,q)^2);
            % Mach no.(1)squared :M12
            M12(s,m,n,q)=((PHIf(m)*w(s,m,n,q)*r11/tan(beta1))^2)/...
               (gama*R*((T01-(((PHIf(m)*w(s,m,n,q)*r11/tan(beta1))^2)/(2*Cp)))));
            % Mach no.(2)squared : M22
            M22(s,m,n,q)=C2(s,m,n,q)^2/(gama*R*(T02(s,m,n,q)-
(C2(s,m,n,q)^2)/(2*Cp)));
            Ro2(s+1,m,n,q) = Ro1(s,m,n,q)*((1+(gama-1)/(2)*M22(s,m,n,q))/(1+(gama-
1)/(2)*M12(s,m,n,q)))...
               ^(-1/(gama-1))*((1+((1+eff)/2)*((gama-
1)/gama)*(U2(s,m,n,q)/sqrt(R*T01))^2*Slipf(s,m,n,q)))...
               ^(1/(gama-1));
            %if  (abs((Ro2(s+1,m,n,q)-Ro2(s,m,n,q)))) <=0.0000001 , break ,  end
         end
         if U2(s,m,n,q) > 603  break  , end
         if  Slipf(s,m,n,q)<= 0.1
            disp('Slip factor very small, so you will get imaginary number, so stop
calculations for this loop')
            break ,  end

         % input power : P
         P(s,m,n,q) = Mractc(s,m,n,q)*(U2(s,m,n,q)*Cth2(s,m,n,q)) ;
         % input torque : T
         T(s,m,n,q) = P(s,m,n,q)/w(s,m,n,q);
         %stagnation temperature of the impeller output :T02
         T02(s,m,n,q) = P(s,m,n,q)/(Mractc(s,m,n,q)*Cp) + T01;
         % stagnation temperature ratio of the impeller out put to the input : T0201r
         T0201r(s,m,n,q) = T02(s,m,n,q)/T01;
         %isentropic stagnation temperature of the compressor exit : T04s
         T04s(s,m,n,q) = eff*(T02(s,m,n,q)-T01) + T01;
```

```
          % stagnation pressure ratio : P04P01r
          P04P01r(s,m,n,q) =(T04s(s,m,n,q)/T01)^(gama/(gama-1)) ;
          % to plot Mract, new Mract (Mractn) is written in the below line
          Mractn(s,m,n,q) = Mractc(s,m,n,q);
       end
       %   rpm(n,q)= w(s,m,n,q)*60/(2*pi);
       figure(1)
       PP  = nonzeros(P(:,m,:,q)); plot(rpm(1:length(PP)),PP,'r-' ); hold on
       figure(2)
       TT = nonzeros(T(:,m,:,q));plot(rpm(1:length(TT)),TT ,'g-'); hold on
       figure(3)
       TT0201r = nonzeros(T0201r(:,m,:,q));plot(rpm(1:length(TT0201r)),TT0201r,'m -
');hold on
       figure(4)
       PP04P01r = nonzeros(P04P01r(:,m,:,q));plot(rpm(1:length(PP04P01r)),PP04P01r,'r-
');hold on
       figure(5)
       MMractn = nonzeros(Mractn(:,m,:,q));plot(rpm(1:length(MMractn)),MMractn,'c-
');hold on

   end

end
%%%%%%%%%%%%%%%%%% restriction program%%%%%%%%%%%%%%

% the program below is written to plot the curves for different constant velocities

PHIfx =tan(beta1)/tan(beta1+alpha); % flow factor :PHIfx
for mx = 1:length(PHIfx)
   U2x= 400:50:600 ;% blade velocity at the impeller tip :U2x

   for  nx = 1:length(U2x);

      for qx= 1:10;% to find the power for different sizes, qx is used
         % r11,r22,rhh and bb are used to refer for different geometries and
         % their definitions are the same as r1,r2,rh and b, respectively
         r11 = (.75 + .25*(qx-1))*r1 ; r22 = ( .75 + .25*(qx-1))*r2 ;
         rhh = (.75 + .25*(qx-1))*rh ; bb  = (.75+ .25*(qx-1))*b ;

         rpmxy(nx)= (U2x(nx)/r22)*60/(2*pi);
        eff=0.8;

         for sx = 1:15 ; %for density and slip factor iteration sx is used
            wx(sx,mx,nx,qx)= U2x(nx)/r22; % angular velocity : wx
            rpmx(nx,qx) = wx(sx,mx,nx,qx)*60/(2*pi); % rotational speed : rpmx
```

```
            % the static density at location 1 (inlet of the impller):Ro1x
            Ro1x = Ro01*(1+(gama-1)/2*(PHIfx*wx(sx,mx,nx,qx)*r11/tan(beta1))^2/...
               (gama*R*(T01-((PHIfx*wx(sx,mx,nx,qx)*r11/tan(beta1))^2/(2*Cp)))))^(-
1/(gama-1));
            % the static density at location 2 (exit of the impeller):Ro2x, first
            % guess for the iteration
            Ro2x(1,mx,nx,qx) = Ro1x;
            Ro1x*pi*(r11^2-rhh^2)*(PHIfx*wx(sx,mx,nx,qx)*r11/tan(beta1));
            % actual mass rate :Mractx
            Mractx(sx,mx,nx,qx) = Ro1x*pi*(r11^2-
rhh^2)*(PHIfx*wx(sx,mx,nx,qx)*r11/tan(beta1));
            Mractcx(sx,mx,nx,qx) = MC*Mractx(sx,mx,nx,qx);% corrected actual mass rate
: Mractcx
            % slip factor : Slipfx
            Slipfx(sx,mx,nx,qx) = (1-(2/Nb*sqrt(cos(beta2))))*...
               (1-
Mractcx(sx,mx,nx,qx)/(Ro2x(sx,mx,nx,qx)*pi^2*r22^2*bb*2*rpmx(nx,qx)/30)*tan(beta2
));
            % exit radial relative velocity of the impeller : Wr2x
            Wr2x(sx,mx,nx,qx)= Mractcx(sx,mx,nx,qx)/(2*pi*r22*bb*Ro2x(sx,mx,nx,qx));
            % absulote tangential velocity at the impller exit : Cth2x
            Cth2x(sx,mx,nx,qx)= Slipfx(sx,mx,nx,qx)*U2x(nx);
            % input power : Pmx (see the comment on Pm)
            Pmx(sx,mx,nx,qx) =Mractcx(sx,mx,nx,qx)*(U2x(nx)*Cth2x(sx,mx,nx,qx)) ;
            % input torque : Tmx(see the comment on Pm)
            Tmx(sx,mx,nx,qx) = Pmx(sx,mx,nx,qx)/wx(sx,mx,nx,qx);
            %stagnation temperature at the impeller output : T02x
            T02x(sx,mx,nx,qx) = Pmx(sx,mx,nx,qx)/(Mractcx(sx,mx,nx,qx)*Cp) + T01;
            % resultant speed at the impller exit: C2x
            C2x(sx,mx,nx,qx)=sqrt((U2x(nx)-
Wr2x(sx,mx,nx,qx)*tan(beta2))^2+Wr2x(sx,mx,nx,qx)^2);
            % Mach no.(1)squared: M12x
            M12x(sx,mx,nx,qx)=((PHIfx*wx(sx,mx,nx,qx)*r11/tan(beta1))^2)/...
               (gama*R*((T01-(((PHIfx*wx(sx,mx,nx,qx)*r11/tan(beta1))^2)/(2*Cp)))));
            % Mach no.(2)squared :M22x
            M22x(sx,mx,nx,qx)=C2x(sx,mx,nx,qx)^2/(gama*R*(T02x(sx,mx,nx,qx)-
(C2x(sx,mx,nx,qx)^2)/(2*Cp)));
            Ro2x(sx+1,mx,nx,qx) = Ro1x*((1+(gama-
1)/(2)*M22x(sx,mx,nx,qx))/(1+(gama-1)/(2)*M12x(sx,mx,nx,qx)))...
               ^(-1/(gama-1))*((1+((1+eff)/2)*((gama-
1)/gama)*(U2x(nx)/sqrt(R*T01))^2*Slipfx(sx,mx,nx,qx)))...
               ^(1/(gama-1));
            %if  abs((Ro2x(sx+1,mx,nx,qx)-Ro2x(sx,mx,nx,qx))) <= 0.0000001 , break ,
end
         end
```

```
        % absolute tangential velocity at the impeller exit : Cth2x
        Cth2x(sx,mx,nx,qx)= Slipfx(sx,mx,nx,qx)*U2x(nx);
        % input power : Px
        Px(sx,mx,nx,qx) =Mractcx(sx,mx,nx,qx)*(U2x(nx)*Cth2x(sx,mx,nx,qx)) ;
        % input torque : Tx
        Tx(sx,mx,nx,qx) = Px(sx,mx,nx,qx)/wx(sx,mx,nx,qx);
        % stagnation temperature ratio of the impeller out put to the input : T0201rx
        T02x(sx,mx,nx,qx) = Px(sx,mx,nx,qx)/(Mractcx(sx,mx,nx,qx)*Cp) + T01;
        % stagnation temperature ratio of the impeller out put to the input : T0201rx
        T0201rx(sx,mx,nx,qx) = T02x(sx,mx,nx,qx)/T01;
        % isentropic stagnation temperature of the comrpessor exit : T04sx
        T04sx(sx,mx,nx,qx) = eff*(T02x(sx,mx,nx,qx)-T01) + T01;
        % stagnation pressure ratio : P04P01rx
        P04P01rx(sx,mx,nx,qx) =(T04sx(sx,mx,nx,qx)/T01)^(gama/(gama-1)) ;

    end

    figure(1)
    PPx  = nonzeros(Px(sx,mx,nx,1:qx)); plot(rpmx(nx,1:qx),PPx,'.-'); hold on
    figure(2)
    TTx = nonzeros(Tx(sx,mx,nx,1:qx)); plot(rpmx(nx,1:qx),TTx ,'.-'); hold on
    figure(3)
    TT0201rx = nonzeros(T0201rx(sx,mx,nx,1:qx)); plot(rpmx(nx,1:qx),TT0201rx,'.-');
    hold on
    figure(4)
    PP04P01rx=nonzeros(P04P01rx(sx,mx,nx,1:qx)); plot(rpmx(nx,1:qx),PP04P01rx,'.-
');
    hold on
    figure(5)
    MMractcx = nonzeros(Mractcx(sx,mx,nx,1:qx)); plot(rpmx(nx,1:qx),MMractcx,'.-');
    hold on

  end
end
hold off

figure(1);grid on
xlabel('rpm'); ylabel('input power ( W )')
title('input power vs rpm for different impeller sizes')
gtext('Z is the reference size where the radiuses: ');
% gtext('r_1 =.025 m,r_2 =.0381 m,r_h =.008m ')
gtext('\beta_1 =67^o')%, \beta_2 =25^o')
gtext('\phi_f=0.7')
% gtext('Nb =14, b=.005 m')
```

```
gtext('.75Z'); gtext('Z');gtext('1.25Z'); gtext('1.5Z');gtext('1.75Z');
gtext('2Z');gtext('2.25Z');gtext('2.5Z');gtext('2.75Z');gtext('3Z')
gtext('U_2=550 m/s'); gtext('500');gtext('450');gtext('400')
% %
figure(2); grid on
xlabel('rpm'); ylabel(' input torque (N-m) ')
title('input torque vs rpm for different impeller sizes')
gtext('Z is the reference size')
%gtext('r_1 =.025 m,r_2 =.0381 m,r_h =.008m ')
gtext('\beta_1 =67^o')%, \beta_2 =25^o')
gtext('\phi_f=0.7')
%gtext('Nb =14, b=.005 m')

gtext('.75Z'); gtext('Z');gtext('1.25Z'); gtext('1.5Z');gtext('1.75Z');
gtext('2Z');gtext('2.25Z');gtext('2.5Z');gtext('2.75Z');gtext('3Z')
gtext('U_2=550 m/s'); gtext('500');gtext('450');gtext('400')

figure(3); grid on
xlabel('rpm');ylabel('T_0_4/ T_0_1')
title('stagnation temperature ratio vs. rpm for different impeller sizes')
gtext('Z is the reference size')
%gtext('r_1 =.025 m,r_2 =.0381 m,r_h =.008m ')
gtext('\beta_1 =67^o')%, \beta_2 =25^o')
gtext('\phi_f=0.7')
%gtext('Nb =14, b=.005 m')

gtext('.75Z'); gtext('Z');gtext('1.25Z'); gtext('1.5Z');gtext('1.75Z');
gtext('2Z');gtext('2.25Z');gtext('2.5Z');gtext('2.75Z');gtext('3Z')
gtext('U_2=550 m/s'); gtext('500');gtext('450');gtext('400')

figure(4); grid on
xlabel('rpm');ylabel('P_0_4/P_0_1 ')
title('stagnation pressure ratio vs. rpm for different impeller sizes')
gtext('Z is the reference size')
%gtext('r_1 =.025 m,r_2 =.0381 m,r_h =.008m ')
gtext('\beta_1 =67^o')%, \beta_2 =25^o')
gtext('\phi_f=0.7')
% gtext('Nb =14, b=.005 m')

gtext('.75Z'); gtext('Z');gtext('1.25Z'); gtext('1.5Z');gtext('1.75Z');
gtext('2Z');gtext('2.25Z');gtext('2.5Z');gtext('2.75Z');gtext('3Z')
gtext('U_2=550 m/s'); gtext('500');gtext('450');gtext('400')
%
figure(5);grid on
xlabel('rpm');ylabel('actual mass flow rate (kg/s)')
```

```
title('actual mass flow rate vs rpm for different impeller sizes')
gtext('Z is the reference size')
%gtext('r_1 =.025 m,r_2 =.0381 m,r_h =.008m ')
gtext('\beta_1 =67^o')%, \beta_2 =25^o')
gtext('\phi_f=0.7')
%gtext('Nb =14, b=.005 m')

gtext('.75Z'); gtext('Z');gtext('1.25Z'); gtext('1.5Z');gtext('1.75Z');
gtext('2Z');gtext('2.25Z');gtext('2.5Z');gtext('2.75Z');gtext('3Z')
gtext('U_2=550 m/s'); gtext('500');gtext('450');gtext('400')
 %%%%%%%%%%%%%%%%%% the end %%%%%%%%%%%%%%%%%%%%
```

Appendix A.3

Third Code

```
% MATLAB SOFTWARE
% this program is written to help on choosing the right driver
% for teh test facility of centrifugal compressors
% this program is written to find the pressure ratio vs different
% impeller sizes of a given
% compressor geometry for different input power and rpm .
% NOTE : SI units are used

%------------------------------ starting the program -------------------------------%

clear all % clear statement for the text
close all % clear statement for the figure(s)
% GIVEN
% rpm, flow factor (PHIf) , impeller size and configuration, inlet stagnation conditions
% MAIN ASSUMPTIONS
% ideal gas and bulk flow

%ANALYSIS

% IMPELLER SIZE
r1 =.025 ;  % inlet tip radius (for the inducer) : r1
r2 =.0381 ; % exit tip radius (for the impeller) : r2
rh =.008 ;  % hub raduis: rh
% IMPELLER CONFIGURATION
beta1 =67*pi/180 ; % inlet tip angles : Beta1 (in radian)
beta2 =25*pi/180 ; % exit tip angles : Beta2 (in radian )
Nb =14 ; % number of the blades : Nb
b=.005 ; % impeller width :b

% GAS PROPERTIES: air
gama = 1.4 ; % specific ratio : gama ,constant
R = 287 ;  % gas constant : R
Cp = 1004 ; % constant pressure specific heat : Cp

% INLET CONDITIONS
T01 =300 ; % stagnation inlet temperature : T01
P01 = 101000 ;% stagnation inlet pressure : P01
Ro01 =1.2 ;% stagnation inlet density : Ro01

% SPECIAL ASSUMPTIONS
MC=.86;%Mass flow rate correction for the assumption of the bulk flow (MC)
alpha= 10*3.1416/180; %the expected angle before stall
%------------------------------ calculations ------------------------------%
```

```
%%%%%%%%%%%% rotational speed restriction program %%%%%%%%%%%%

PHIfxx = tan(beta1)/tan(beta1+alpha);
for mxx = 1:length(PHIfxx)

   rpmxx  =[30000 50000 70000 100000]; % rotational speed : rpmxx
   for  nxx = 1:length(rpmxx);

      Qxx=46; % the maximum iteration for qxx

      for qxx= 1:Qxx, % to find the power for different sizes, qxx is used
         Zxx(qxx)=0.7+.05*qxx; % the relative size of the compressor comparing to Zxx
         % r11,r22,rhh and bb are used to refer for different geometries and
         % their definitions are the same as r1,r2,rh and b, respectively

         r11 = (.75 + .05*(qxx-1))*r1 ;  r22 = ( .75 + .05*(qxx-1))*r2 ;
         rhh = (.75 + .05*(qxx-1))*rh ;  bb  = (.75+ .05*(qxx-1))*b ;
         % eff : is the efficiency of the compressor
         eff= 0.8;

          for sxx = 1:50;  %for density and slip factor iteration sxx is used
            wxx(sxx,mxx,nxx,qxx)= rpmxx(nxx)*2*pi/60; % angular velocity : wxx
            if ((PHIfxx(mxx)*wxx(sxx,mxx,nxx,qxx)*r11/tan(beta1))^2/(2*Cp))> (T01-10)
               disp('PHIfxx*wxx*r11/tan(beta1))^2/(2*Cp))> T01, so you will get
imaginary number, so stop calculations for this loop')
               break ,  end
            % blade velocity at the impeller exit :U2xx
            U2xx(sxx,mxx,nxx,qxx)= wxx(sxx,mxx,nxx,qxx)*r22;
            % the static density at location 1 (inlet of the impeller):Ro1xx
            Ro1xx = Ro01*(1+(gama-
1)/2*(PHIfxx(mxx)*wxx(sxx,mxx,nxx,qxx)*r11/tan(beta1))^2/...
               (gama*R*(T01-
((PHIfxx(mxx)*wxx(sxx,mxx,nxx,qxx)*r11/tan(beta1))^2/(2*Cp)))))^(-1/(gama-1));
            % the static density at location 2 (exit of the impeller):Ro2xx, first guess for the
iteration
            Ro2xx(1,mxx,nxx,qxx) = Ro1xx;
            % actual mass rate :Mractxx
            Mractxx(sxx,mxx,nxx,qxx)= Ro1xx*pi*(r11^2-
rhh^2)*(PHIfxx(mxx)*wxx(sxx,mxx,nxx,qxx)*r11/tan(beta1));
            Mractcxx(sxx,mxx,nxx,qxx) = MC*Mractxx(sxx,mxx,nxx,qxx); % corrected
actual mass rate : Mractcxx
            % slip factor : Slipfxx
            Slipfxx(sxx,mxx,nxx,qxx) = (1-(2/Nb*sqrt(cos(beta2))))*...
```

```
            (1-
Mractcxx(sxx,mxx,nxx,qxx)/(Ro2xx(sxx,mxx,nxx,qxx)*pi^2*r22^2*bb*2*rpmxx(nxx)/3
0)*tan(beta2));
          if  Slipfxx(sxx,mxx,nxx,qxx)<= 0.1
             break ,  end
          % exit radial relative velocity of the impeller : Wr2xx
          Wr2xx(sxx,mxx,nxx,qxx)=
Mractcxx(sxx,mxx,nxx,qxx)/(2*pi*r22*bb*Ro2xx(sxx,mxx,nxx,qxx));
          % absolute tangential velocity at the impeller exit : Cth2xx
          Cth2xx(sxx,mxx,nxx,qxx)=
Slipfxx(sxx,mxx,nxx,qxx)*U2xx(sxx,mxx,nxx,qxx);
          % input power : Pmxx (this value of the power for the iteration inside the s
loop and
          % does not represent the actual power which are used for the pressure ratio
calculation)
          % this distinguishing between the two power (Pmxx and Pxx, below) is
important to get the
          % rigth plot
          Pmxx(sxx,mxx,nxx,qxx)
=Mractcxx(sxx,mxx,nxx,qxx)*(U2xx(sxx,mxx,nxx,qxx)*Cth2xx(sxx,mxx,nxx,qxx)) ;
          % input torque : Tmxx (see the comment on Pmx)
          Tmxx(sxx,mxx,nxx,qxx) = Pmxx(sxx,mxx,nxx,qxx)/wxx(sxx,mxx,nxx,qxx);
          %stagnation temperature at the impeller output : T02xx
          T02xx(sxx,mxx,nxx,qxx) =
Pmxx(sxx,mxx,nxx,qxx)/(Mractcxx(sxx,mxx,nxx,qxx)*Cp) + T01;
          % resultant speed at the impeller exit: C2xx
          C2xx(sxx,mxx,nxx,qxx)=sqrt((U2xx(sxx,mxx,nxx,qxx)-
Wr2xx(sxx,mxx,nxx,qxx)*tan(beta2))^2+Wr2xx(sxx,mxx,nxx,qxx)^2);
          % Mach no.(1)squared: M12xx

M12xx(sxx,mxx,nxx,qxx)=((PHIfxx(mxx)*wxx(sxx,mxx,nxx,qxx)*r11/tan(beta1))^2)/...
            (gama*R*((T01-
(((PHIfxx(mxx)*wxx(sxx,mxx,nxx,qxx)*r11/tan(beta1))^2)/(2*Cp)))));
          % Mach no.(2)squared :M22xx

M22xx(sxx,mxx,nxx,qxx)=C2xx(sxx,mxx,nxx,qxx)^2/(gama*R*(T02xx(sxx,mxx,nxx,qx
x)-(C2xx(sxx,mxx,nxx,qxx)^2)/(2*Cp)));
          Ro2xx(sxx+1,mxx,nxx,qxx) = Ro1xx*((1+(gama-
1)/(2)*M22xx(sxx,mxx,nxx,qxx))/(1+(gama-1)/(2)*M12xx(sxx,mxx,nxx,qxx)))...
            ^(-1/(gama-1))*((1+((1+eff)/2)*((gama-
1)/gama)*(U2xx(sxx,mxx,nxx,qxx)/sqrt(R*T01))^2*Slipfxx(sxx,mxx,nxx,qxx)))...
            ^(1/(gama-1));
          if  abs((Ro2xx(sxx+1,mxx,nxx,qxx)-Ro2xx(sxx,mxx,nxx,qxx))) <= 0.00001 ,
break , end
        end
```

```
        if  Slipfxx(sxx,mxx,nxx,qxx)<= 0.1
           disp('Slip factor very small, so you will get imaginary number, so stop
calculations for this loop')
           break ,  end
        % absolute tangential velocity at the impeller exit : Cth2xx
        Cth2xx(sxx,mxx,nxx,qxx)= Slipfxx(sxx,mxx,nxx,qxx)*U2xx(sxx,mxx,nxx,qxx);
        %input power : Pxx
        Pxx(sxx,mxx,nxx,qxx)
=Mractcxx(sxx,mxx,nxx,qxx)*(U2xx(sxx,mxx,nxx,qxx)*Cth2xx(sxx,mxx,nxx,qxx)) ;
        % input torque : Txx
        Txx(sxx,mxx,nxx,qxx) = Pxx(sxx,mxx,nxx,qxx)/wxx(sxx,mxx,nxx,qxx);
        %stagnation temperature of the impeller output :T02xx
        T02xx(sxx,mxx,nxx,qxx) =
Pxx(sxx,mxx,nxx,qxx)/(Mractcxx(sxx,mxx,nxx,qxx)*Cp) + T01;
        % stagnation temperature ratio of the impeller out put to the input : T0201rxx
        T0201rxx(sxx,mxx,nxx,qxx) = T02xx(sxx,mxx,nxx,qxx)/T01;
        %isentropic stagnation temperature of the compressor exit : T04sxx
        T04sxx(sxx,mxx,nxx,qxx) = eff*(T02xx(sxx,mxx,nxx,qxx)-T01) + T01;
        % stagnation pressure ratio : P04P01rxx
        P04P01rxx(sxx,mxx,nxx,qxx) =(T04sxx(sxx,mxx,nxx,qxx)/T01)^(gama/(gama-1))
;
        %U2xx(sxx,mxx,nxx,qxx)= wxx(sxx,mxx,nxx,qxx)*r22;
      end
   end
end
PP04P01rxx1  = nonzeros(P04P01rxx(:,mxx,1,:));
ZZxx1= nonzeros(Zxx(1:length(PP04P01rxx1)));
PP04P01rxx2  = nonzeros(P04P01rxx(:,mxx,2,:));
ZZxx2= nonzeros(Zxx(1:length(PP04P01rxx2)));
PP04P01rxx3  = nonzeros(P04P01rxx(:,mxx,3,:));
ZZxx3= nonzeros(Zxx(1:length(PP04P01rxx3)));
PP04P01rxx4  = nonzeros(P04P01rxx(:,mxx,4,:));
ZZxx4= nonzeros(Zxx(1:length(PP04P01rxx4)));
%         PP04P01rxx5 = nonzeros(P04P01rxx(:,mxx,5,:));
%        ZZxx5= nonzeros(Zxx(1:length(PP04P01rxx5)));
figure(1)
plot( ZZxx1 ,PP04P01rxx1,'.-',ZZxx2 ,PP04P01rxx2,'.-',ZZxx3 ,PP04P01rxx3,'.-',ZZxx4
,PP04P01rxx4,'.-')%,ZZxx5 ,PP04P01rxx5,'.-')
hold on
%%%%%%%%%% input power restriction program %%%%%%%%%%%%%%
%
 PHIfxxx = tan(beta1)/tan(beta1+alpha);
for mxxx = 1:length(PHIfxxx)
   Pxxx=   [100000 200000 350000 500000];
   Pmxxx=  [100000 200000 350000 500000];
```

```
   for  bxxx = 1:length(Pxxx);
      QXXX=46; %Qxxx refer to the maximum size.
      for qxxx= QXXX:-1:1 % to find the power for different sizes, qxxx is used
         Zxxx(qxxx)=0.75+.05*(QXXX-qxxx);  % the relative size of the compressor
comparing to Zxxx
         % r11,r22,rhh and bb are used to refer for different geometries and
         % their definitions are the same as r1,r2,rh and b, respectively. The reference
         % size Z refer to r1,r2,rh and b.

         % impller size and it is constant with the others variables
         r11 = (0.75 + .05*(QXXX-qxxx))*r1 ; r22 = (0.75 + .05*(QXXX-qxxx))*r2 ;
         rhh = (0.75 + .05*(QXXX-qxxx))*rh ; bb  = (0.75 + .05*(QXXX-qxxx))*b ;

         for nxxx=1:1500% loop for rpmxxx iteration

            % The equations for rpmxxx(1) were taken from the plot of the rpm vs power
            % (another program) then the values of the data were extracted to excel
software
            % where the trendline function was used to find the equations of those curves
            % also some modifications are done through trial and error to improve the
            % the rpmxxx equations (multiplying/ dividing by 2 or ...)
            % these factor may change if the power is not in the given range

            if      Zxxx(qxxx)>=2.875
               rpmxxx(1,qxxx,bxxx) =  414.8/4*Pxxx(bxxx)^0.3489;
               %
            elseif   Zxxx(qxxx)>=2.625 & Zxxx(qxxx)<2.875
               rpmxxx(1,qxxx,bxxx)=   511.84/4*Pxxx(bxxx)^0.3439;
            elseif   Zxxx(qxxx)>=2.375  & Zxxx(qxxx)<2.625
               rpmxxx(1,qxxx,bxxx) =  573.22/4*Pxxx(bxxx)^0.348;
            elseif   Zxxx(qxxx)>=2.125  & Zxxx(qxxx)<2.375
               rpmxxx(1,qxxx,bxxx) =  791.53/4*Pxxx(bxxx)^0.3369;
            elseif   Zxxx(qxxx)>=1.875  & Zxxx(qxxx)<2.125
               rpmxxx(1,qxxx,bxxx) =  826.13/4*Pxxx(bxxx)^0.3488;
            elseif   Zxxx(qxxx)>=1.625  & Zxxx(qxxx)<1.875
               rpmxxx(1,qxxx,bxxx) =  1047.2/4*Pxxx(bxxx)^0.3479;
            elseif   Zxxx(qxxx)>=1.375 & Zxxx(qxxx)<1.625
               rpmxxx(1,qxxx,bxxx) =  0.0000000006/20000*Pxxx(bxxx)^2.9257;
            elseif   Zxxx(qxxx)>=1.125  & Zxxx(qxxx)<1.375
               rpmxxx(1,qxxx,bxxx) =  1859.3/12*Pxxx(bxxx)^0.3481;
            elseif   Zxxx(qxxx)>=.875   & Zxxx(qxxx)< 1.125
               rpmxxx(1,qxxx,bxxx) =  3666.1/6*Pxxx(bxxx)^0.3218;
            else
               rpmxxx(1,qxxx,bxxx) =  8999.6/7*Pxxx(bxxx)^0.2817;
            end
```

```
            % eff : is the efficiency of the compressor
           eff =0.8;

              wxxx1(mxxx,nxxx,qxxx,bxxx)= rpmxxx(nxxx,qxxx,bxxx)*2*pi/60;%
angular velocity : wxxx
              if
((PHIfxxx(mxxx)*wxxx1(mxxx,nxxx,qxxx,bxxx)*r11/tan(beta1))^2/(2*Cp))> (T01-10)
                 disp('PHIfxxx*wxxx*r11/tan(beta1))^2/(2*Cp))> T01, so you will get
imaginary number, so stop calculations for this loop')
                 nxxx=nxxx-1;
                 break ,  end
            for sxxx = 1:50; %for density and slip factor iteration sxxx is used
              wxxx(sxxx,mxxx,nxxx,qxxx,bxxx)= rpmxxx(nxxx,qxxx,bxxx)*2*pi/60;%
angular velocity : wxxx
              % blade velocity at the impeller exit :U2xxx
              U2xxx(sxxx,mxxx,nxxx,qxxx,bxxx)=
wxxx(sxxx,mxxx,nxxx,qxxx,bxxx)*r22 ;
              % the static density at location 1 (inlet of the impeller):Ro1xxx
              Ro1xxx = Ro01*(1+(gama-
1)/2*(PHIfxxx(mxxx)*wxxx(sxxx,mxxx,nxxx,qxxx,bxxx)*r11/tan(beta1))^2/...
                 (gama*R*(T01-
((PHIfxxx(mxxx)*wxxx(sxxx,mxxx,nxxx,qxxx,bxxx)*r11/tan(beta1))^2/(2*Cp)))))^(-
1/(gama-1));
              % the static density at location 2 (exit of the impeller):Ro2xxx, first guess for
the iteration
              Ro2xxx(1,mxxx,nxxx,qxxx,bxxx) = Ro1xxx;
              % actual mass flow rate :Mractxxx
              Mractxxx(sxxx,mxxx,nxxx,qxxx,bxxx)=  Ro1xxx*pi*(r11^2-
rhh^2)*(PHIfxxx(mxxx)*wxxx(sxxx,mxxx,nxxx,qxxx,bxxx)*r11/tan(beta1));
              % corrected actual mass flow rate : Mractcxxx
              Mractcxxx(sxxx,mxxx,nxxx,qxxx,bxxx) =
MC*Mractxxx(sxxx,mxxx,nxxx,qxxx,bxxx);
              % slip factor: Slipfxxx
              Slipfxxx(sxxx,mxxx,nxxx,qxxx,bxxx) = (1-(2/Nb*sqrt(cos(beta2))))*...
                 (1-
Mractcxxx(sxxx,mxxx,nxxx,qxxx,bxxx)/(Ro2xxx(sxxx,mxxx,nxxx,qxxx,bxxx)*pi^2*r22
^2*bb*2*rpmxxx(nxxx,qxxx,bxxx)/30)*tan(beta2));
              if  Slipfxxx(sxxx,mxxx,nxxx,qxxx,bxxx)<= 0.1
              break ,  end
              % exit radial relative velocity of the impeller : Wr2xxx
              Wr2xxx(sxxx,mxxx,nxxx,qxxx,bxxx)=
Mractcxxx(sxxx,mxxx,nxxx,qxxx,bxxx)/(2*pi*r22*bb*Ro2xxx(sxxx,mxxx,nxxx,qxxx,bx
xx));
              % resultant speed at the impeller exit: C2xxx
```

```
C2xxx(sxxx,mxxx,nxxx,qxxx,bxxx)=sqrt((U2xxx(sxxx,mxxx,nxxx,qxxx,bxxx)-
Wr2xxx(sxxx,mxxx,nxxx,qxxx,bxxx)*tan(beta2))^2 ...
                +Wr2xxx(sxxx,mxxx,nxxx,qxxx,bxxx)^2);
            % absolute tangential velocity at the impeller exit : Cth2xxx
            Cth2mxxx(sxxx,mxxx,nxxx,qxxx,bxxx)=
Slipfxxx(sxxx,mxxx,nxxx,qxxx,bxxx)*U2xxx(sxxx,mxxx,nxxx,qxxx,bxxx);
            % input torque : Tmxxx (see the comment on Pmxx)
            Tmxxx(sxxx,mxxx,nxxx,qxxx,bxxx) =
Pmxxx(bxxx)/wxxx(sxxx,mxxx,nxxx,qxxx,bxxx);
            %stagnation temperature at the impeller output : T02xxx
            T02mxxx(sxxx,mxxx,nxxx,qxxx,bxxx) =
Pmxxx(bxxx)/(Mractcxxx(sxxx,mxxx,nxxx,qxxx,bxxx)*Cp) + T01;
            % Mach no.(1)squared: M12xxx

M12xxx(sxxx,mxxx,nxxx,qxxx,bxxx)=(PHIfxxx(mxxx)*(wxxx(sxxx,mxxx,nxxx,qxxx,bx
xx)*r11/tan(beta1))^2)/...
                (gama*R*((T01-
((PHIfxxx(mxxx)*(wxxx(sxxx,mxxx,nxxx,qxxx,bxxx)*r11/tan(beta1))^2)/(2*Cp)))));
            % Mach no.(2)squared :M22xxx

M22xxx(sxxx,mxxx,nxxx,qxxx,bxxx)=C2xxx(sxxx,mxxx,nxxx,qxxx,bxxx)^2/ ...
                (gama*R*(T02mxxx(sxxx,mxxx,nxxx,qxxx,bxxx)-
(C2xxx(sxxx,mxxx,nxxx,qxxx,bxxx)^2)/(2*Cp)));
            Ro2xxx(sxxx+1,mxxx,nxxx,qxxx,bxxx) = Ro1xxx*((1+(gama-
1)/(2)*M22xxx(sxxx,mxxx,nxxx,qxxx,bxxx))/(1+(gama-
1)/(2)*M12xxx(sxxx,mxxx,nxxx,qxxx,bxxx)))...
                ^(-1/(gama-1))*((1+((1+eff)/2)*((gama-
1)/gama)*(U2xxx(sxxx,mxxx,nxxx,qxxx,bxxx)/sqrt(R*T01))^2*Slipfxxx(sxxx,mxxx,nxx
x,qxxx,bxxx)))...
                ^(1/(gama-1));
            if  abs((Ro2xxx(sxxx+1,mxxx,nxxx,qxxx,bxxx)-
Ro2xxx(sxxx,mxxx,nxxx,qxxx,bxxx))) <= 0.00001 , break , end
          end

          if ((Pmxxx(bxxx)-
(Mractcxxx(sxxx,mxxx,nxxx,qxxx,bxxx)*U2xxx(sxxx,mxxx,nxxx,qxxx,bxxx)*...
                Cth2mxxx(sxxx,mxxx,nxxx,qxxx,bxxx)))<= 50) , break ,end
           % this criteria is OK. Not necessary to be very small since the effect of the
change in rpm value is small
           rpmxxx(nxxx+1,qxxx,bxxx)=rpmxxx(nxxx,qxxx,bxxx)+350;

        end
        % absolute tangential velocity at the impeller exit : Cth2xxx
```

```
        Cth2xxx(sxxx,mxxx,nxxx,qxxx,bxxx)=
Slipfxxx(sxxx,mxxx,nxxx,qxxx,bxxx)*U2xxx(sxxx,mxxx,nxxx,qxxx,bxxx);
        % input torque : Txxx
        Txxx(sxxx,mxxx,nxxx,qxxx,bxxx) =
Pxxx(bxxx)/wxxx(sxxx,mxxx,nxxx,qxxx,bxxx);
        %stagnation temperature of the impeller output :T02xxx
        T02xxx(sxxx,mxxx,nxxx,qxxx,bxxx) =
Pxxx(bxxx)/(Mractcxxx(sxxx,mxxx,nxxx,qxxx,bxxx)*Cp) + T01;
        %ratio of the stagnation temperature of the impeller exit to the inlet
        T0201rxxx(sxxx,mxxx,nxxx,qxxx,bxxx) =
T02xxx(sxxx,mxxx,nxxx,qxxx,bxxx)/T01;
        %isentropic stagnation temperature of the compressor exit : T04sxxx
        T04sxxx(sxxx,mxxx,nxxx,qxxx,bxxx) =
eff*(T02xxx(sxxx,mxxx,nxxx,qxxx,bxxx)-T01) + T01;
        % stagnation pressure ratio : P04P01r
        P04P01rxxx(sxxx,mxxx,nxxx,qxxx,bxxx)
=(T04sxxx(sxxx,mxxx,nxxx,qxxx,bxxx)/T01)^(gama/(gama-1)) ;

      end

   end
end
PP04P01rxxx1  = nonzeros(P04P01rxxx(:,mxxx,:,:,1));
ZZxxx1= nonzeros(Zxxx(1:length(PP04P01rxxx1)));
PP04P01rxxx2  = nonzeros(P04P01rxxx(:,mxxx,:,:,2));
ZZxxx2= nonzeros(Zxxx(1:length(PP04P01rxxx2)));
PP04P01rxxx3  = nonzeros(P04P01rxxx(:,mxxx,:,:,3));
ZZxxx3= nonzeros(Zxxx(1:length(PP04P01rxxx3)));
PP04P01rxxx4  = nonzeros(P04P01rxxx(:,mxxx,:,:,4));
ZZxxx4= nonzeros(Zxxx(1:length(PP04P01rxxx4)));
% PP04P01rxxx5  = nonzeros(P04P01rxxx(:,mxxx,:,:,5));
% ZZxxx5= nonzeros(Zxxx(1:length(PP04P01rxxx5)));
figure(1)
plot(ZZxxx1 ,PP04P01rxxx1,'ob-'); hold on
plot(ZZxxx2 ,PP04P01rxxx2,'or-'); hold on
plot(ZZxxx3 ,PP04P01rxxx3,'og-'); hold on
plot(ZZxxx4 ,PP04P01rxxx4,'om-'); hold on
% plot(ZZxxx5 ,PP04P01rxxx5,'oc-');
hold off;
grid on
title('Pressure ratio vs compressor size for different constant rpm and input power')

xlabel('compressor size(Z)')
ylabel('total pressure ratio(P_0_4/P_0_1)')
gtext('operating limit curve for a given:')
```

```
gtext('\beta_1=67^o, \beta_2=25^o,')
gtext('r_1/r_2= 1.524,'); gtext('at Z=1, r_1=.025m')
gtext('\phi_f=0.7'); gtext('eff= 80%')
gtext('30krpm');  gtext('50krpm'); gtext('70krpm'); gtext('100krpm');
gtext('100kW'); gtext('200kW'); gtext('350kW');  gtext('500kW')
legend('30krpm','50krpm','70krpm','100krpm','100kW','200kW','350kW','500kW',-1)
```

Appendix B

Flow Chart

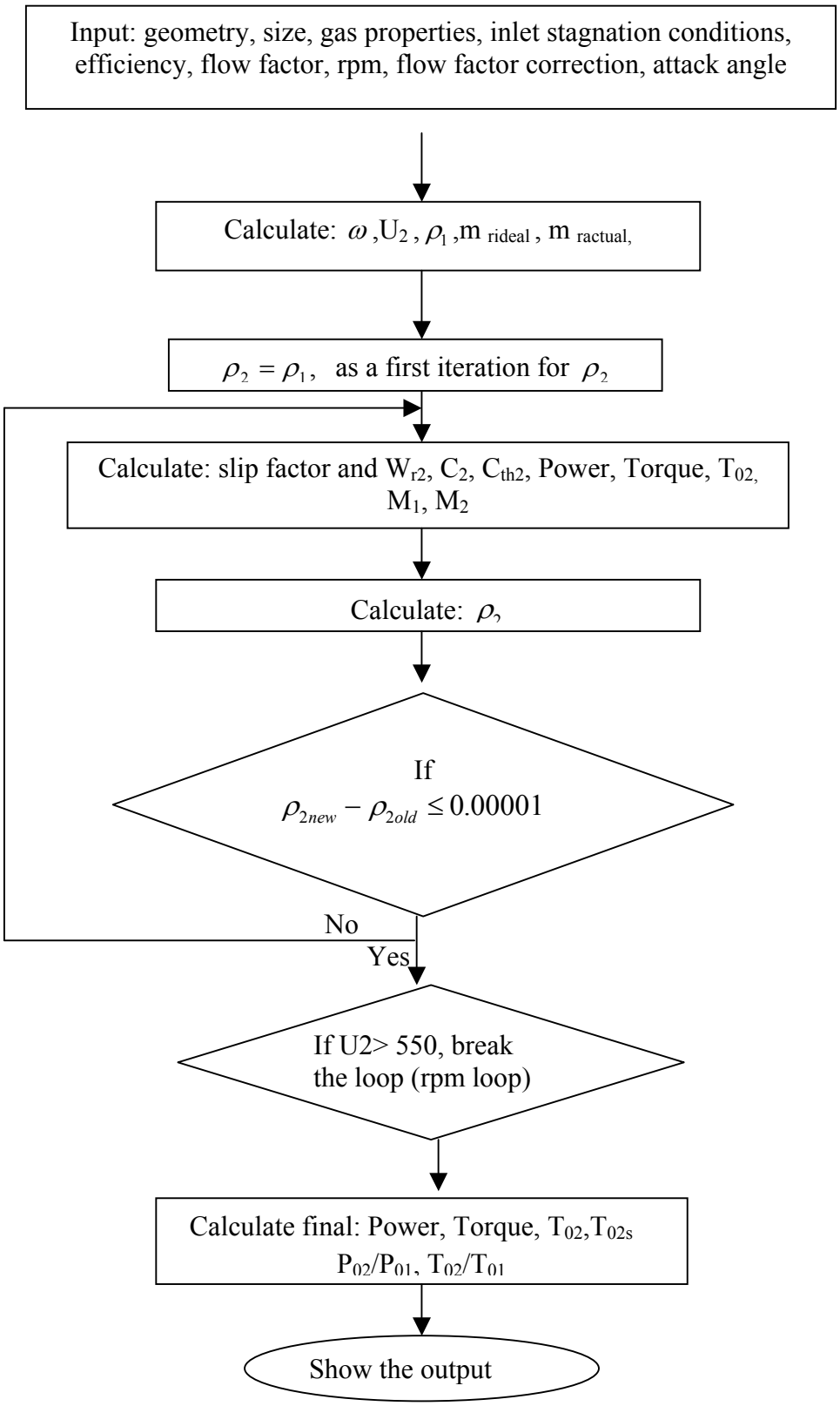

General flow chart of the codes

Nomenclature

A	area
b	impeller width
C	absolute velocity of the impeller
C_θ	tangential velocity of the impeller
C_p	constant pressure specific heat
C_{z1}	absolute tangential velocity at the impeller inlet
d	compressor discharge conditions
ΔP	differential static pressure of the flow meter
H	enthalpy
$\dot{m}$	mass flow rate
M	Mach number
$Mech$	mechanical
N_b	number of the blades in the impeller
P	pressure
Pr	pressure ratio
P	power
ρ_1	static density at the impeller (compressor) inlet
ρ_2	static density at the impeller exit
Q	flow rate
r_1	inlet radius of the impeller
r_2	exit radius of the impeller
r_h	hub radius
R	gas constant
R	result (used for the uncertainty analysis)
rpm	rotational speed per minute
T	temperature

τ	input torque
U_B	bias uncertainty
U_p	precision uncertainty
U	impeller tangential velocity
v:	velocity
W	work
W_{r_2}	exit radial relative velocity of the impeller
Z	blade size

Subscripts

$_{0201r}$	ratio of the impeller exit with the inlet
01	inlet impeller (compressor) stagnation condition
02	exit impeller stagnation condition
02s	isentropic exit impeller stagnation condition
04	exit compressor stagnation condition
1	impeller inlet
2	impeller exit
4	compressor exit
act	actual case
cr	compressor rotor
c	compressor stage
f	flow meter
i	compressor inlet conditions
I	piping inlet
ideal	idea case
imp	impeller
tt	total-to-total
Z	axial inlet of the impeller
Z	is the reference size

Greek letters

β	impeller angle
δ_{ik}	kronecker delta
γ	specific heat ratio
σ_S	slip factor
η	efficiency
ϕ_f	flow factor
Ω	angular velocity
ζ	correlation coefficient of the bias limit

REFERENCES

1. Al-Zubaidy, Sarim and Dahgan, Mahdi, 1992, " Perfomance Prediction Method for low Pressure Ratio Centrifugal compressor," ASE *Technical Paper Series 921732* p 1-8.

2. Arima, T., Sonoda, T., Shirotori, M and Yamaguchi, Y., 1998, " Computation of Subsonic and Transonic Compressor Rotor Flow Taking Account of Reynolds Stress Anisotropy," ASME, *98-GT-423*.

3. Beihoff, B., 1996, " A Survey of Torque Transudation Methodologies for Industrial Application," *IEEE*, 0-7803-3148-6-5/96 pp 220-229.

4. Boyce, M., 2002, "Gas Turbine Engineering Handbook," *Gulf Professional Publishing*, pp 635 & 638.

5. Boyce, M., 2003 "Centrifugal Compressor: a basic guide" Penn Well Corporation, pp 552.

6. Capece, V. R., 1982 " Investigation of Turbocharger Stall: I-Facility Design and Construction and Initial Performance Data," PhD Thesis, *Massachusetts Institute of Technology*.

7. Chen, J., Fletcher, D. F., Haynes, B. S. and Hooper, J. D., (1998),"Validation of the Cobra Probe Using Turbulence Measurement in a Fully Developed Pipe Flow," *13th Australian Fluid Mechanics Conference,* 3-18 December.

8. Chevron Co., December 1988 "Compressor Manual," Sec. 170, pp 100-36.

9. Clayton, R. P., Leong, W. U. A., Sanatian, R., Issa, R. I. and Xi, G., 1998, " A Numerical Study of the Three-Dimensional Turbulent Flow in the Impeller of a High-Speed Centrifugal Compressor," ASME, *98-GT-49*.

10. Colantuoni, S. and Colella, A., 1993, " Aerodesign and Performance Analysis of a Radial Transonic Impeller for a 9:1 Pressure Ratio Compressor," ASME *Journal of Turbomachinery*, Vol. 115, pp. 573-581.

11. Eisenlohr, Gernot; Dalbert, Peter; Krain, Hartmut; Pröll, Hartwing; Richter, Franz-Arno and Rohne, Karl-Heinz, 1998, " Analysis of the Transonic Flow at the Inlet of a High Pressure Ratio Centrifugal Impeller," ASME paper *98-GT-24*.

12. Ebi, Günter; Reckermann, Matthias; Zappe, Hans P. and Söchtig, Jürgen (1999), "An Integrated-Optical, Non-Contact Torque Measurement Micro-system," *Optical Engineering,* Vol. 38, pp. 240-245.

13. Engeda, A., 1997, " Comparative Rotating Stall and Surge Characteristic of a Centrifugal Compressor With Three Different Types of Diffusers," ASME, *97-GT-245*.

14. Erhard, J. and Gehrer, A., 2000, "Design And Construction Of A Transonic Test-Turbine Facility," ASME TURBOEXPO, *2000-GT-480.*

15. Fink, D. A., 1984, " An Experimental Investigation of Centrifugal Compressor Surge and Stall Phenomena in turbochargers," MS Thesis, *Massachusetts Institute of Technology.*

16. Fink, D. A., 1988, " Surge Dynamics and Unsteady Flow Phenomena in Centrifugal Compressors," PhD Thesis, *Massachusetts Institute of Technology.*

17. Hill, P. and Peterson, C. (1992), "Mechanics and Thermodynamics of Propulsion," 2nd edition, *Addison Wesley*.

18. Hunziker, R., Dickmann, H-P and Emmrich, R., 2001," Numerical and experimental investigation of a centrifugal compressor with an inducer casing bleed system," IMechE, *part A*, Vol. 215, pp 783-791.

19. Justen, F., Ziegler, K.U. and Gallus, H.E., 1999, " Experimental Investigation of Unsteady Flow Phenomena in a Centrifugal Compressor Vaned Diffuser of Variable Geometry," ASME *Journal of Turbomachinery*, Vol. 121 pp 763-771.

20. Kim, Y., Engeda, A. Aungier, R. and Direnzi, G., 2001, " The Influence of Inlet Flow Distortion on the Performance of a Centrifugal Compressor and the Development of an Improved Inlet Using Numerical Simulation," IMechE, Vol 215 *part A*, 323-338.

21. Köppel, P., Roduner, C., Kupferschmied, P. and Gyarmathy, G., 2000, " On the Development and Application of the Fast-Response Aerodynamic Probe System in Turbomachines- Part3: Comparison of Averaging Methods Applied to Centrifugal Compressor Measurements," ASME, *Journal of Turbomachinery*, Vol. 122 pp 527-536.

22. Krain, H. and Hoffmann, B., 1998, " Flow Physics in High Pressure Ratio Centrifugal Compressors," ASME, 9 pp *FEDME98-4853*.

23. Krain, K., Hoffmann, B. and Pak, H., 1995, " Aerodynamics of a Centrifugal Compressor Impeller with Transonic Inlet Conditions," ASME, 9 pp *95-GT-79*.

24. Liberti, J.-L. Di, Wilmsen, B. and Engeda, A.,1996, " The Effect of the Vaneless Diffuser width on the Performance of a Centrifugal Compressor," ASME, FED-Vol.237, Fluid Engineering Division Conference N. 2, pp 797-803.

25. Masutani, Joy; Koga, Jun and Kawashima, Yasuhiro, 1999, " Development of High-Speed, Compact Centrifugal Compressor Stage," *Mitsubishi Heavy Industries, Ltd, Technical Review*, Vol. 36 no., pp 6-10.

26. Nikuradse, J., (1932)"Gesetzmässigkeit der turbulenten Ströomung in glatten Rohren ," Forschg. Arb. Ing. -Wes. No. 356.

27. Omega Engineering Inc., " Practical guidelines for Temperature measurement," pp Z-15.

28. Rodgers, C., 1997, "Development of a High-Specific-Speed Centrifugal Compressor," ASME, *Journal of Turbomachinery*, Vol. 119 pp 501-505.

29. Roduner, C., Köppel, P., Kupferschmied, P. and Gyarmathy, G., 1999, "Comparison of Measurement Data at the Impeller Exit of a Centrifugal Compressor Measured With Both Pneumatic and Fast-Response Probes," ASME, *Journal of Turbomachinery*, Vol. 121 pp 609-618.

30. Roduner, C., Kupferschmied, P., Köppel, P., and Gyarmathy, G., 2000, "On the Development and Application of the Fast-Response Aerodynamic Probe System in Turbomachines- Part 2: Flow, Surge and Stall in a Centrifugal Compressor," ASME, *Journal of Turbomachinery*, Vol. 122 pp 517-526.

31. Schlechtriem, S. and Lötzerich, M., 1997, " Breakdown of Tip Leakage Vortices in Compressor at Flow Conditions Close to Stall," ASME, *97-GT-41*.

32. Schlichting, H., 1979, " Boundary Layer Theory", McGraw-Hill, 7th edition.

33. Shirley, Gregory B., 1998, " An Experimental Investigation of Low Reynolds Number, high Mach Number Centrifugal Compressor," Master Thesis, Massachusetts Institute of Technology ".

34. Reunanen, Arttu, (2001), *"* Experimental and Numerical Analysis of Different Volutes in a Centrifugal Compressor,*"* Dissertation, *Lappeenranta University of Technology,* Finland.

35. Saudi Armco, 2001, "Rotating Equipment short course," *AGE102.08*, pp 3-4.

36. Saxena, M. N., (2000), "Optimize Gas Turbine –Driven Centrifugal Compressors," *Hydrocarbon Processing*, November 2000, pp 61-64.

37. Tullis, Iain D.C., (2000), " the laser torquemeter and implications of Speckle Decorrelation on Torque Measurement," *PhD thesis,* Loughborough University, UK.

38. Walsh, P. and Fletcher P., (1998), *"*Gas Turbine Perfomance,*"* *Blackwell Science Ltd and ASME,* pp 530-531.

39. Wernet, P. M., Bright, M. M. and Skoch, G. J., 2001, " An Investigation of Surge in a High-Speed Centrifugal Compressor Using digital PIV," ASME, *Journal of Turbomachinery*, Vol. 123 pp 418-428.

40. Wiesner, F. J., (1967), " A Review of Slip Factors for Centrifugal Compressor Impeller," *Trans. ASME Series A. J. Eng. For Power*, 89, pp 588-592.

41. Yun, Hayong and Smith, Jr., J. L., 1996, "Centrifugal Compressor for Automotive Air Conditioners- Component Design" *proceedings of the ASME Advanced Energy Systems Division*, pp 115-122.

VITA

- Fahad A. AL-SULAIMAN.
- Received Bachelor of Science (B.Sc.) degree in Mechanical Engineering from King Fahd University of Petroleum & Minerals, Dhahran Saudi Arabia in Jan. 2001.
- Joined Mechanical Engineering Department of King Fahd University of petroleum & Minerals, Dhahran Saudi Arabia, as a M.Sc. student since Feb. 2001.